PROGRESS REPORT

Industrial Products from Vegetable Oils

20130204

March 2017

Funded by The Agriculture Development Fund

Prepared by Dr. Martin J.T. Reaney
Chair of Lipid Quality and Utilization
University of Saskatchewan

TABLE OF CONTENTS

EXECUTIVE SUMMARY

Previous progress:

1. Conversion of Glycerol to Monoglyceride

Magnesium and calcium oxide were used as an effective catalyst mixture to produce monoacyl glycerol from biodiesel waste. We subsequently found that magnesium turnings were a superior catalyst for glycerolysis of triglycerides. **The reaction can add substantial value to glycerol remaining from a biodiesel process.**

2. Production of Lithium Catalysts, High Quality Glycerol and Lithium Grease

The improved glycerol and lithium grease have substantially more value than the crude glycerol produced by a normal biodiesel reaction.

3. Trans-vaccenic Acid (TVA) for Clinical Trials

We have also completed the first good manufacturing practice (GMP) run at the pilot plant where we scaled up the production of TVA. This marks an important step in the evolution of the Bioprocessing Pilot Plant as we have demonstrated the capability of conducting processes for human trials. We have prepared 94.9% of TVA and 1.8% of *cis*-vaccenic acid. Oleic acid was used as internal standard.

4. Enriched Gondoic Acid Methyl Ester

5. Drop-in Fuel

We developed analytical procedures to measure branched and unbranched alkane in drop in fuels. The method also determines undesired fatty alcohol, fatty aldehyde, fatty ester and alkene as side products.

6. Bleached Flaxseed Oil

Lipid quality and utilization (LQU) has developed rapid bleaching methods based on high vacuum bleaching. The vacuum refined flaxseed oil dries 40% faster than crude flaxseed oil and the pigment level is comparable to sun-bleached flaxseed oil.

7. Flax Meal Antioxidant

Flaxseed meal contains the most powerful antioxidant system for linolenic acid rich oils

known. LQU has identified its constituents.

8. Oxygen-17 NMR Spectroscopy

We have demonstrated the first example of using ^{17}O NMR to monitor the production of first generation biodiesel (fatty acid methyl ester) and MG production. ^{17}O NMR can be a very powerful tool for the investigation of oxygen functionalities in the complex mixtures present in synthetic biofuels.

9. Triglyceride Molecular Distillation

We have enriched light short chain lipids in coconut oil using a molecular distillation process as a model process. This method could be used to produce other enriched TG species from complex mixtures.

10. Cannabidiol

LQU developed rapid methods for CBD quantification based on ^{1}H NMR and GC-MS. The hempseed oil sample contain trace amount of CBD, which can be detected by GC-MS. The CBD level is lower than 20 ppm based on ^{1}H NMR spectra.

This year progress:

1. Pilot Scale Low Temperature Flaxseed Oil Refining Process

LQU has developed a low temperature refining method for flaxseed oil refining. This method combines the peptide isolation process and glycerol refining process. Compared to direct evaporation methods, solvent extraction with glycerol is efficient and reliable.

2. Flaxseed Oil Decolorization for Paint Industry

LQU has developed a general method for flaxseed oil decolorization by using 5% activated charcoal (NORIT®KB-EVN from CABOT). This method can be applied to all the major flax varieties.

3. Linalool Content by Whole Seeds Solid State NMR

LQU has developed a method to collect the whole seeds NMR spectra of coriander seed. The spectra quality is high enough to measure minor difference among seeds. ^{13}C NMR spectrum of

intact seeds can be collected without using ^{13}C labeled seeds.

4. Determining Flaxseed Oil Oxidation by NMR

LQU has developed a quick method for direct measurement of oxidized lipid product. This method has been successfully applied to monitor the oxidation status of flaxseed oil food products.

LIST OF ABBREVIATIONS

ω-3	Omega-3
ALA	α-Linolenic acid
$CDCl_3$	Deuterated chloroform
DMSO-d_6	Dimethyl sulfoxide-d_6
LQU	Lipid quality and utilization
NMR	Nuclear magnetic resonance
PF	Peptide free
PUFA	Polyunsaturated fatty acid
TMS	Tetramethylsilane

RESEARCH WORK

1. Pilot Scale Low Temperature Flaxseed Oil Refining Process

1.1. Introduction

Flaxseed is the richest plant source of the omega-3 (ω-3) fatty acid i.e. α-linolenic acid (ALA). Flaxseed oil is low in saturated fatty acids (9 %), moderate in monosaturated fatty acids (18 %), and rich in polyunsaturated fatty acid (73 %). Of all lipids in flaxseed oil, ALA is the major fatty acid ranging from 39.00 to 60.42 % followed by oleic, linoleic, palmitic and stearic acids. Flaxseed oil provides an excellent ω-6:ω-3 fatty acid ratio of approximately 0.3:1. Although flaxseed oil is naturally high in anti-oxidants like tocopherols and beta-carotene, flaxseed oil is easily oxidized after extraction and becomes more unstable with refining. The bioavailability of ALA is dependent on the type of flax ingested. Oil may be extracted from flaxseed by pressing or cold pressing. Although it is considered important to avoid heat during pressing flaxseed, cold pressing is not associated with an empirical benefit. Mild processing temperatures might not kill bacterial populations present in seeds and these organisms might persist in both meal and oil products. Oilseed meal is frequently contaminated with salmonella for example. Also, oil-degrading enzymes such as lipoxygenase found in flaxseed can degrade the oil. These enzymes can be inactivated by heating which in turn preserves oil quality. The objective of this study is to address all these issues with a newly developed low temperature refining method.

1.2. Materials and Methods

Flaxseed oil was provided by Prairie Tide Chemicals Inc. (Saskatoon, SK, Canada). Food grade glycerol was purchased from a local supplier. The thin film processor (Artisan, Waltham, MA, USA) equipped with a continuous feeding pump and cooling system was employed for low temperature ethanol evaporation. Proton NMR spectra of flaxseed oil and glycerol phase were recorded on a 500 MHz Avance spectrometer (Bruker, Rheinstetten, Germany) equipped with an autosampler and an inverse triple resonance probe (TXI, 5mm). Spectra (solvent $CDCl_3$) were

collected at 298 K with 128 scans.

1.3. Results and Discussion

The crude flaxseed oil contains cyclolinopeptides, which contribute a strong bitterness. Lipids Quality Utilization (LQU) has developed an efficient approach to recover these valuable peptides and produce refined flaxseed oil. This approach is based on liquid extraction with ethanol solution at ambient temperatures. The ethanol solution used in this process can denature the protein and kill the bacteria. The refined flaxseed oil contains about 4% ethanol. The residual ethanol can be evaporated under reduced pressure at elevated temperatures. This project aims to develop an ethanol removal method at room temperature at pilot scale.

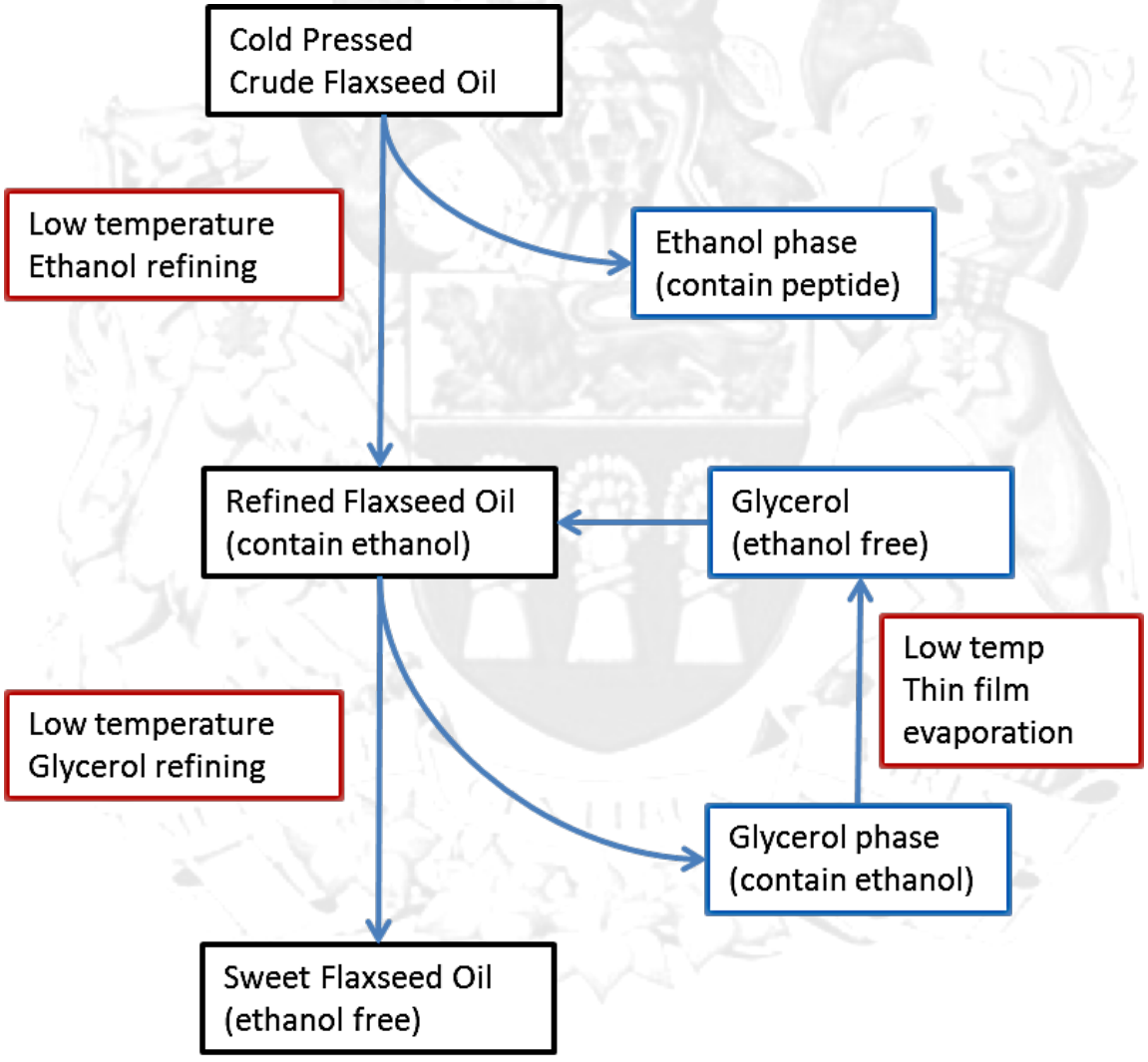

Figure 1.1 Low temperature flaxseed oil refining.

Figure 1.1 shows a schematic of how a typical plant for flaxseed oil low temperature refining may be organized. Cold pressed crude flaxseed oil is received and transferred to the tank for ethanol refining. The ethanol solution was separated and drained for peptide isolation. Ethanol free glycerol (5%, w/w) was added into this refined flaxseed oil. To improve the extraction efficiency, the glycerol refining step was repeated four times in a counter current mode (Figure 1.2).

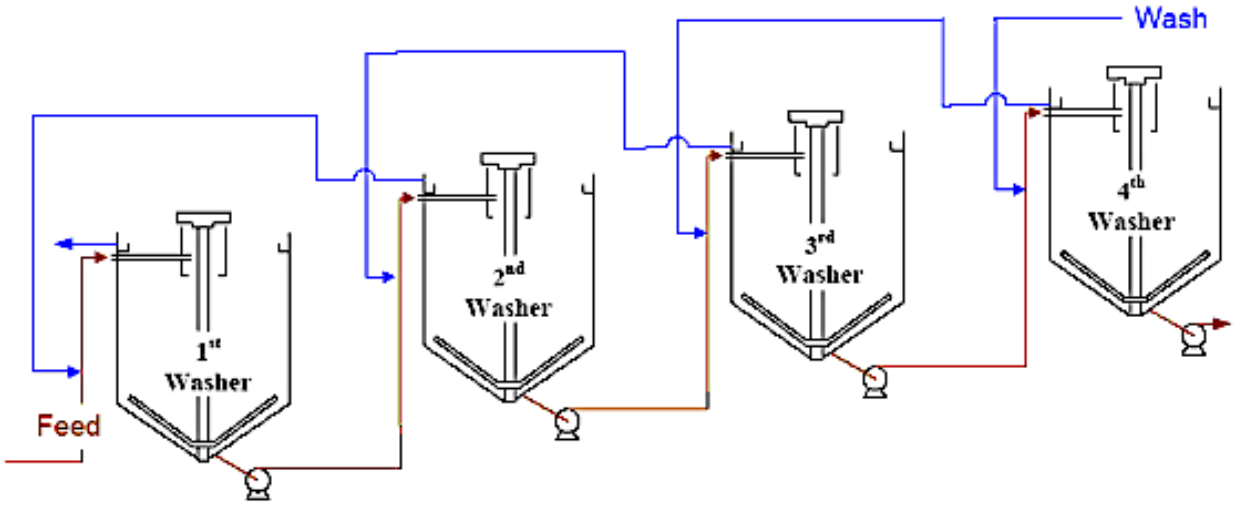

Figure 1.2 Countercurrent flow for glycerol refining.

The glycerol phase (containing ethanol) was stripped with a Rototherm thin film evaporator. The following shows the operate principle of Rototherm (Figure 1.3).

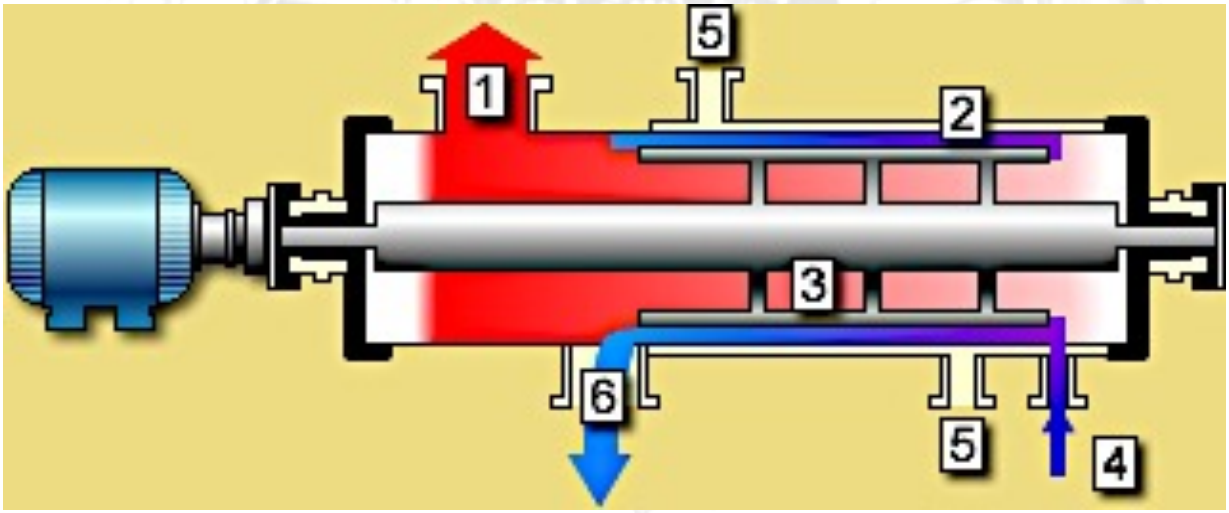

Figure 1.3 Glycerol stripping with Rototherm thin film evaporator. [1] Ethanol Vapor Out, [2] Process Wall, [3] Rotor Blades, [4] Crude Glycerol Feed In, [5] Heating Oil In/Out, and [6] Discharge of Stripped Glycerol.

The crude glycerol was injected into the Rototherm and heated at 70 °C under a vacuum (15 mbar) to evaporate the ethanol. The flow rate is controlled by a feeding pump at 20 L/h. Mixing intensity was set to its maximum at 720 rpm.

The Rototherm was equipped with a Delta Therm oil heater manufactured by Delta T Systems Inc., which was able to operate at temperatures up to 260 °C. The temperature of the reaction mixture (measured by thermo probe inside the reactor) is affected by the heating capacity, flow rate and the rate of evaporation. At the best condition (flow rate 20 L/h, spin rate 720 rpm, vacuum 15 mbar), the reaction mixture can reach the desired temperature (70 °C) with the heater set at temperature as high as 135 °C. Initially, the heater was set at 100% capacity until the desired temperature was reached. The heater was then controlled to maintain the set temperature. The glycerol (containing trace flaxseed oil) starts to turn red above 90 °C.

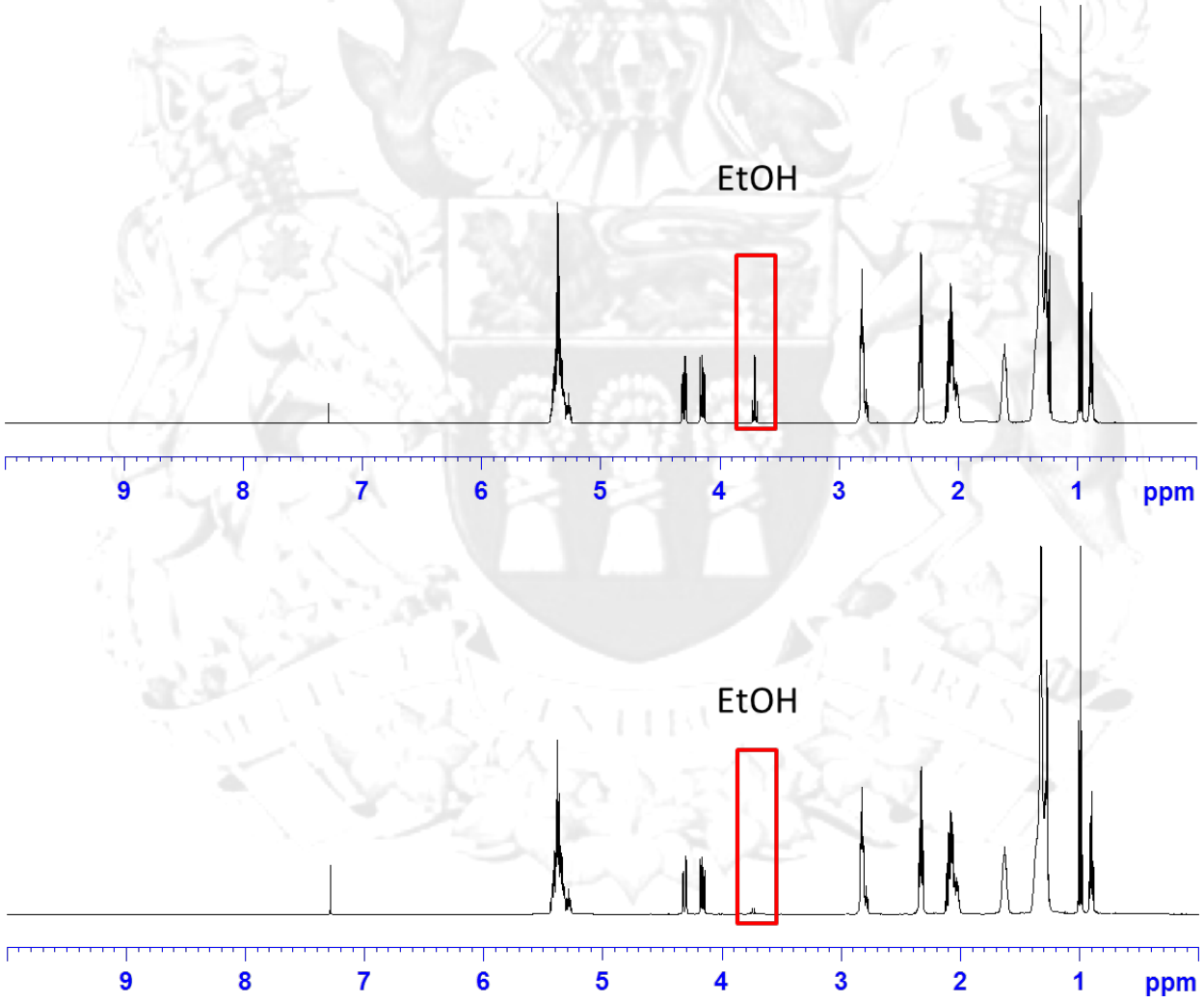

Figure 1.4 ^{1}H-NMR spectra of the flaxseed oil before and after glycerol refining.

The ^{1}H-NMR spectra of flaxseed oil after glycerol refining step is essentially free of ethanol (Figure 1.4). The whole refining process of this sweet flaxseed oil is under very mild conditions.

1.4. Conclusions

LQU has developed a low temperate refining method for flaxseed oil refining. This method combines the peptide isolation process and glycerol refining process. Compared to direct evaporation methods, solvent extraction with glycerol is relatively efficient and reliable.

2. FLAXSEED OIL DECOLORIZATION FOR PAINT INDUSTRY

2.1. Introduction

Flaxseed oil is commonly used in painting. Six historic methods have been used by painters to afford refined oil products that dry hard and do not form yellow discoloration after drying. Refining involves treatments that include refining by contact of flaxseed oil with sand, water, salt water, ethanol water mixtures, snow, and oxygen. The exposure of flaxseed oil to light is also described. These refining methods increase oil drying rate and are effectively used on both cold pressed oils and refined flaxseed oils. These methods are adapted by professional painters and hobbyists for preparation of small volumes of paint oil. This project aims to develop a convenient method for large scale production of high quality paint oil from flaxseed oil.

2.2. Materials and Methods

Flaxseed oil was provided by Prairie Tide Chemicals Inc. (PTC, Saskatoon, SK, Canada). UV-Visible spectra of flaxseed oil were collect on a UV-Vis spectrophotometer (GENESYS 10S Thermo Fisher Scientific, Waltham, MA USA). Abbreviation used in decolorization process study in Table 2.1 (Sangster's cold pressed organic flaxseed oil, peptide free (PF) oil: control peptide free sweet flaxseed oil; and commercial oil).

Table 2.1 Abbreviation used in decolorization process study.

Abbreviation	Absorbent	Supplier	Product Information
JS-15-13-A	Alumina	Sigma	Alumina oxide 60-120 mesh
JS-15-13-S	Silica	Sigma	Silica gel 60-120 mesh
JS-15-13-R	Silica	Sigma	Silica gel pH=1
JS-15-13-C	Charcoal	EMD	Activated powder Nord SX-4 CX0657-1
Res	resin	DOW	DOW ion-exchange resin
Res_heat	resin	DOW	DOW ion-exchange resin (72 ^{o}C)
Char_AG60	Charcoal	Sigma	Activated, granular 20-60 mesh C3014-500G
Char_A	Charcoal	EMD	Activated powder Nord SX-4 CX0657-1
Char_BDH	Charcoal	BDH	Decolorizing powder, activated B33032
GCB	Charcoal	Bioriginal	Graphitized carbon black
Si_Gel60	Silica	Sigma	Silica gel 60-120 mesh
Si_R40F	Silica	SORBSIL	Average particle size 14-22 microns
Si_R92	Silica	SORBSIL	Average particle size 14-22 microns
PF	Oil	PTC	Purified flaxseed oil (peptide free)

2.3. Results and Discussion

For an efficient decolorization process, the absorbent agent used (commonly bleaching earth), is of primary importance. In particular, its type and dosage affect the decolorization of oil, but also the oil yield due to considerable amounts of oil retention. The operational parameters of the decolorization process, namely, temperature/vacuum, contact time, handling, and mixing of absorbent agent, should also be properly selected to attain sufficient decolorization of oil and minimize oil losses.

2.3.1. Different absorbent agent screen

The basic absorbents used in flaxseed oil decolorization are alumina oxide, synthetic amorphous silica, acid activated silica and activated carbon. These four absorbents were quickly tested at high loading (>20%). Colorless flaxseed oil can be generated in all the cases (Figure 2.1). These results were further confirmed by UV-Vis spectra (Figure 2.2). However, under standard loading conditions (5%), only charcoal (BDH) treated flaxseed oil can meet specifications (Figure 2.3).

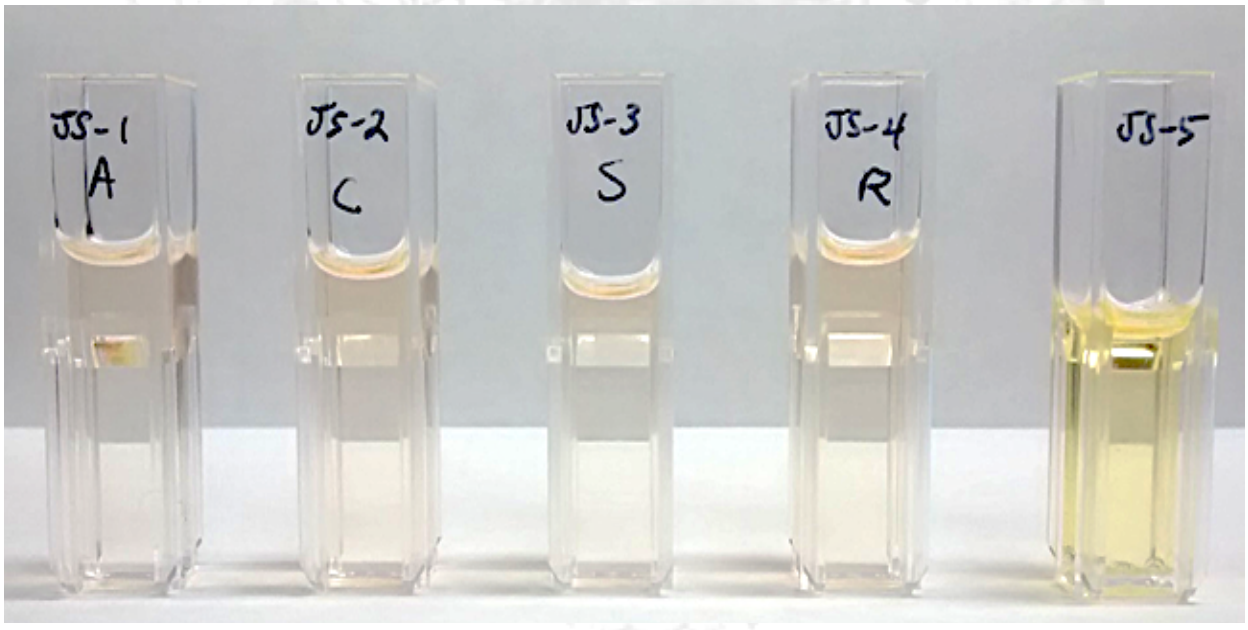

Figure 2.1 Flaxseed oil decolorization at high absorbent loading.

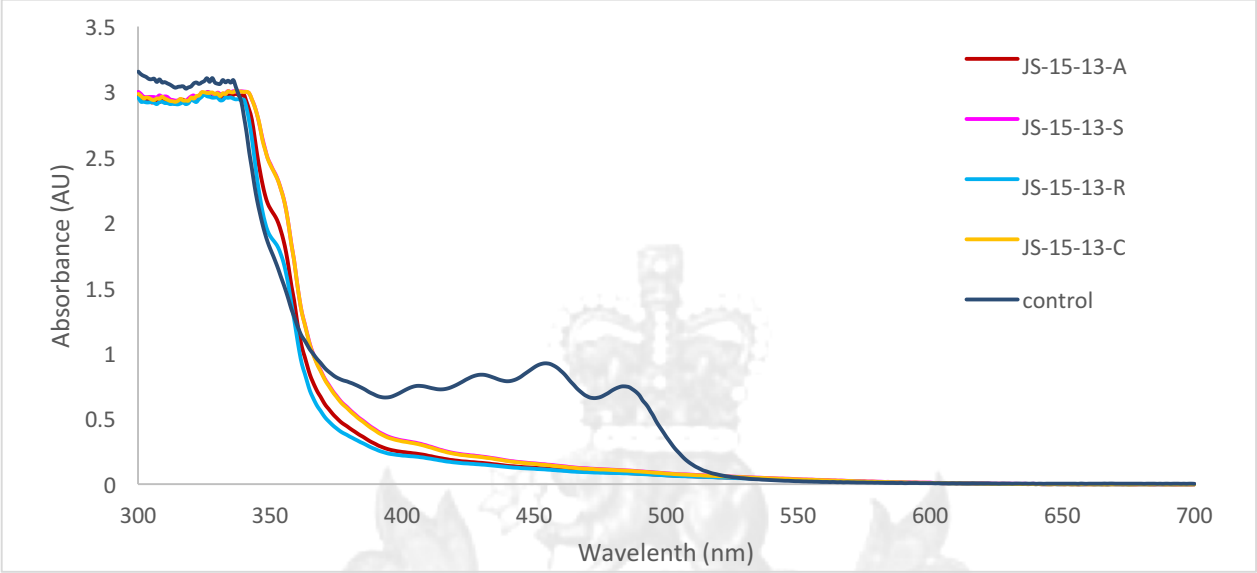

Figure 2.2 UV-Vis spectra of flaxseed oil decolorization at high absorbent loading.

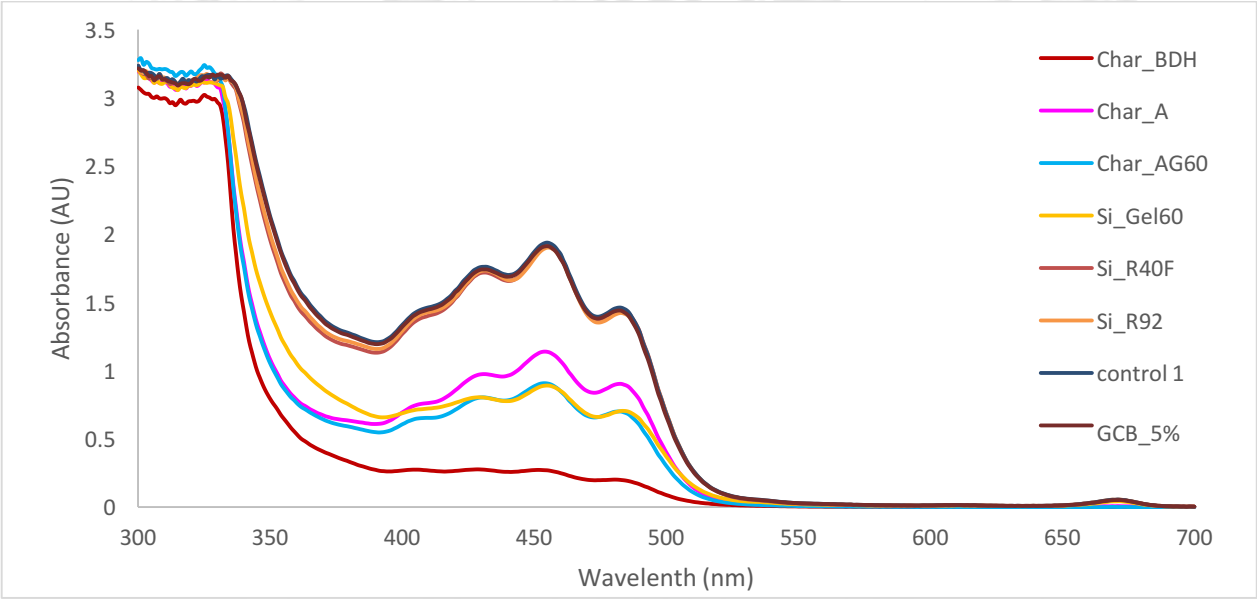

Figure 2.3 UV-Vis spectra of flaxseed oil decolorization at standard absorbent loading.

2.3.2. Decolorization condition optimization (temperature)

The dosage and absorbent type, as well as the operation conditions, such as temperature and contact time, are important parameters for the decolorization process of flaxseed oil.

Decolorization of PF flaxseed oil is more efficient at an elevated temperature (60 °C). Commercial flaxseed oil is not as sensitive to the operation temperature (Figures 2.4 and 2.5).

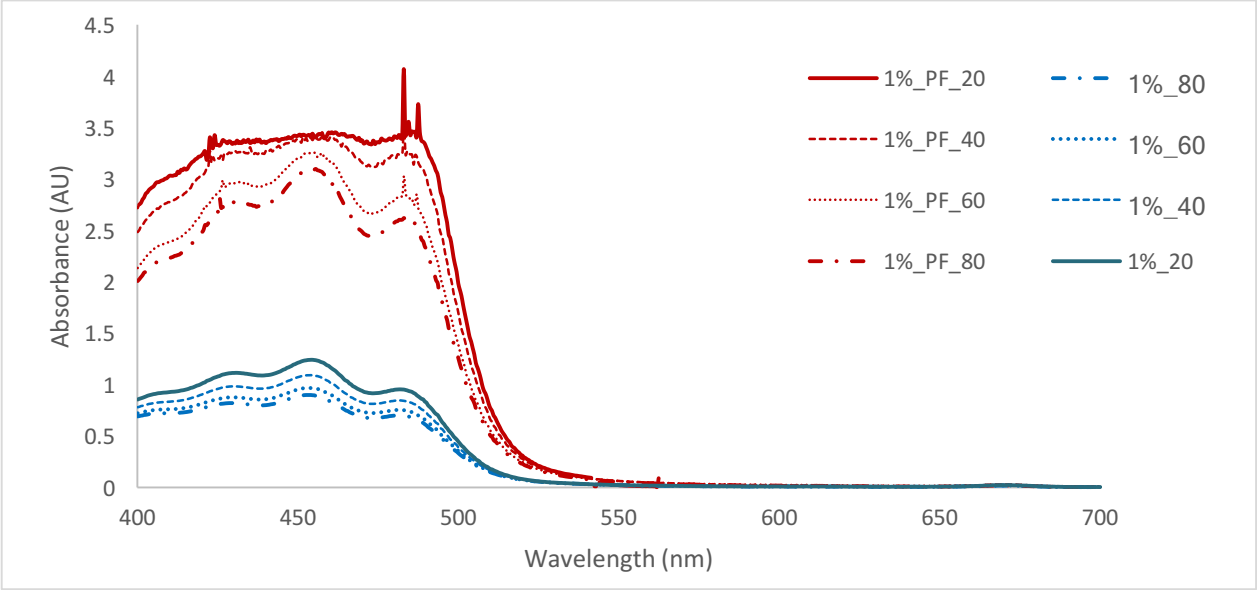

Figure 2.4 Commercial flaxseed oil and PF oil treated with 1% BDH charcoal at different temperatures.

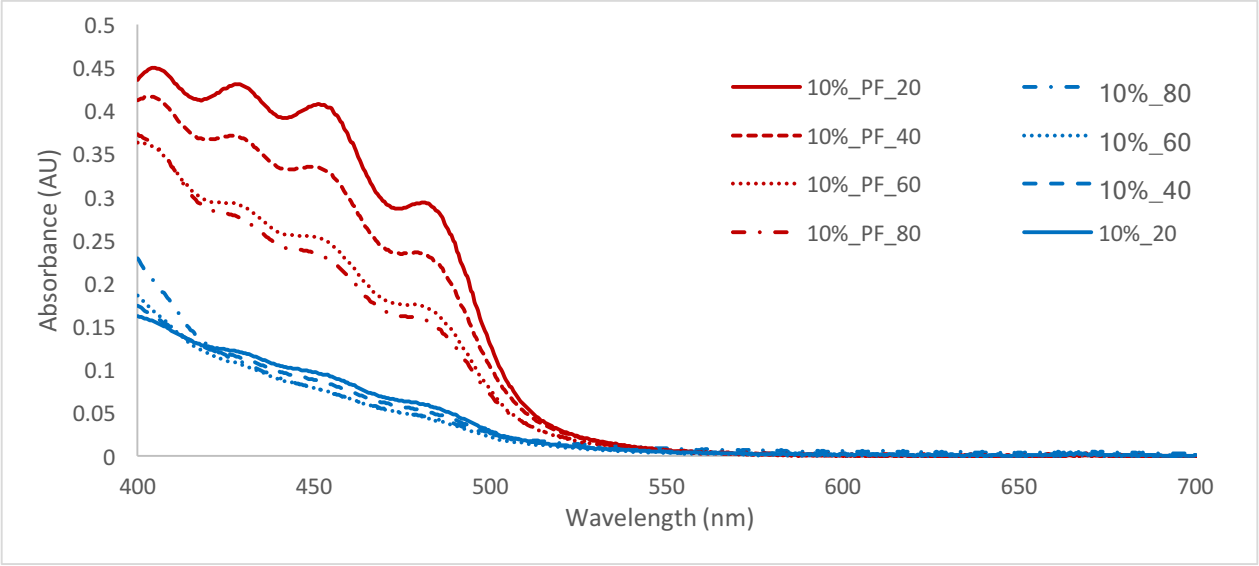

Figure 2.5 Commercial flaxseed oil and PF oil treated with 10% BDH charcoal at different temperatures.

2.3.3. Decolorization condition optimization (contact time)

The above results suggested that for both commercial flaxseed oil and PF flaxseed oil, the decolorization process can be completed within 24 h (Figures 2.6-2.9).

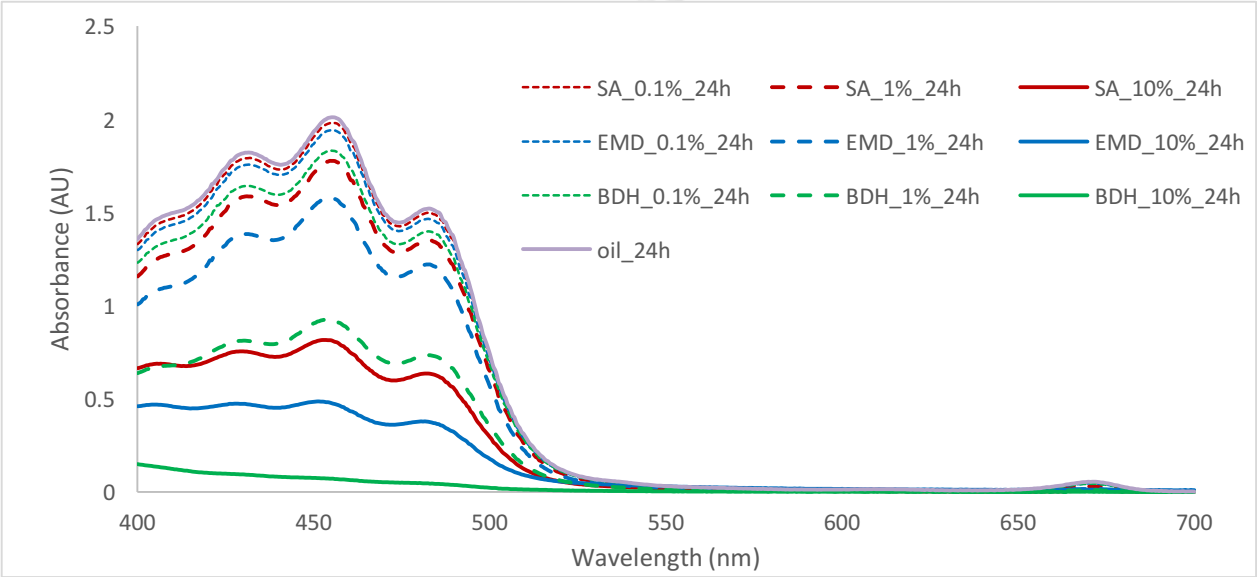

Figure 2.6 Commercial flaxseed oil 24 h decolorization result.

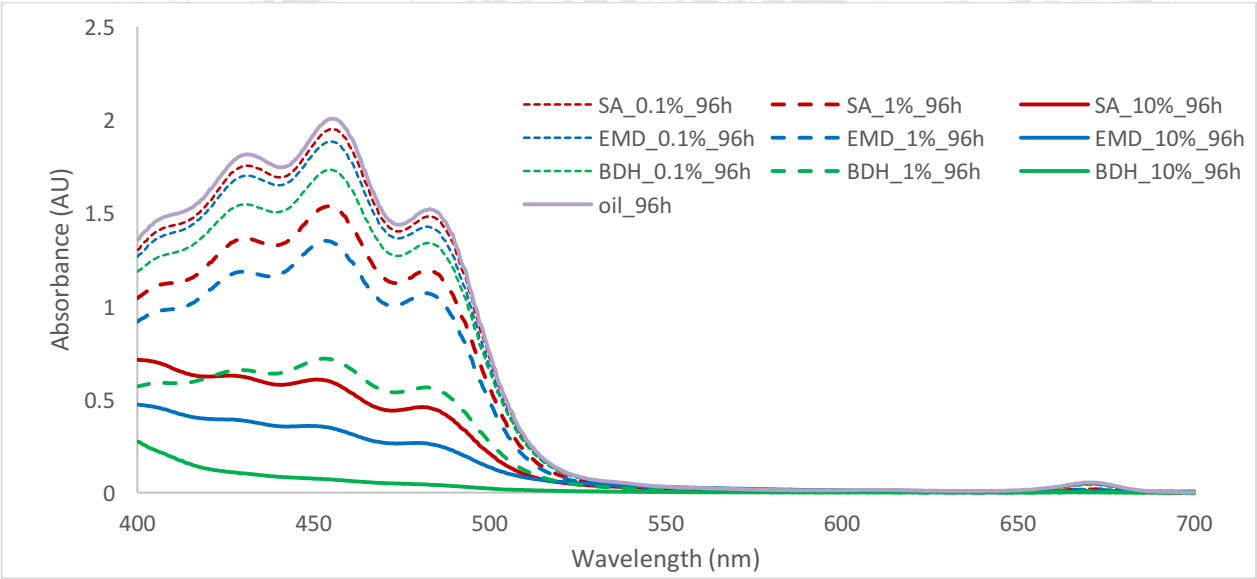

Figure 2.7 Commercial flaxseed oil 96 h decolorization result.

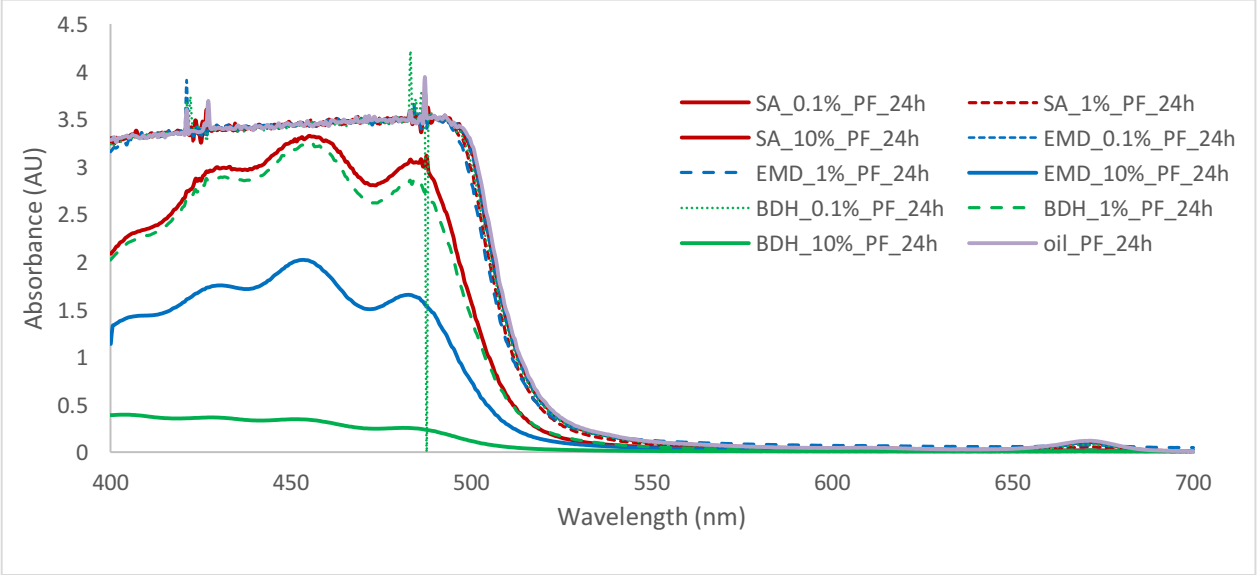

Figure 5.8 PF flaxseed oil 24 h decolorization result.

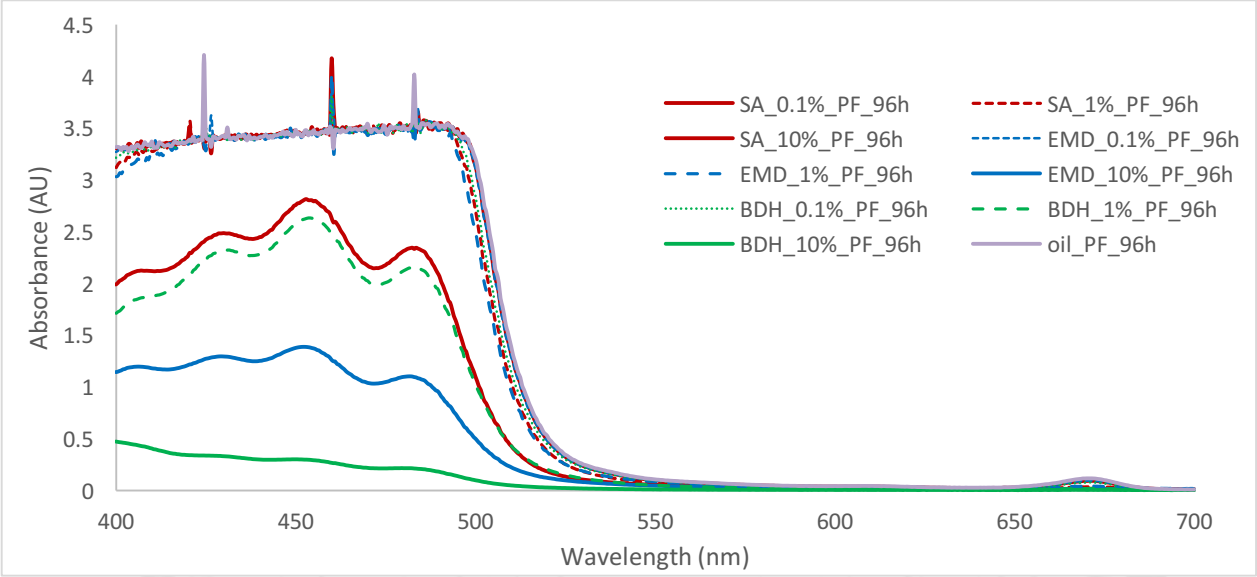

Figure 2.9 PF flaxseed oil 96 h decolorization result.

2.3.4. Decolorization condition optimization (absorbent loading and handling)

Best decolorization results can be achieved with 5% BDH charcoal within 2 h contact time (Figures 2.10 and 2.11).

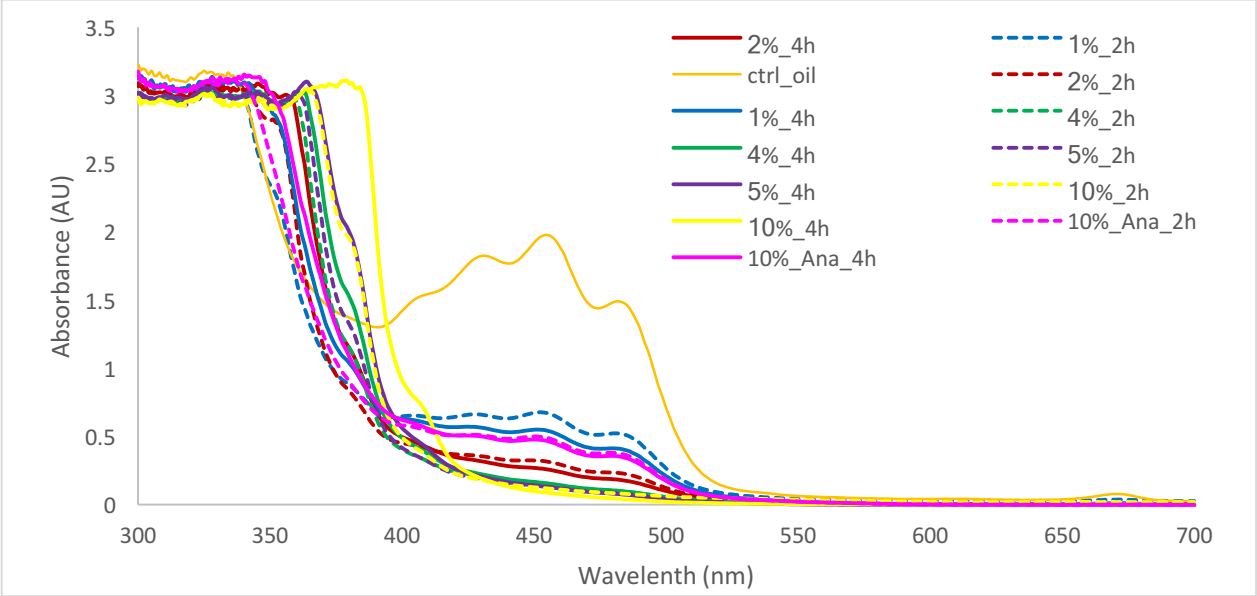

Figure 2.10. Commercial flaxseed oil decolorization with different loading (BDH charcoal).

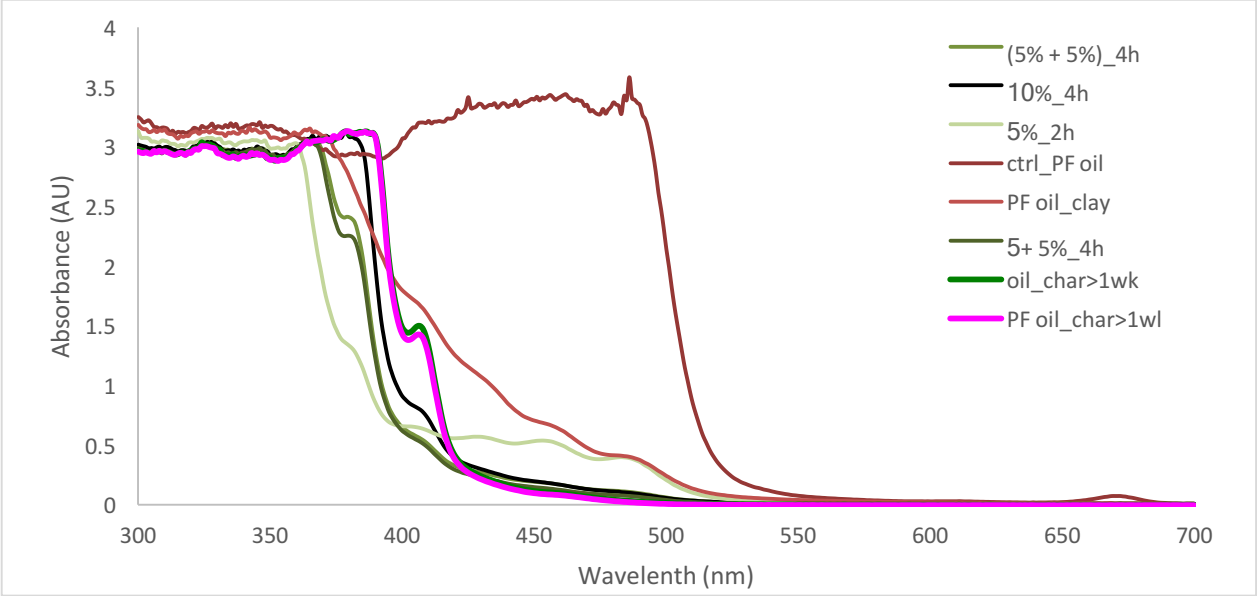

Figure 2.11. Commercial flaxseed oil decolorization with different absorbents loading and handling (BDH charcoal).

2.3.5. Decolorization condition optimization (charcoal screen)

Best decolorization results were achieved with a poorly labeled bottle of BDH charcoal which

is no longer commercially available. It took tremendous effort to find a comparable commercial charcoal product. The charcoal products from major North American and Chinese suppliers were screened (Figures 2.12 and 2.13).

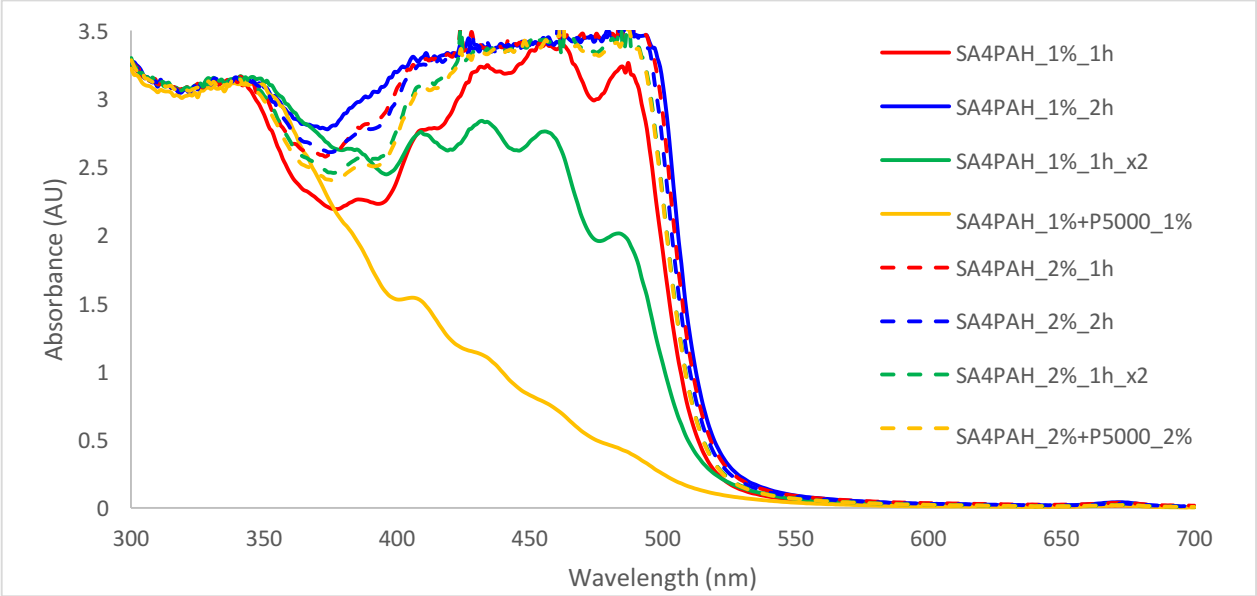

Figure 2.12 Screen of commercial charcoal products for decolorization process-1.

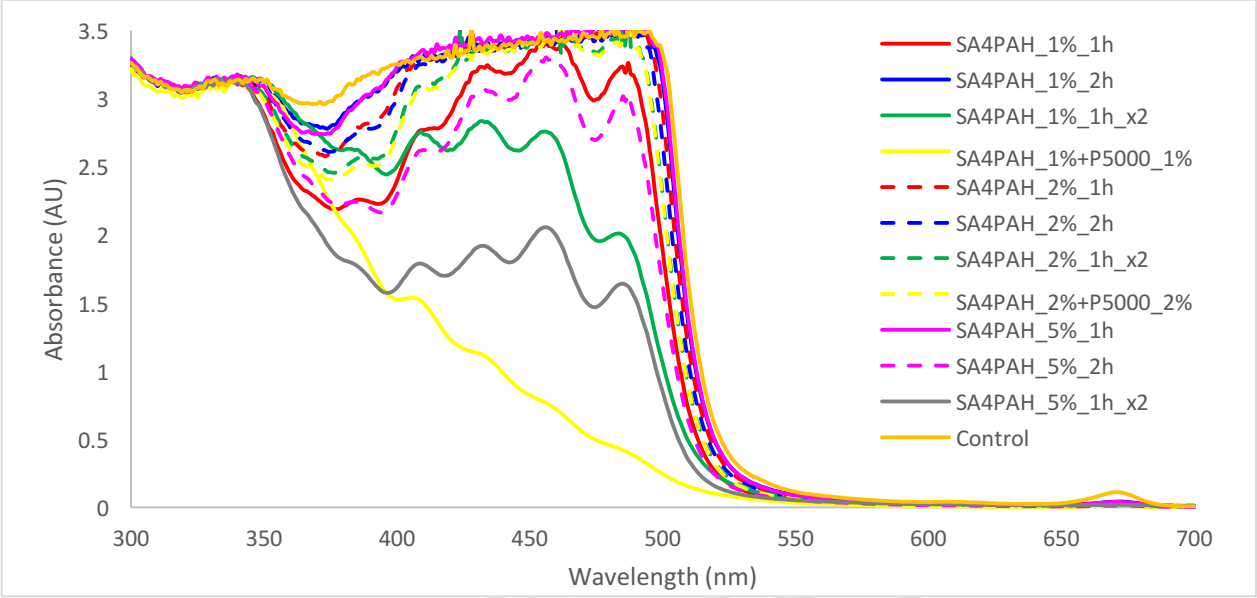

Figure 2.13 Screen of commercial charcoal products for decolorization process-2.

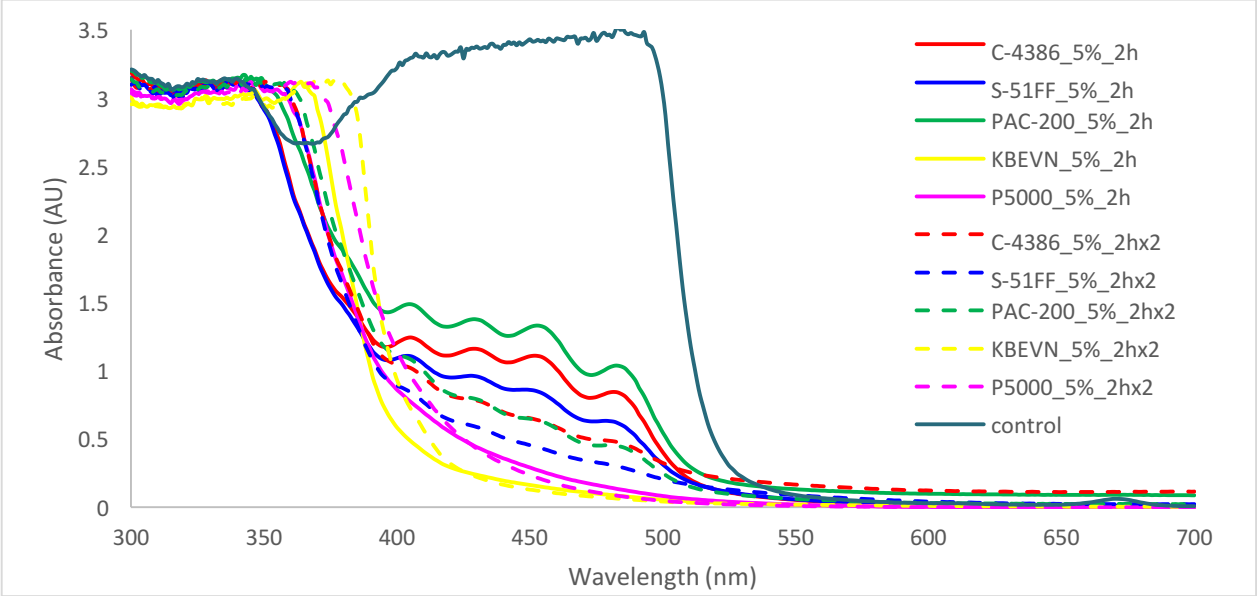

Figure 2.14 Screen of commercial charcoal products for decolorization process-3.

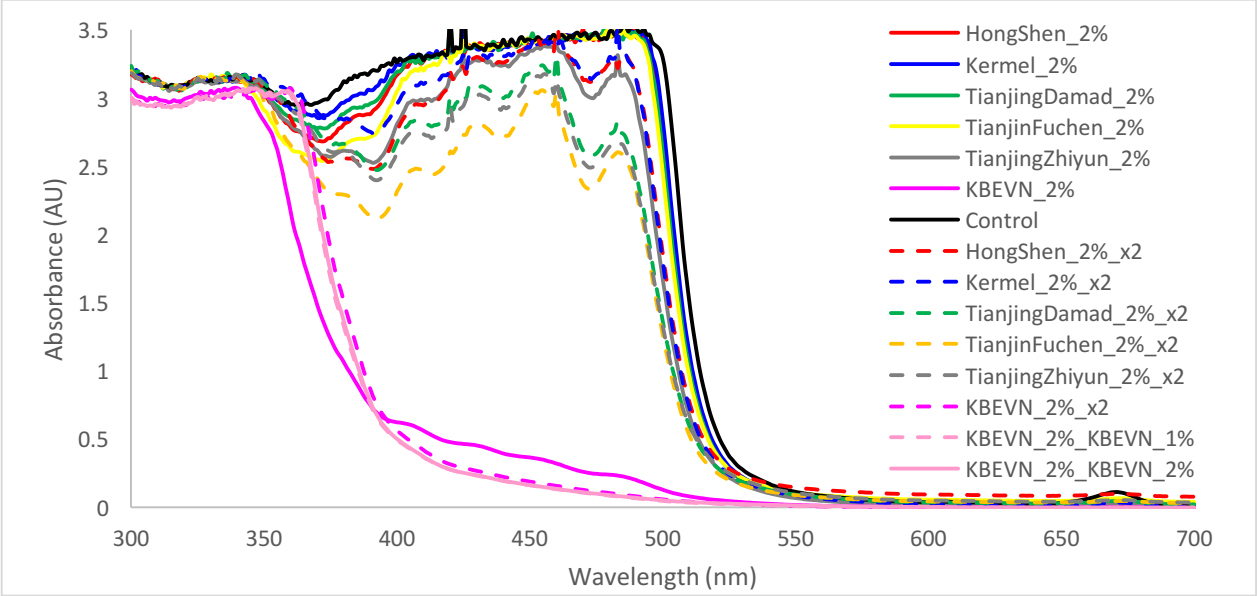

Figure 2.15 Screen of commercial charcoal products for decolorization process-4.

Fortunately, the charcoal product NORIT®KB-EVN, a chemically activated carbon from CABOT, exhibited similar reactivity as BDH (Figure 2.16).

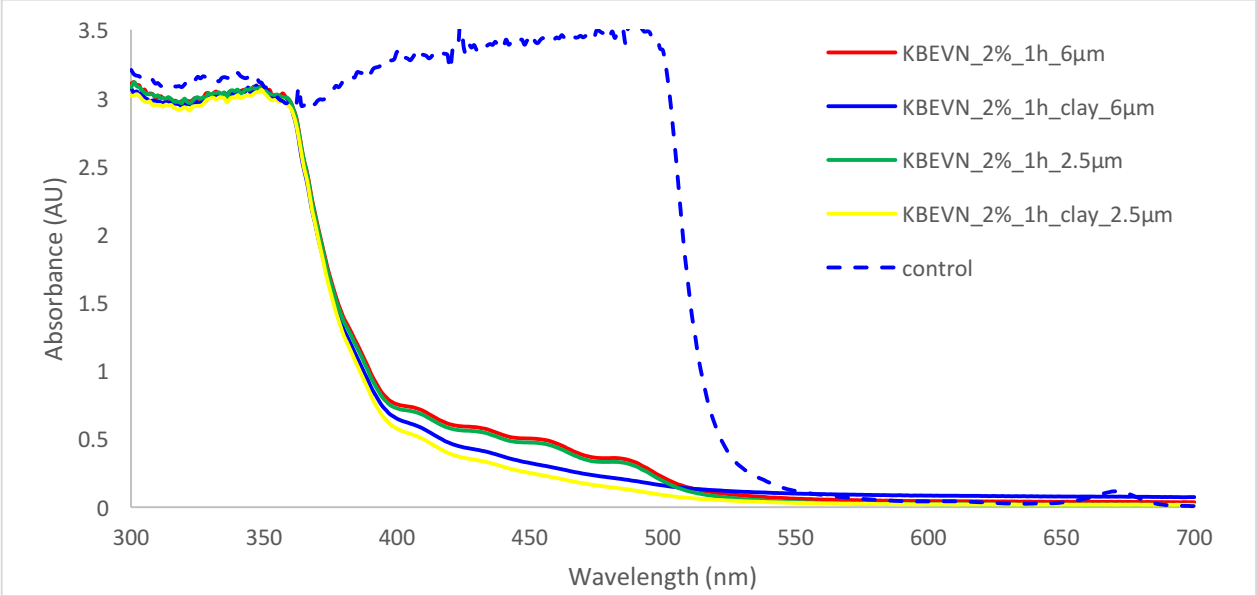

Figure 2.16 Screen of commercial charcoal products for decolorization process-5.

2.3.5. Decolorization condition application

To test the limit and the scope of this method, five different flax varieties: CDC Sorrel (Sorrel), CDC Glas (Glas), AAC Bravo (Bravo), Prairie Sapphire (Psapph) and Sanctuary (Sanct) were tested. The results of decolorization were shown in Figures 2.17-2.22.

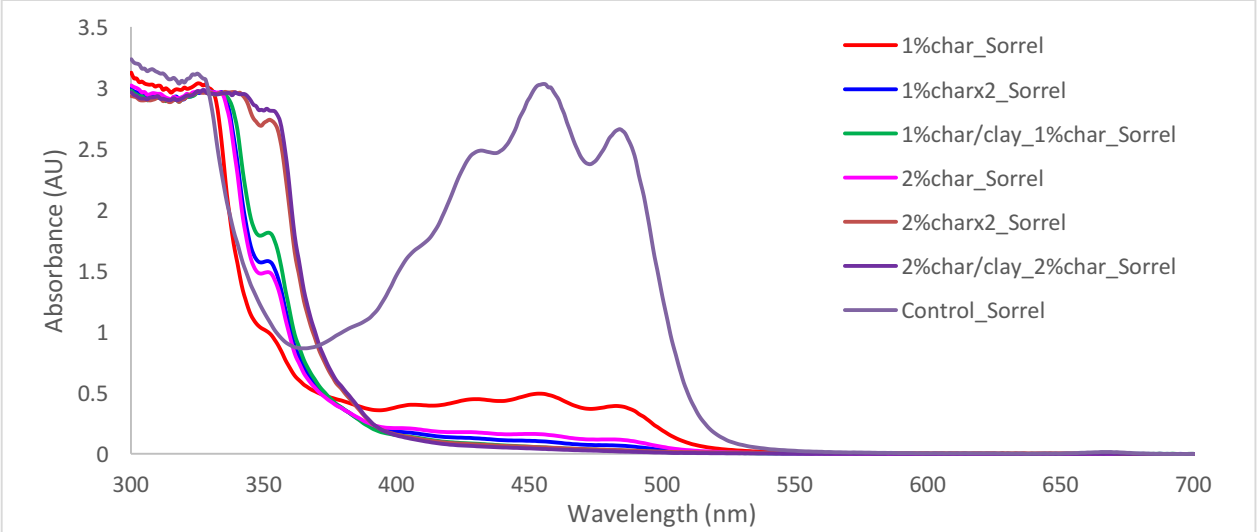

Figure 2.17 Decolorization of CDC Sorrel with NORIT®KB-EVN.

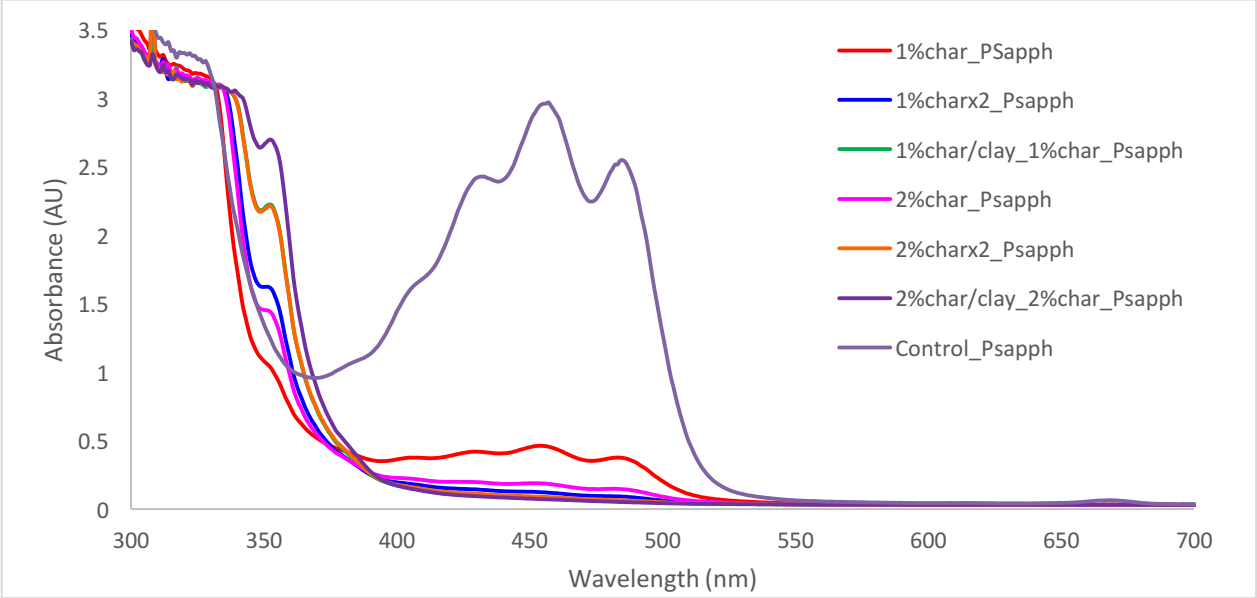

Figure 2.18 Decolorization of Prairie Sapphire with NORIT®KB-EVN.

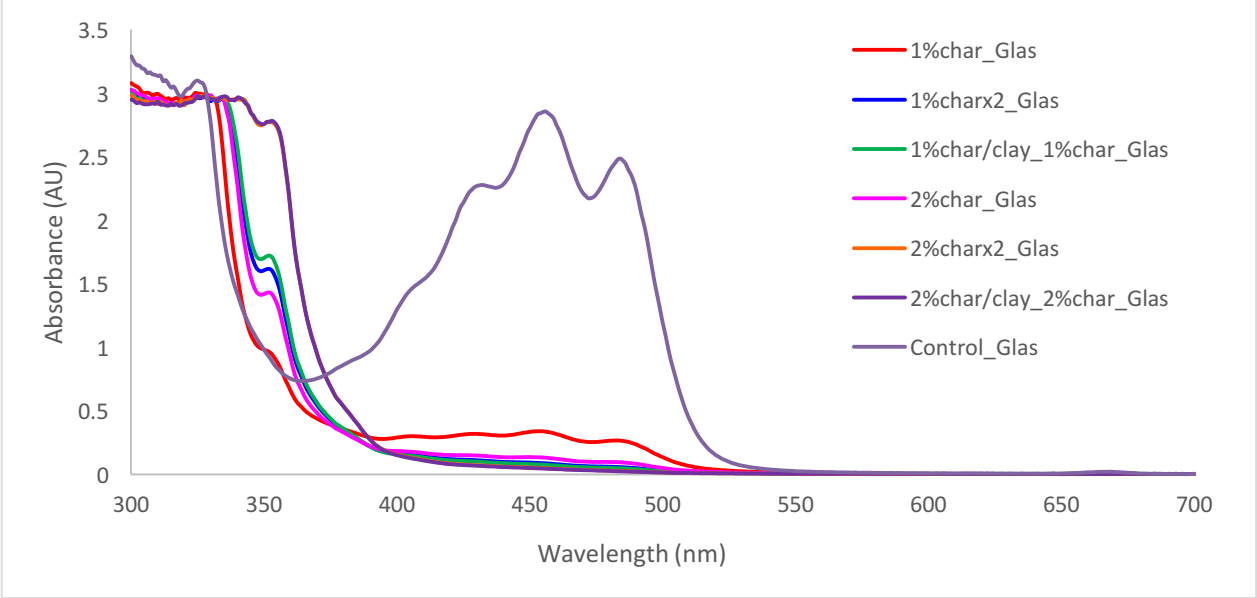

Figure 2.19 Decolorization of CDC Glas with NORIT®KB-EVN.

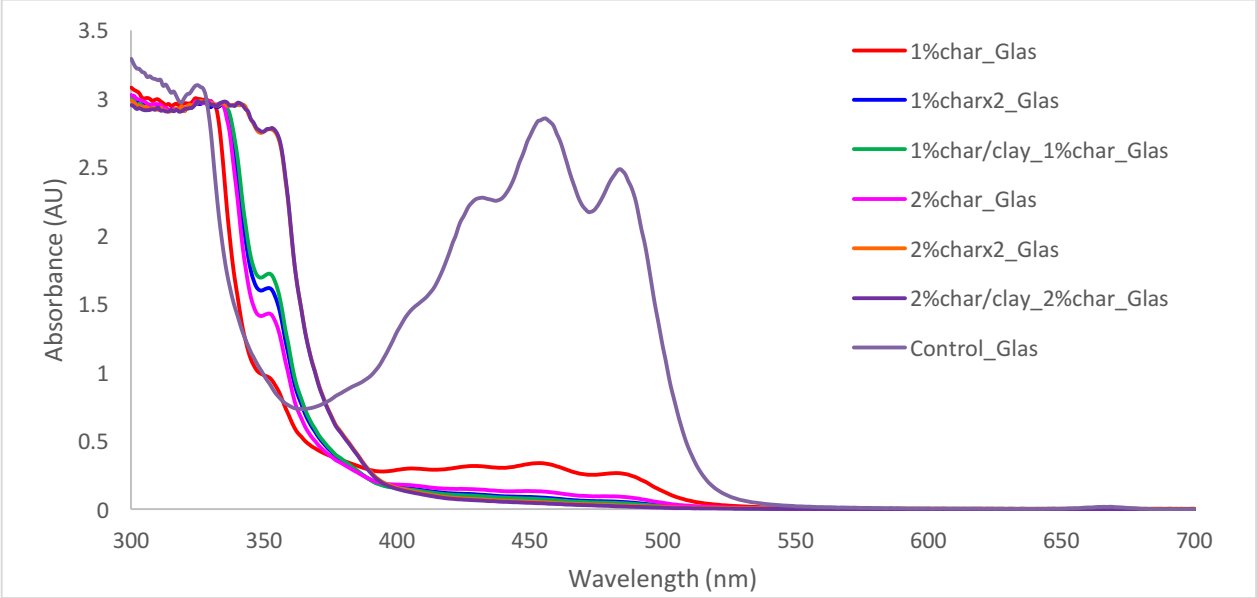

Figure 2.20 Decolorization of CDC Glas with NORIT®KB-EVN.

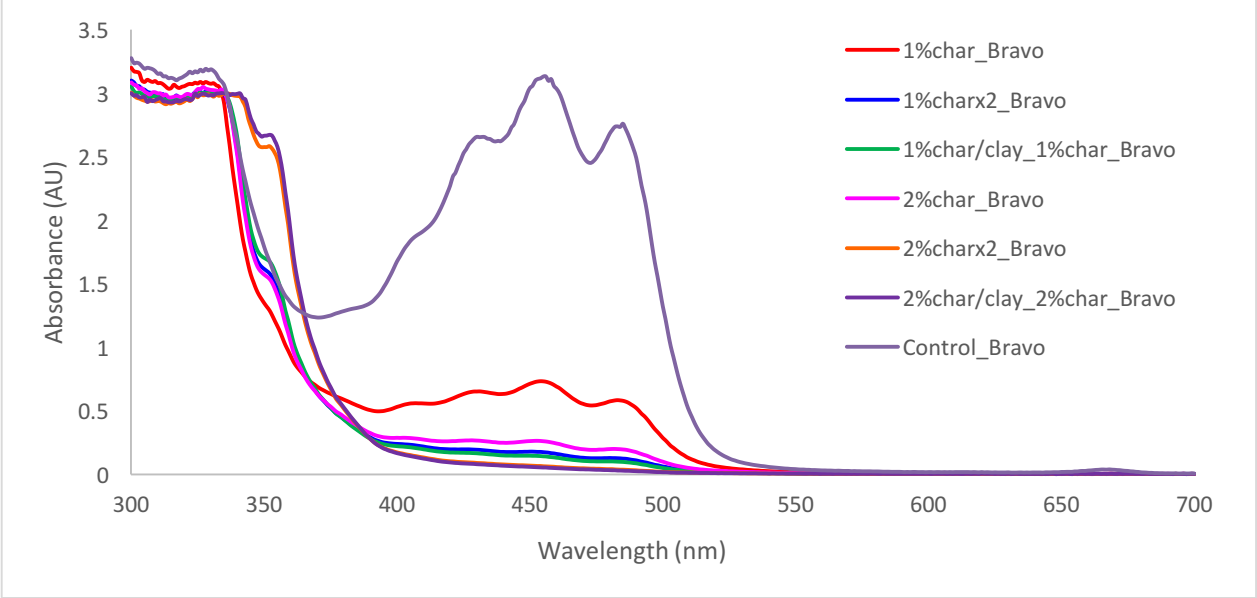

Figure 2.21 Decolorization of AAC Bravo with NORIT®KB-EVN.

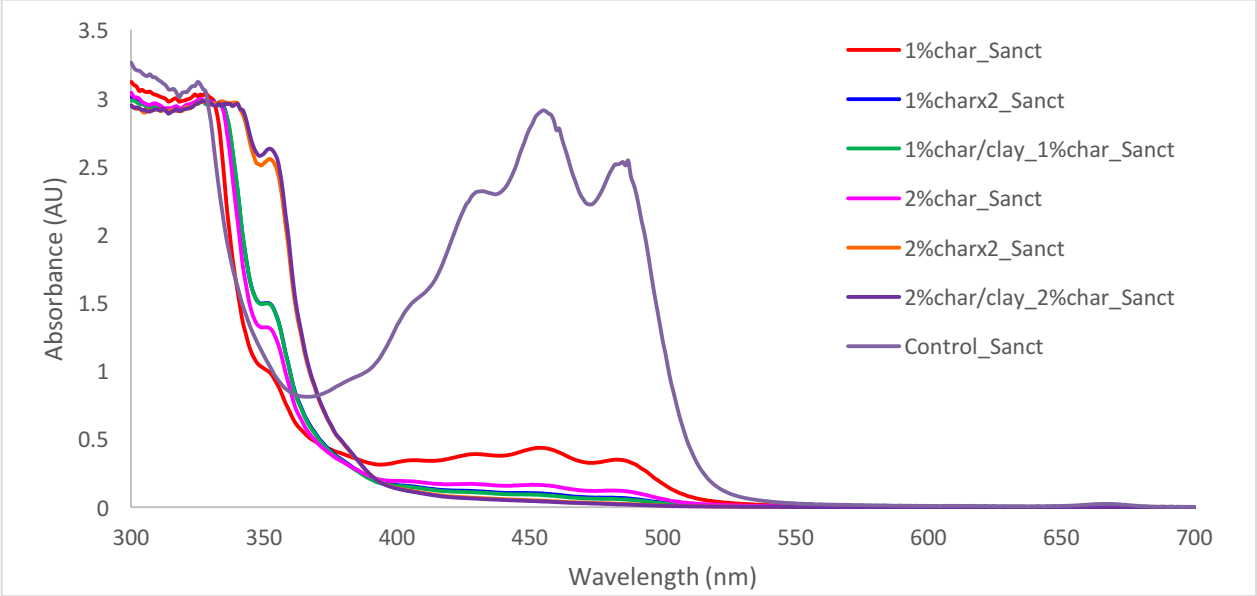

Figure 2.22 Decolorization of Sanctuary with NORIT®KB-EVN.

2.4. Conclusions

LQU has developed a general method for flaxseed oil decolorization by using 5% activated charcoal (NORIT®KB-EVN from CABOT). This method can be applied to all the major flax varieties.

3. LINALOOL CONTENT BY WHOLE SEEDS SOLID STATE NMR

3.1. Introduction

Recently, NMR spectroscopy has been applied to analyze seed oil and protein composition, but often requires extensive and time-consuming sample preparation. One study used canola seeds that were initially milled into flour, dissolved in a buffer solution, and centrifuged prior to collection of the supernatant for NMR analysis. Such methods of sample preparation can be detrimental as they potentially perturb the structure and native chemical and physical interactions that influence analyte kinetics across phase boundaries, which are important for analysis. For oilseed breeders, selection of single seeds allows for more rapid development of cultivars than the analysis of bulk seed samples from a single plant. One requirement of a successful single seed analysis method is that it must preserve viability. Solid state NMR of single seeds can be a rapid, low-cost method for use as a selection tool in plant breeding. This project aims to develop a method to collect the whole seeds NMR spectra of coriander seed.

3.2. Materials and Methods

Samples of coriander were taken from field experiments (University of Saskatchewan). Deuterated solvents and tetramethylsilane (TMS) were purchased from Sigma-Aldrich Chemical Co. All NMR measurements were performed on a 500 MHz Bruker Avance III spectrometer at a spinning speed of 6666 Hz using a prototype CMP MAS 4 mm 1H– 13C– 19F– 2H probe fitted with an actively shielded Z gradient (Bruker BioSpin) at 298 K.

3.3. Results and Discussion

Seeds remained intact and were not damaged during the spinning process. Only one seed was used and fit into the rotor, deuterated chloroform ($CDCl_3$) was employed as an external lock. The rotor was sealed using a top insert made from Kel-F, a Kel-F sealing screw, and a Kel-F cap. Figure 3.1 shows the ^1H spectrum of single coriander seed (CDC major). The resolution of the spectrum is comparable to solution state NMR. The coupling constant of linalool signal (4.9~5.7 ppm) can be measured accurately. Minor component such as cymene (6.85 ppm) can be detected and analyzed.

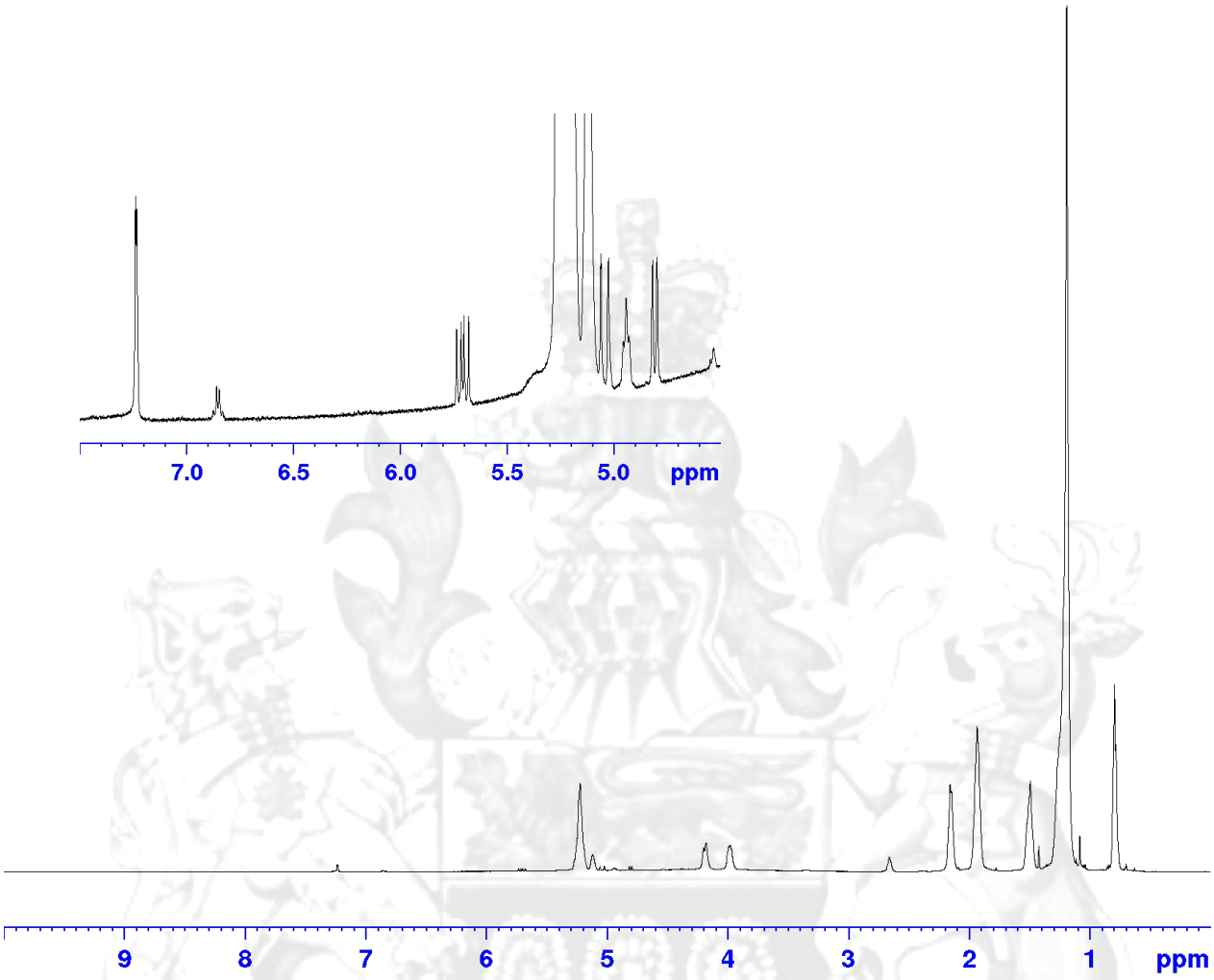

Figure 3.1 Single seed solid state ^{1}H-NMR of CDC major.

Based on the ^{1}H spectrum, this CDC major seed contains about 3.9% linalool and 0.1% cymene. The oil contains 81.1% of mono-unsaturated fatty acid (C18:1) and 12.9% of di-unsaturated fatty acid (C18:2). Figure 3.2 is the ^{1}H spectrum of single coriander seed (CDC Linalool). The ^{1}H spectrum suggested that it contains a higher level of linalool (8.6%), and lower level of cymene (0.08%).

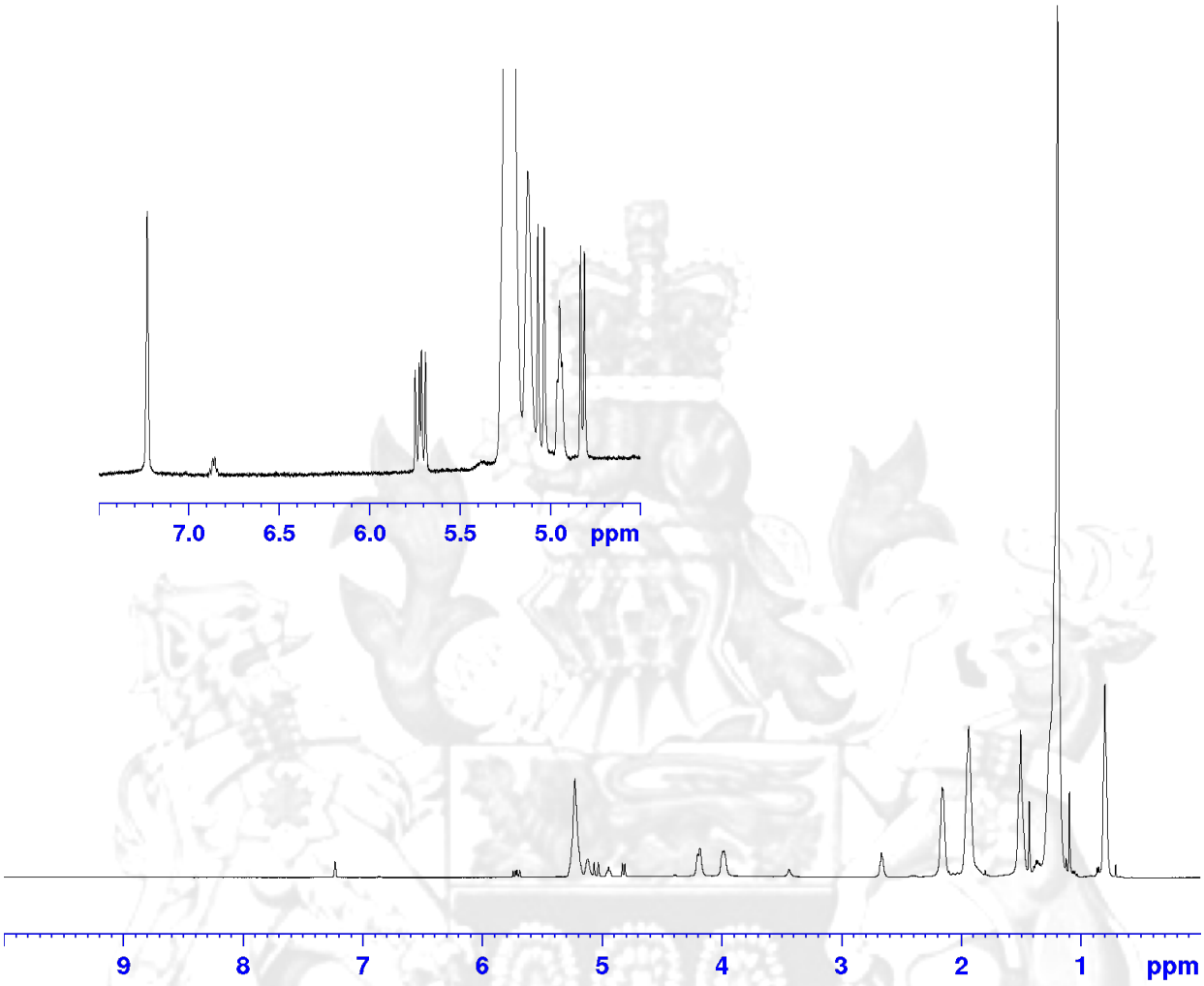

Figure 3.2 Single seed solid state ^{1}H-NMR of CDC Linalool.

The ^{13}C spectra of the coriander seeds were collected as well (Figures 3.3 and 3.4). The quality of the spectrum is compatible to those obtained from ^{13}C-labeled seeds. Uniformly ^{13}C-enriched seeds need to be produced in specially designed airtight, high-irradiance growth chambers. Plants need to be grown from ^{13}C-labeled seeds in a closed atmosphere containing 97% atom % $^{13}CO_2$ from the seedling stage until full maturity.

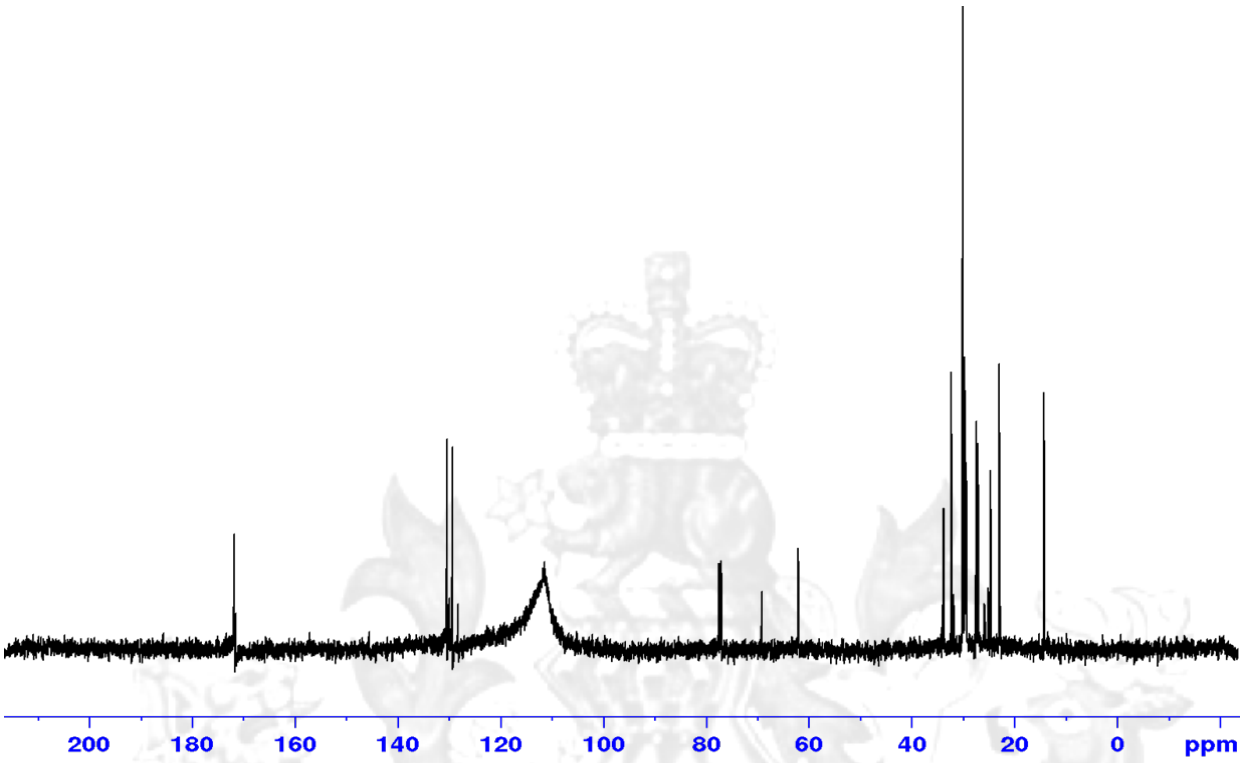

Figure 3.3 Single seed solid state ^{13}C NMR of CDC major.

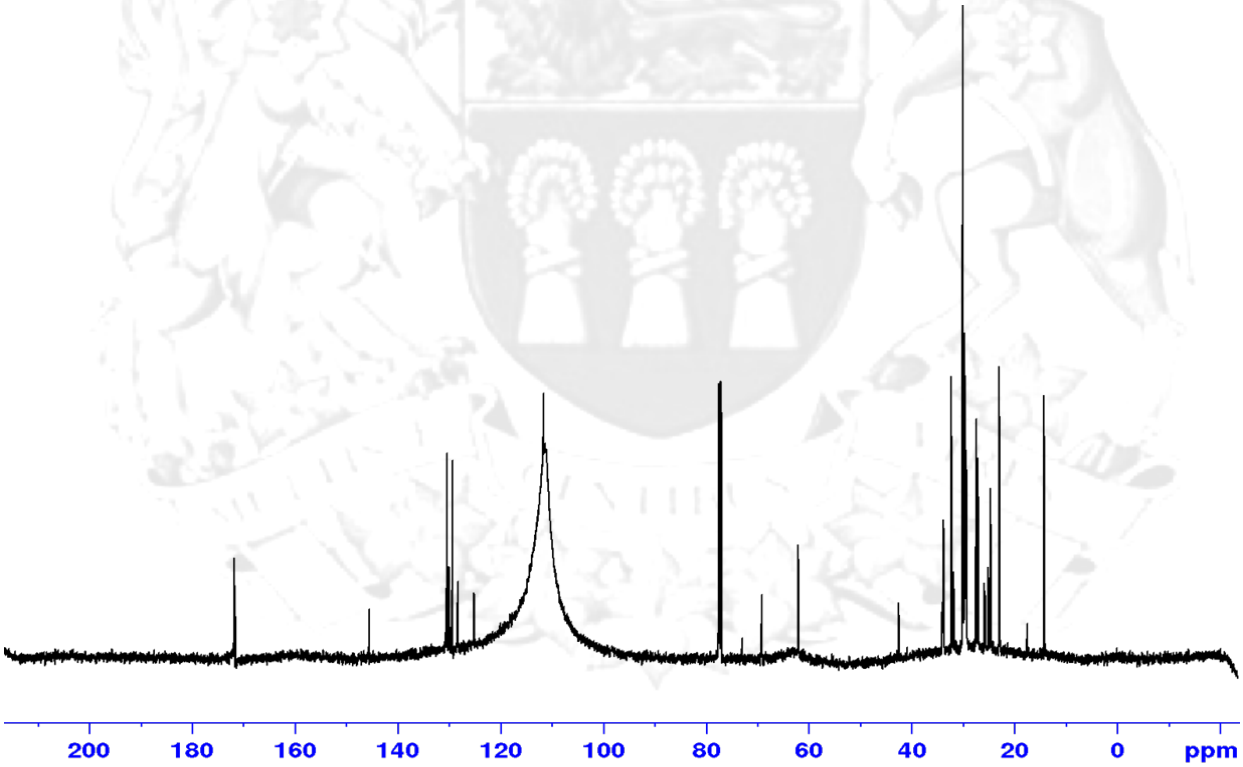

Figure 3.4 Single seed solid state ^{13}C NMR of CDC Linalool.

The single seed ^{1}H-NMR can be done in 20 min, which allow rapid screening seeds for oil composition. The results of five single CDC Linalool were listed in Table 3.1.

Table 3. 1 Single Seed Sample Solid State NMR Results.

	Mass (mg)	Cymene %	Linalool %	C18:1 %	C18:2 %	Sterol %
Seed 1	54	0.010	6.230	74.54	15.13	2.22
Seed 2	65	0.014	6.501	75.64	14.91	3.03
Seed 3	46	0.014	5.814	73.62	15.25	2.35
Seed 4	43	0.005	5.407	75.16	15.88	2.20
Seed 5	53	0.003	4.913	73.83	15.43	1.84

3.4. Conclusions

LQU has developed a method to collect the whole seeds NMR spectra of coriander seed. The spectra quality is high enough to measure minor difference among seeds. ^{13}C NMR spectrum of intact seeds can be collected without using ^{13}C labeled seeds.

4. Determining Flaxseed Oil Oxidation by NMR

4.1. Introduction

Lipid oxidation is the most important factor limiting the shelf life of polyunsaturated oils such as flaxseed oils. Numerous methods are available to determine lipid oxidation, but none of them provide a completely satisfactory description of the oxidative status. It is therefore necessary to develop methods both to replace the traditional chemical methods and to obtain a better understanding of the oxidation processes of lipids. In addition, it is important to develop methods to avoid the use of harmful chemicals. Flaxseed oils are highly susceptible to oxidation based on their high polyunsaturated fatty acid (PUFA) content. During auto-oxidation, hydroperoxides are formed as primary oxidation products; these are unstable and react further to give a complex set of secondary products such as aldehydes, ketones, alcohols, and acids. The objective of this study is to develop a method to quantify these intermediates and monitor the oxidation status of flaxseed oil.

4.2. Materials and Methods

Materials. Flaxseed oil was provided by Prairie Tide Chemicals Inc. (Saskatoon, SK, Canada). Deuterated solvents and TMS were purchased from Sigma-Aldrich Chemical Co.

Sample preparation. The sample (250 mg) was dissolved in 0.6 mL of a mixture of $CDCl_3$ and Dimethyl sulfoxide-d_6 (DMSO-d_6, v/v 5:1), with a small proportion of TMS acting as an internal reference. Two or three balls of the molecular sieve were then added to the sample. After 20 min of shaking, this mixture was placed in a 5-mm diameter NMR tube.

NMR method. The ^{1}H -NMR spectra were recorded on a Bruker 400 MHz spectrometer operating at 400.17 MHz. The acquisition parameters were: spectral width 20.5396 ppm, relaxation delay 1 s, acquisition time 7.97 s, number of scans 128. The experiment was carried out at 300 K using a flip angle of 30°. The T1 measurements were performed to ensure that saturation effects did not influence the repeatability of the intensities. The T1 values of the hydroperoxide protons were in the same order of magnitude of the triacylglyceride protons which were approximately between 0.4 and 3 s. All data were processed using Bruker's TOPSPIN-NMR software (version 2.1, Bruker, Rheinstetten, Germany).

4.3. Results and Discussion

In $CDCl_3$, the OOH protons of hydroperoxides provide peaks in the region of 7.5-8.7 ppm. In the presence of a small amount of DMSO-d_6, this signal will provide a much narrower peak and a downfield shift to 10-12 ppm. Figure 4.1 presents the ^{1}H-NMR spectrum of the flaxseed oil. The region between 10.6 and 11.5 ppm has been enlarged to see the peroxide signals. This characteristic hydroperoxide signal pattern of flaxseed oil is mainly contributed by oxidized linolenic acid.

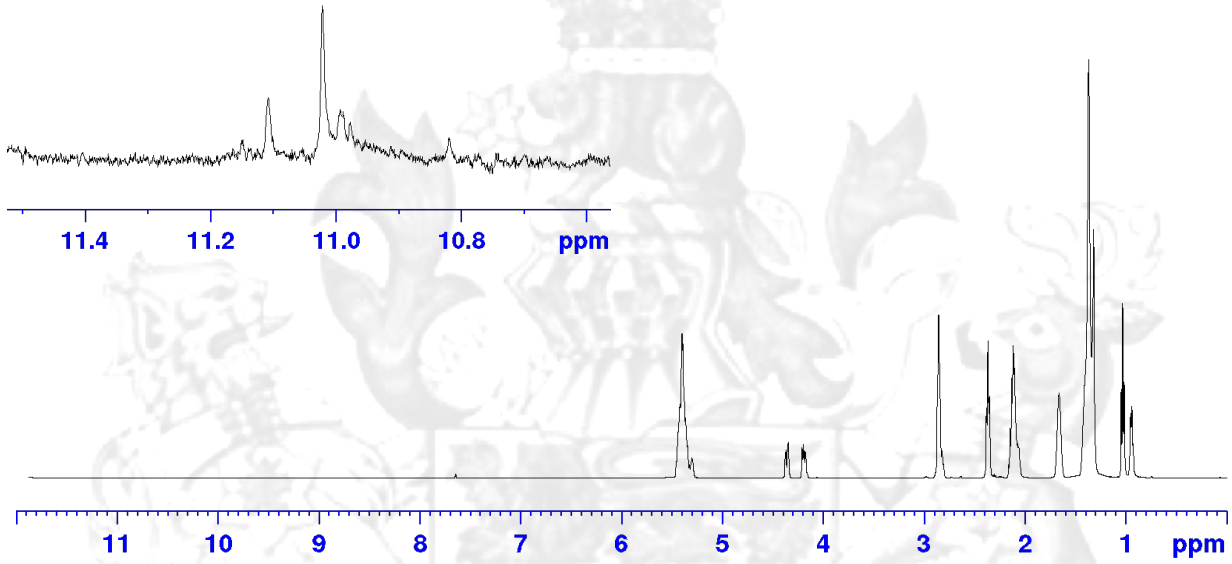

Figure 4.1 ^{1}H spectrum of oxidized flaxseed oil.

The first application of this NMR technique is to compare the oxidative stability of food products made with the flaxseed oil of six different varieties and the decolorized sweet flaxseed oil of CDC Glas. The seven flaxseed oils were mixed with salted butter, unsalted butter and coconut oil at 20/80 ratio. These flaxseed oil blends were then stored in a fridge at 4 °C. To check the quality of these blended food products, the ^{1}H-NMR spectra of each sample was collected at day 0, day 7, day 14, day 28, and day 60 (Figure 31-40). The flaxseed oil blend products made with unsalted butter and salted butter were very stable (Figures 4.2-4.5). No detectable oxidative product signal was detected until day 14 (Figures 4.6 and 4.7). The oxidation was very slow even after 60 days of storage (Figures 4.8-4.11).

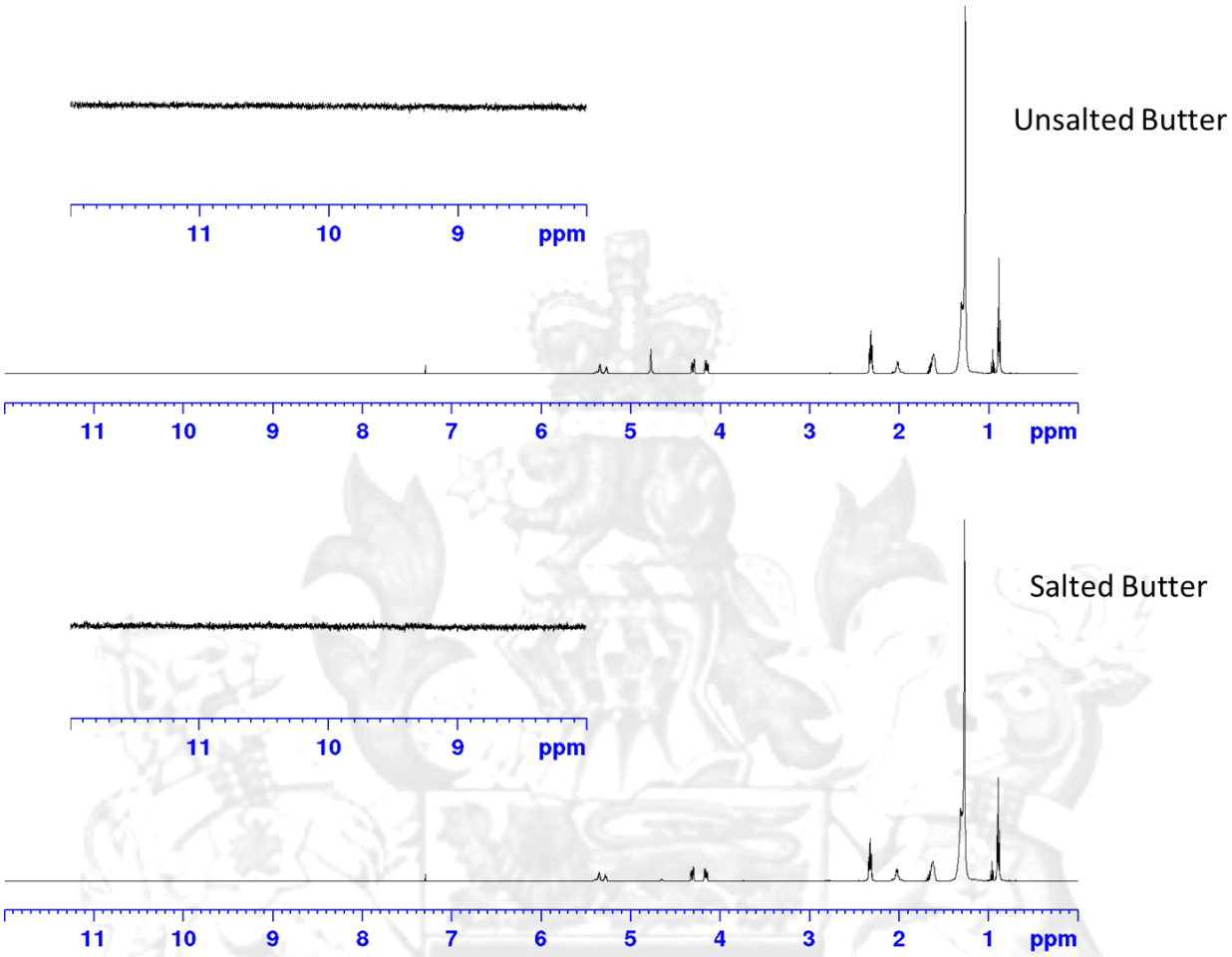

Figure 4.2 ^{1}H-NMR spectrum of unsalted butter and salted butter at day 0.

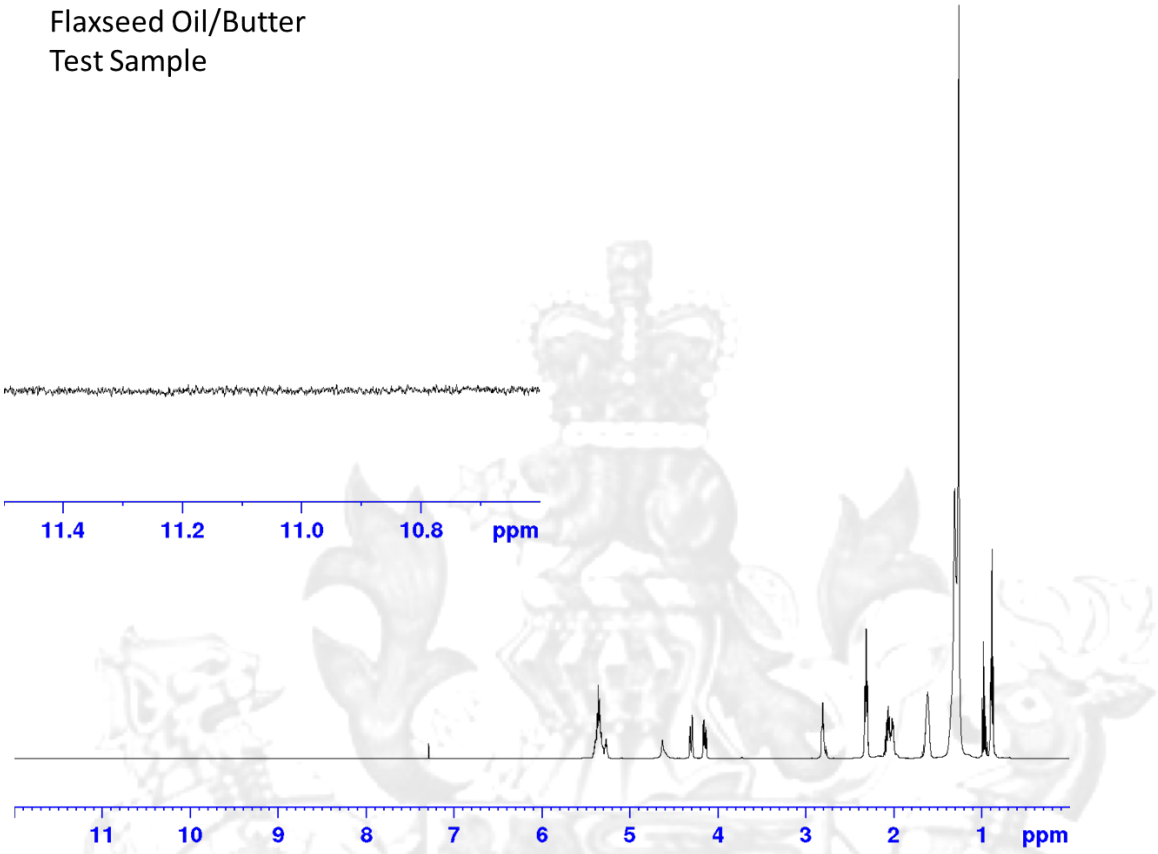

Figure 4.3 ^{1}H-NMR spectrum of flaxseed oil butter blend at day 0.

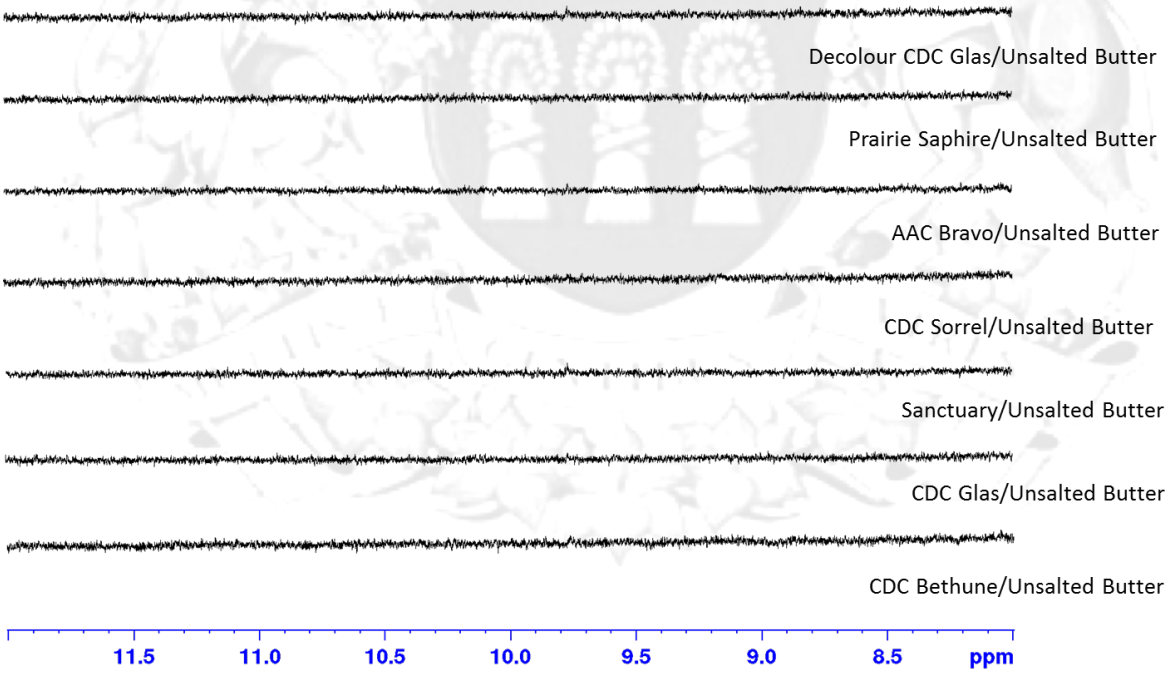

Figure 4.4 ^{1}H-NMR spectrum of flaxseed oil and unsalted butter blend at day 7.

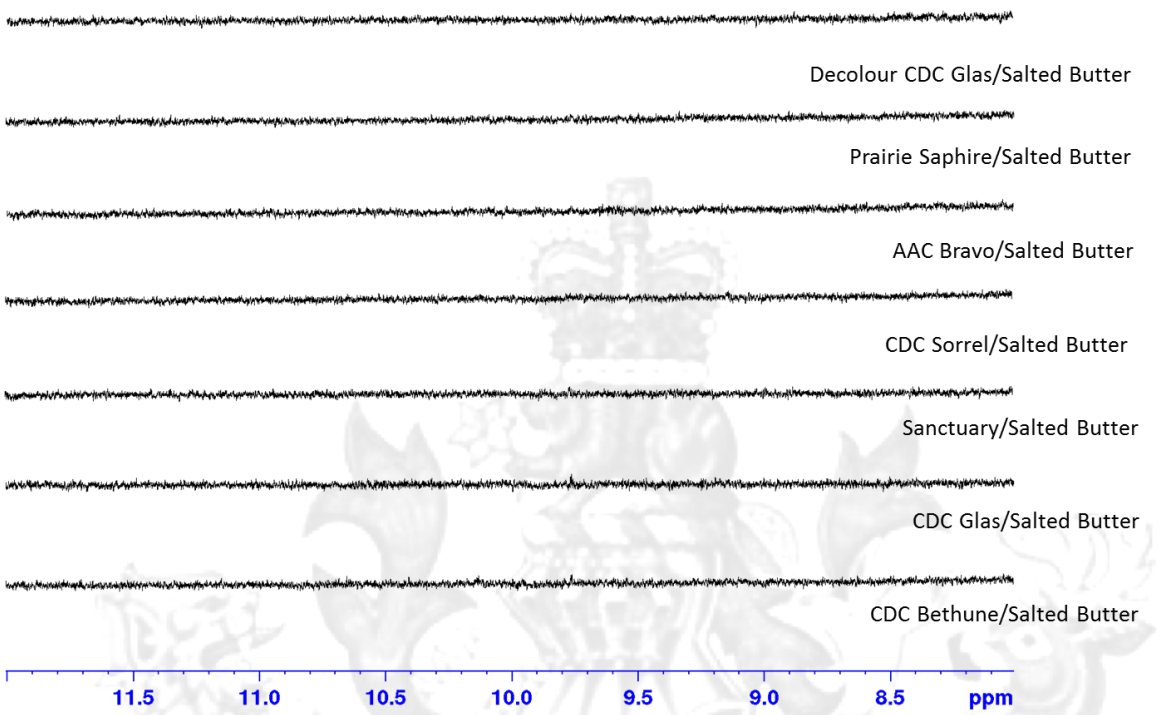

Figure 4.5 ^{1}H-NMR spectrum of flaxseed oil and salted butter blend at day 7.

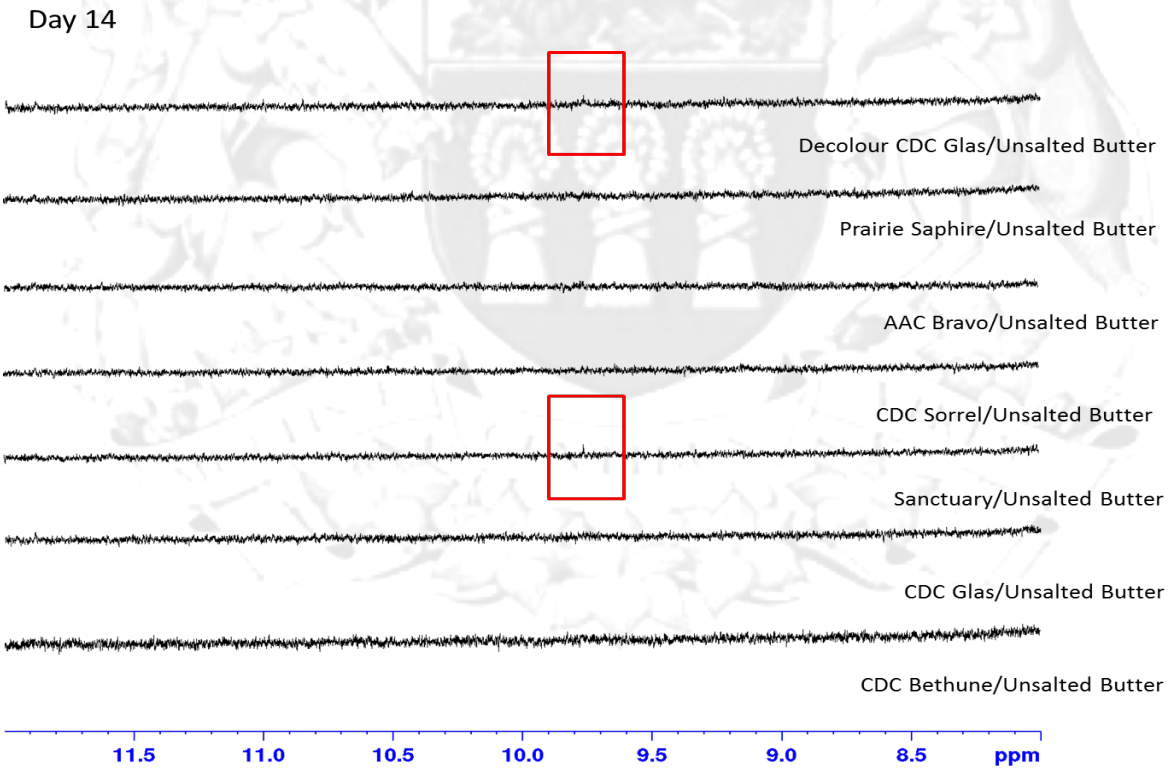

Figure 4.6 ^{1}H-NMR spectrum of flaxseed oil and unsalted butter blend at day 14.

Day 14

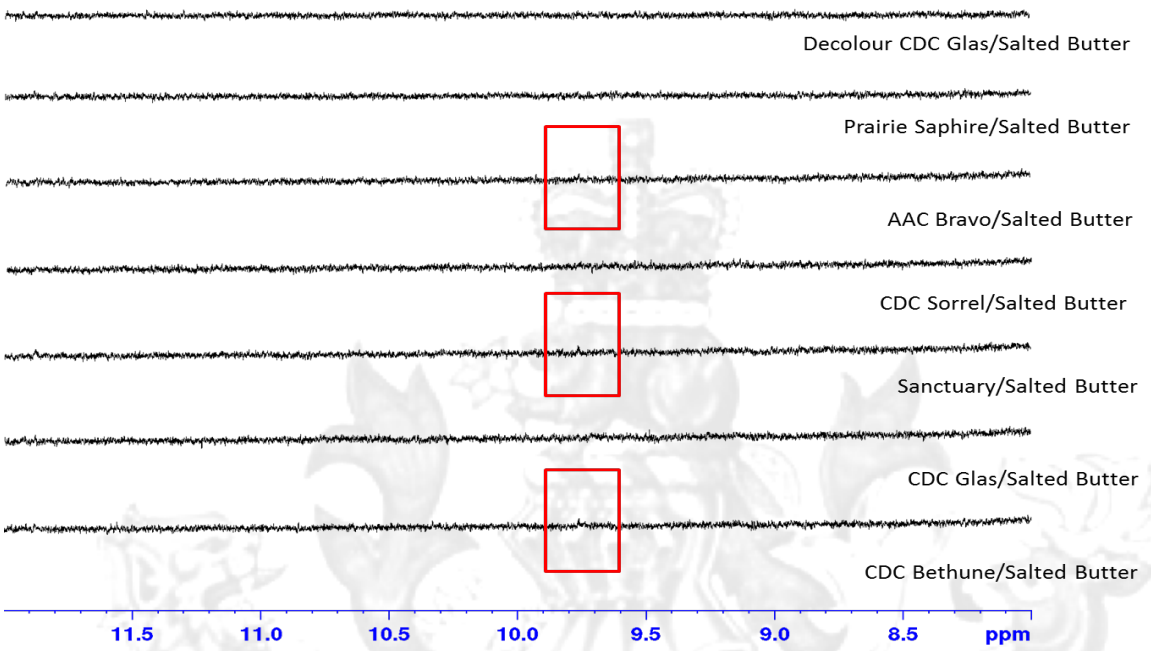

Figure 4.7 ^{1}H-NMR spectrum of flaxseed oil and salted butter blend at day 14.

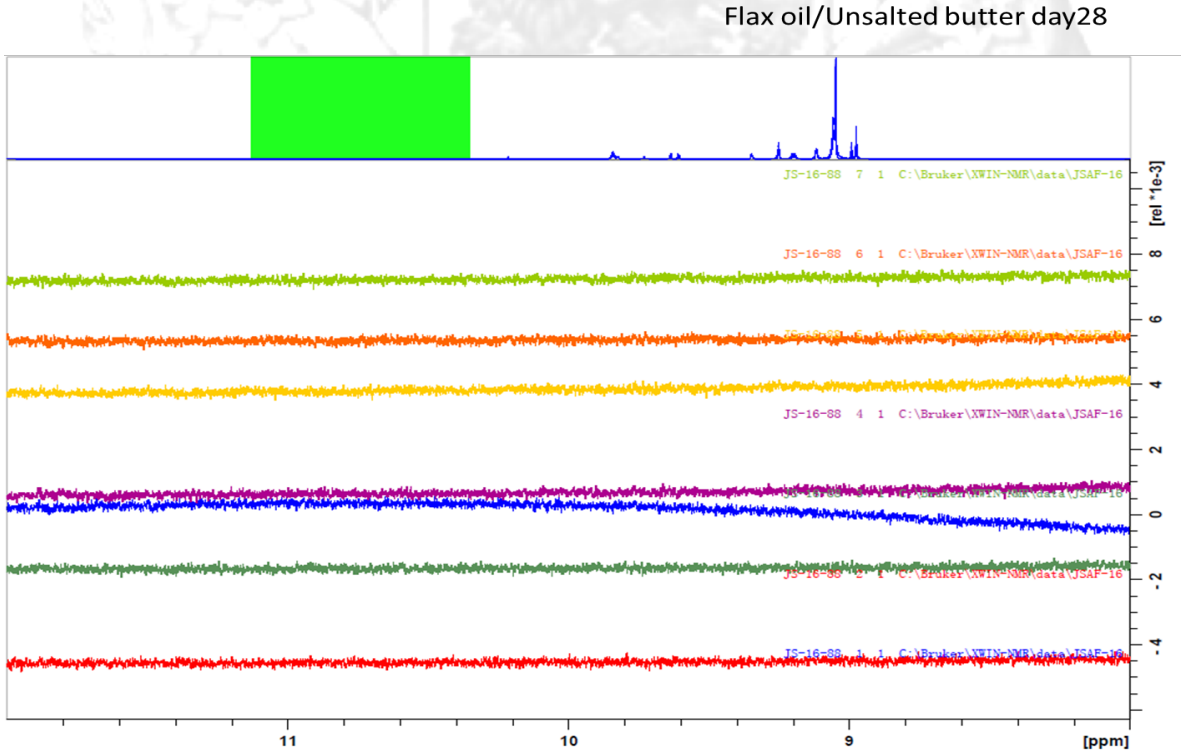

Figure 4.8 ^{1}H-NMR spectrum of flaxseed oil and unsalted butter blend at day 28.

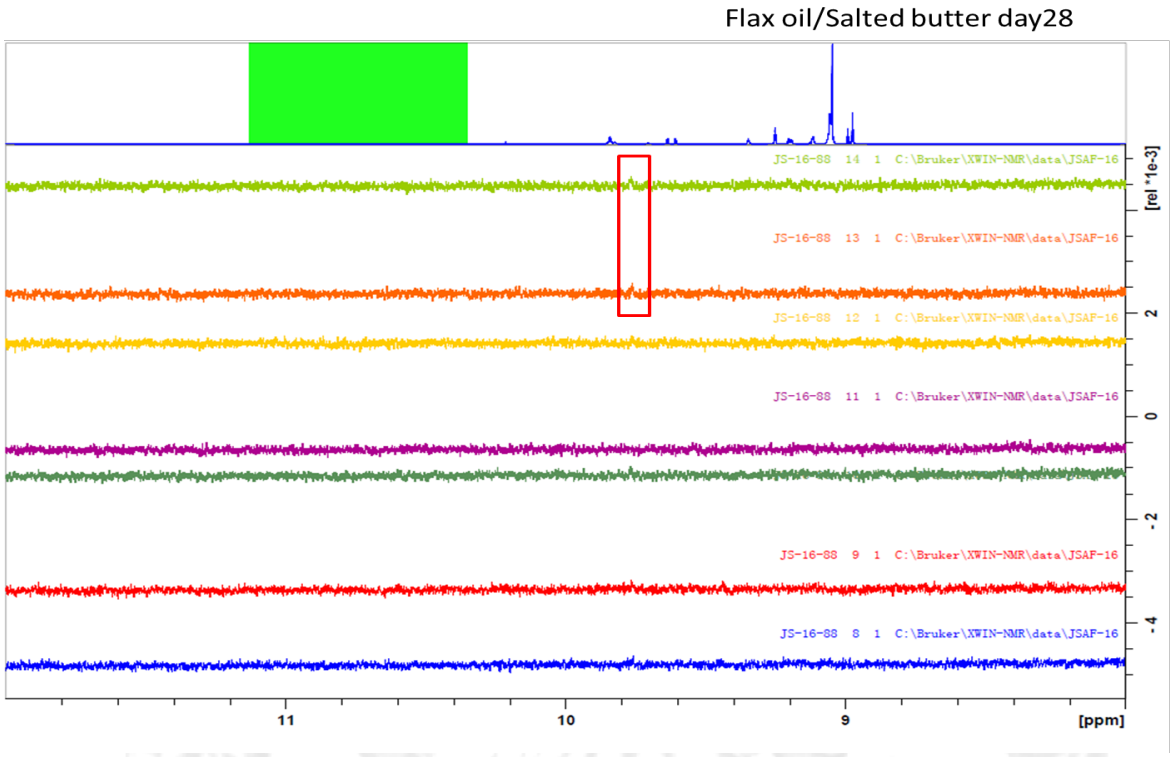

Figure 4.9 ^{1}H-NMR spectrum of flaxseed oil and salted butter blend at day 28.

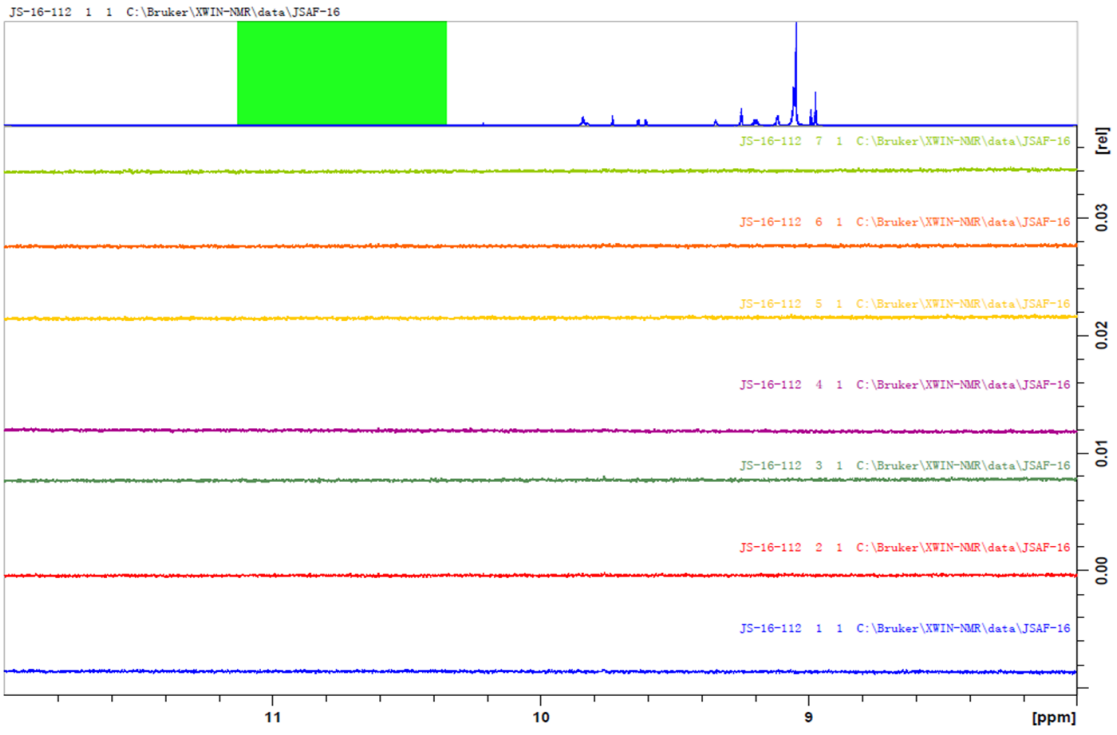

Figure 4.10 ^{1}H-NMR spectrum of flaxseed oil and unsalted butter blend at day 60.

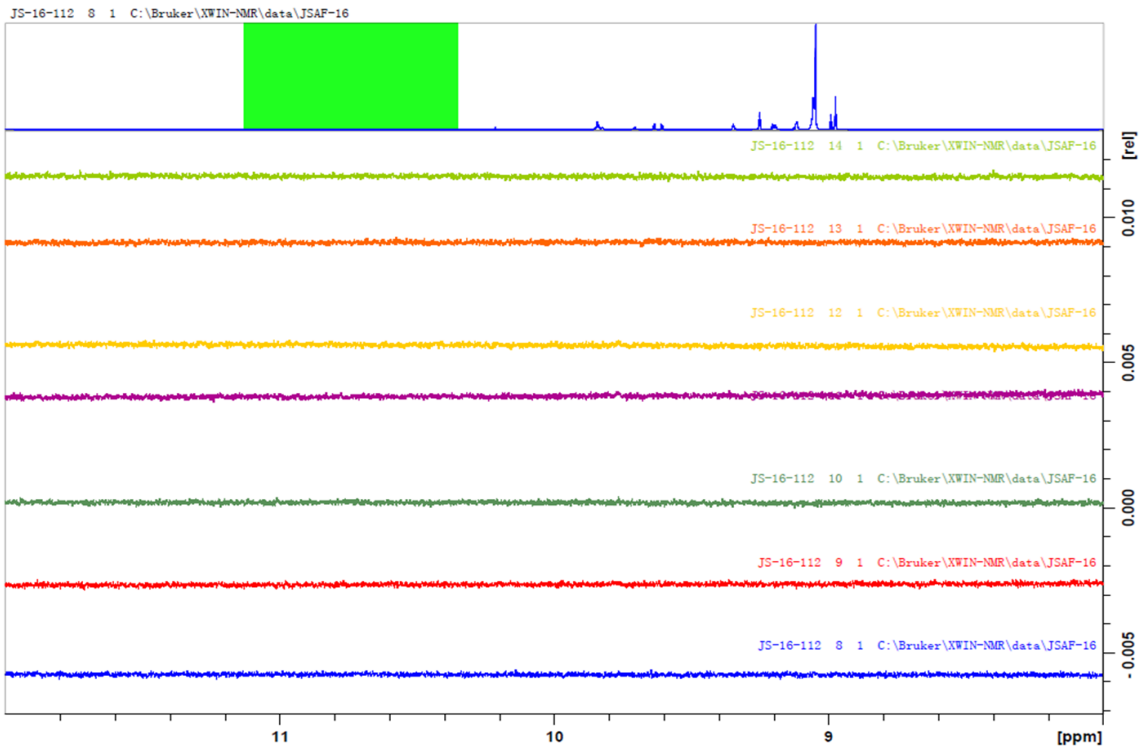

Figure 4.11 ^{1}H-NMR spectrum of flaxseed oil and salted butter blend at day 60.

4.4. Conclusions

LQU has developed a quick method for direct measurement of oxidized lipid product. This method has been successfully applied to monitor the oxidation status of flaxseed oil food products.

APPENDICES

APPENDIX A

Sun, G, Y Li, Z Cai, Y Teng, Y Wang, MJT Reaney (2017) K_2CO_3-loaded hydrotalcite: A promising heterogeneous solid base catalyst for biolubricant base oil production from waste cooking oils. *Applied Catalysis B: Environmental.* 209, 118–127.

Applied Catalysis B: Environmental 209 (2017) 118–127

Contents lists available at ScienceDirect

Applied Catalysis B: Environmental

journal homepage: www.elsevier.com/locate/apcatb

K_2CO_3-loaded hydrotalcite: A promising heterogeneous solid base catalyst for biolubricant base oil production from waste cooking oils

Guo Sun[a,b,1], Ying Li[a,b,1], Zizhe Cai[c], Yinglai Teng[a,b], Yong Wang[a,b,*], Martin J.T. Reaney[d]

[a] Guangdong Saskatchewan Oilseed Joint Laboratory, Department of Food Science and Engineering, Jinan University, Guangzhou 510632, China
[b] Guangdong Engineering Technology Research Center for Oils and Fats Biorefinery, Guangzhou 510632, China
[c] School of Pharmaceutical Sciences, Sun Yat-Sen University, Guangzhou 510006, China
[d] University of Saskatchewan, Department of Plant Science, Saskatoon, SK S7N 5A8, Canada

ARTICLE INFO

Article history:
Received 29 November 2016
Received in revised form 23 February 2017
Accepted 28 February 2017
Available online 1 March 2017

Keywords:
Hydrotalcite/K_2CO_3 heterogeneous catalyst
Trimethylolpropane fatty acid triester
Biolubricant base oil
Characterization
Recycling

ABSTRACT

Hydrotalcite (HT) loaded with potassium carbonate (K_2CO_3) was originally applied as a promising heterogeneous solid base catalyst for the production of trimethylolpropane fatty acid triester (TFATE) as the biolubricant base oil through transesterification of fatty acid methyl esters (FAME) from waste cooking oils and trimethylolpropane (TMP), in which FAME to TMP ratio (3:1), catalyst dosage (2% w/w), pressure (300 Pa), temperature (160 °C) and time (2 h) were optimized in order to obtain the best TFATE yield (80.6%). Based on the above, K_2CO_3 dosage (30% w/w) and calcination temperature (500 °C) in the preparation of HT/K_2CO_3 catalyst were optimized to improve the TFATE yield to 93.9% along with 97.7% of conversion rate of FAME (CRF). The catalyst recycling was also investigated to determine the suitable reactivated method. Besides, HT/K_2CO_3 catalysts in various states were characterized for better comprehension of their functional mechanisms and appropriate potential applications.

1. Introduction

For continuous environmental deterioration caused by the leakage of mineral-based lubricants, the worldwide requirement for sustainable development and eco-friendly products are currently on the rise [1]. As the Global Industry Analysts estimated [2], the global aggregate demand of lubricants will reach 4.13 hm^3 by 2017. Hence, it is inevitable to employ bio-based oils instead of mineral ones which account for 85–90% of global lubricant base oils produced every year. Although biolubricant like vegetable oils can be used as either an alternative with almost the same function in the machine protection or biolubricant base oils, the higher production cost is the main bottleneck for its development compared to conventional lubricants [3,4]. Moreover, there are other four types of biolubricant base oils including polyalphaolefins, polyalkylene glycols, dibasic acid esters and polyol ester [5], among which trimethylolpropane fatty acid triester (TFATE) as a type of polyol ester has proved to be a potential biolubricant base stock due to its favorable lubricity, stability, biodegradability and physicochemical properties, as compared to another pentaerythritol fatty ester [6,7]. Furthermore, the transesterfication of fatty acid methyl ester (FAME) and trimethylolpropane (TMP) was reportedly preferred to the esterification of free fatty acids (FFA) with TMP because of its low cost, energy efficient and higher yield as well [8].

The transesterification catalyst for TFATE production was normally classified into enzyme, heterogeneous, homogeneous base and acid catalysts [9–12]. Thereinto, using less corrosive heterogeneous catalyst can not only eliminate procedures like neutralization and washing, but also can be recycled after simple filtration [13]. As previously reported, a range of heterogeneous base catalysts have been widely studied for biodiesel production [14–17]. Nevertheless, the preparation of such catalysts is relatively complicated involving high temperature and pressure in general [18,19]. Hydrotalcite (HT) is commonly a di-hydroxyl complex metal oxide possessing layered and porous structures, which can be recognized as catalyst carrier, ion-exchange and composite materials. HT loaded with potassium carbonate (HT/K_2CO_3) had been discussed for improving the catalyst activity in biodiesel productions [20]. The calcination of HT/K_2CO_3 at higher temperatures (≥400 °C) can decompose the carbonate into its metal oxide form, which generates highly dispersed active sites on the HT surface for various catalytic reactions. Nonetheless, such catalyst in biolubricant

* Corresponding author at: Guangdong Saskatchewan Oilseed Joint Laboratory, Department of Food Science and Engineering, Jinan University, Guangzhou 510632, China.
E-mail addresses: wangyjnu@hotmail.com, twyong@jnu.edu.cn (Y. Wang).
[1] Ying Li and Guo Sun contributed equally to this work and should be considered as co-first authors.

http://dx.doi.org/10.1016/j.apcatb.2017.02.078
0926-3373/

productions has rarely been studied, as well as its elaborate characterization, optimal preparation and recycling.

Considering the above, a thorough study of HT/K_2CO_3 reutilized for the production of TFATEs as biolubricant base oils was hereby provided using economically available waste cooking oils (WCO) in China as the feedstock. Firstly, a preliminary single-effect study for the TFATE production was conducted in terms of FAME to TMP ratio, catalyst dosage, reaction pressure, temperature and time. Subsequently, both the preparation and the recycling of HT/K_2CO_3 catalyst were optimized for obtaining desirable mass fraction of TFATE (MFT) and conversion rate of FAME (CRF). Regarding the characterization of HT/K_2CO_3 catalysts in various states, a series of modern methods were employed to expound the relationship between structural changes and catalytic activity concerning their catalytic active sites, microstructures, thermo-stability, metal ion leaching, specific surface areas, pore sizes and volumes for better comprehension of their functional mechanisms in future biolubricant base oil production.

2. Experimental

2.1. Materials

WCO with an acid value of 78.8 mg KOH/g and an initial moisture content of 0.6% from restaurants were provided by Balis Waste Treatment in Guangzhou, China, in which remaining food and water were removed by filtration after settling. The main components in WCO were FFA (38.7%), diacylglycerol (5.4%) and triacylglycerol (55.9%). TMP was obtained from Keoumi Chemical Reagent in Tianjin, China. Solid superacid of sulfated zirconia supported alumina (SO_4^{2-}/ZrO^{2-}:Al_2O_3) was purchased from Taide Chemical Scientific in Shandong, China. HT was supplied by Tiantang Chemical in Hunan, China. K_2CO_3 (>99%) and all other chemical reagents were of analytical grade from Fuyu Chemical in Tianjin, China.

2.2. HT/K_2CO_3 preparation and optimization

The HT/K_2CO_3 catalyst was prepared according to our developed method [21]. On one hand, 25 g of HT and 5 g of K_2CO_3 were mixed with 100 mL of distilled water in a flask of 250 mL for 24 h reaction at 80 °C, in which agitation was implemented for the first hour only. The resultant slurry was then oven dried at 80 °C for 5 h, followed by grinding and calcination at 600 °C for 6 h to form the solid base catalyst for the single factor experiment in the following transesterifications. On the other hand, different K_2CO_3 dosages (15, 20, 25 and 30%) and calcination temperatures (400, 500, 600 and 700 °C) were characterized based on the optimal conditions from single-factor experiments above, in which 100 mL of distilled water was poured into 50 g of HT/K_2CO_3 mixture instead here.

2.3. HT/K_2CO_3 characterization

HT/K_2CO_3 catalysts in various states were firstly pressed into KBr pellets for a qualitative Fourier Transform infrared spectroscopy (FT-IR), in which the spectra were recorded over 32 scans by a 640-IR spectrometer (Varian, USA) in a transmission mode from 4000 to 400 cm^{-1} with a resolution of 1 cm^{-1}. X-ray diffraction (XRD) was then conducted using an MSAL XD-II X-ray diffractomter from Persee in Beijing, China with Cu Kα radiation (λ = 0.15418 nm). All samples were measured at 36 kV and 20 mA scanning from 10 to 80° at 4°/min. Thermogravimetry/differential thermal analysis (TG-DTA) was carried out on the samples heating up to 950 °C at 10 °C/min in an air flow with a Mettler Toledo TGA/SDTA85 from USA. The microstructure was observed by an ULTRA-55 field emission scanning electron microscope (FESEM) from ZEISS, Germany at a magnification of 20000×. The property of HT/K_2CO_3 was also measured by an automatic specific surface area/pore size distribution analyzer (BET sorp-mini II, ASAP010 Micromeritics instrument, USA), which was purged with helium gas during operation. The isotherms were generated by sweeping nitrogen onto the catalysts in a bath containing liquid nitrogen at 77 K. The relative pressure range was set at 2–99 kPa for adsorption and 97–31 kPa for desorption.

2.4. HT/K_2CO_3 application for TFATE production using WCO

The pathway of TFATE production (Fig. 1) starts with the production of WCO-FAME via a two-step process [22]. Firstly, WCO was filtered to remove solid particles before the esterification with glycerol catalyzed by solid superacid to lower the content of free fatty acids. The catalyst was removed by filtration and the esterified WCO was then transesterified with methanol to produce crude FAME using the KOH catalyst. Methanol and water remaining in the crude FAME were vacuum evaporated (5000 Pa, 50 °C), before which the reaction product was washed with hot water (80 °C) twice to remove residual glycerol and soap. The prepared WCO-FAME was analyzed by GC-FID after and fractionated by a MD80 molecular distillation (MD) apparatus (Handway Technology, Foshan, China) equipped with a falling film evaporator (0.1 m^2) and an internal condenser (0.05 m^2). A jacketed glass vessel with a flow regulation valve was used to load the WCO-FAME into the MD equipment at 40 mL/h. The operating parameters were as follows: pressure (<0.1 Pa), wiped film speed (300 rpm), temperature for distillation, condensation and feeding tank was 140 °C, 50 °C and 110 °C, respectively. Distillates and residues were separately discharged into glass flasks by gravity, among which the purified WCO-FAME was added dropwise to the mixture of TMP and HT/K_2CO_3 catalyst for the TFATE production in a three-necked flask equipped with a condenser and a constant-pressure dropping funnel. This second transesterification was evaluated in terms of FAME to TMP molar ratio (2.5:1, 2.8:1, 3:1, 3.3:1 and 3.6:1), catalyst dosage (0.5, 1.0, 1.5, 2.0 and 2.5%, w/w), reaction pressure (100, 200, 300, 400, and 500 Pa), temperature (130, 140, 150, 160 and 170 °C) and time (1, 1.5, 2.0, 2.5 and 3 h) under the prescribed magnetic stirring of 300 rpm. After the reaction, the HT/K_2CO_3 catalyst simply filtrated from the TFATE product was recycled and the TFATE was collected for further analyses.

2.5. FAME and TFATE analysis

The composition of fatty acid and TMP esters was determined by an Agilent 7820A gas chromatography (Agilent Technologies, Palo Alto, USA) equipped with a flame ionization detector (FID) [23]. For FAME analysis, fatty acids were transmethylated to their methyl esters in GC-FID using a DB-wax capillary column (10 m × 0.1 mm × 0.2 μm) with nitrogen as the carrier gas at a flow rate of 0.17 mL/min. The temperature of injector and detector was 240 °C. Samples were dissolved in hexane at a concentration of 10.0 mg/mL, 0.5 μL of which was withdrawn and injected with a split ratio of 30:1. The oven temperature was programmed to increase from 100 to 220 °C at 100 °C/min, held at 220 °C for 2 min, then heated from 220 to 240 °C at 40 °C/min and maintained for 4 min at 240 °C.

For TFATE analysis, a DB-1HT capillary column (15 m × 0.25 mm × 0.1 μm) was employed using nitrogen as the carrier gas at a flow rate of 4.41 mL/min. The temperature for injector and detector was 380 °C and 400 °C, respectively. The oven temperature was operated as follows: the initial temperature set at 50 °C was heated to 220 °C at 50 °C/min, then increased at 30 °C/min to 290 °C, then increased at 40 °C/min to 330 °C for 2 min interval and at 30 °C/min from 330 to 370 °C, held for another 3 min at 370 °C. Samples were dissolved in hexane at 10.0 mg/mL

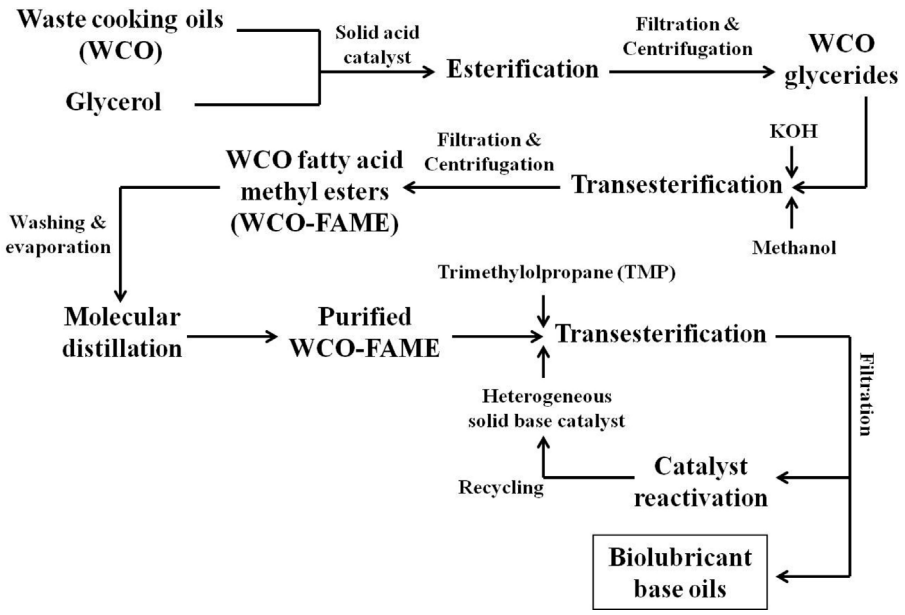

Fig. 1. Process diagram of biolubricant base oil production from waste cooking oils catalyzed by HT/K_2CO_3.

and 0.5 μL of sample was injected with the split ratio of 20:1. Data were collected and processed with Aglient EZchrom Elite software. Both FAME and TFATE analytical results were expressed as relative percentages of the total fatty acid esters.

According to GC-FID results obtained, the mass fraction of TFATE (MFT) and the conversion rate of FAME (CRF) could be calculated as follows,

$$\text{MFT}\ (\%) = \frac{A_{tri}}{A_{tri} + A_{di} + A_{mono} + A_{FAME}} \times 100\% \quad (1)$$

where A_{tri}, A_{di}, A_{mono} and A_{FAME} are the peak area of TFATE, trimethylolpropane fatty acid diester (TFADE) and monoester (TFAME) and FAME, respectively.

$$\text{CRF}\ (\%) = \frac{\frac{R_{tri}}{M_{tri}} \times 3 + \frac{R_{di}}{M_{di}} \times 2 + \frac{R_{mono}}{M_{mono}}}{\frac{R_{tri}}{M_{tri}} \times 3 + \frac{R_{di}}{M_{di}} \times 2 + \frac{R_{mono}}{M_{mono}} + \frac{R_{FAME}}{M_{FAME}}} \times \frac{M}{3} \times k \times 100\% \quad (2)$$

where R_{tri}, R_{di}, R_{mono} and R_{FAME} indicate the mass fraction of TFATE, TFADE, TFAME and FAME, respectively. M specifies the molar ratio of FAME to TMP. k stands for the GC coefficient (1/1.1), M_{tri}, M_{di}, M_{mo} and M_{fame} represent the relative mass of TFATE, TFADE, TFAME and FAME in a sample, respectively [24].

2.6. Analysis of metal ion leaching

The metal ion leaching was traced by inductively coupled plasma-atomic emission spectrometry (ICP-AES) (Optima 2000DV ICP-AES, Perkin Elmer, USA). Samples were prepared at 160 °C for 2 h using FAME to TMP molar ratio (3.5:1) and catalyst dosage (2% w/w), which were carbonized and incinerated at 600 °C for 4 h. The ashed samples were dissolved in 5 mL of nitric acid and diluted to 50 mL with distilled water for analysis using the following conditions: 1.1 kW of forward power, 30 °C of oven temperature, 0.2 L/min for auxiliary gas flow rate, 15 L/min for nebulizer gas flow rate, 0.8 L/min for plasma gas flow rate and 1.5 mL/min for the pump sample quantity. All determinations were performed in triplicate.

2.7. Recycling of HT/K_2CO_3 catalyst

The recycling of HT/K_2CO_3 catalyst from vacuum filtration was investigated using five reactivated methods below:

a Direct reuse;
b Hexane treatment: 5.0 g of recovered HT/K_2CO_3 catalyst placed in a centrifuge tube of 50 mL was washed thrice with 50 mL of n-hexane, which was vacuum dried at 40 °C for 2 h to remove n-hexane, and then at 80 °C for 5 h to remove water;
c Calcination after hexane treatment: HT/K_2CO_3 from the method above was calcinated in a muffle oven at 600 °C for 5 h;
d Hexane and methanol treatment: HT/K_2CO_3 from the second method was washed with 50 mL of methanol in the centrifuge tube by vortex mixing to eliminate the formed soap within, which was then centrifuged at 2000 rpm and vacuum dried at 40 °C for 2 h to remove methanol and at 80 °C for 5 h to remove water;
e Calcination after hexane treatment and impregnation: HT/K_2CO_3 from the second method was impregnated with a K_2CO_3 solution of 5%.

The resulting slurry was oven dried at 80 °C for 5 h and then calcinated in a muffle oven at 600 °C for 5 h. The efficiency of five reactivated catalysts for the TFATE production was assessed as compared to the new-made catalyst under the same transesterification conditions.

3. Results and discussion

3.1. The composition of FAME from WCO

As Table 1 represented, nine WCO-based FAMEs were characterized with 61.1% of unsaturation degree, which leads to desirable low-temperature properties and oxidative stability for producing TFATE as the base oil for biolubricant [1]. The three major components in the WCO-based FAME are methyl oleate (36.11 ± 1.58%), methyl palmitate (31.87 ±1.10%) and methyl linoleate (21.71 ± 1.06%), which was consistent with the composition in the blend of soybean and palm oil [23]. The physiochemical property of TFATE depends largely on the fatty acid composition. The average molecular weight ($M_{average}$) of WCO FAME could be calculated as 286 Da in light of Eq. (3), which helps to determine the specific dosage of TMP used in the following transesterifications.

$$M_{average} = \frac{100}{\frac{m_1}{M_1} + \frac{m_2}{M_2} + \ldots + \frac{m_x}{M_X}} \quad (3)$$

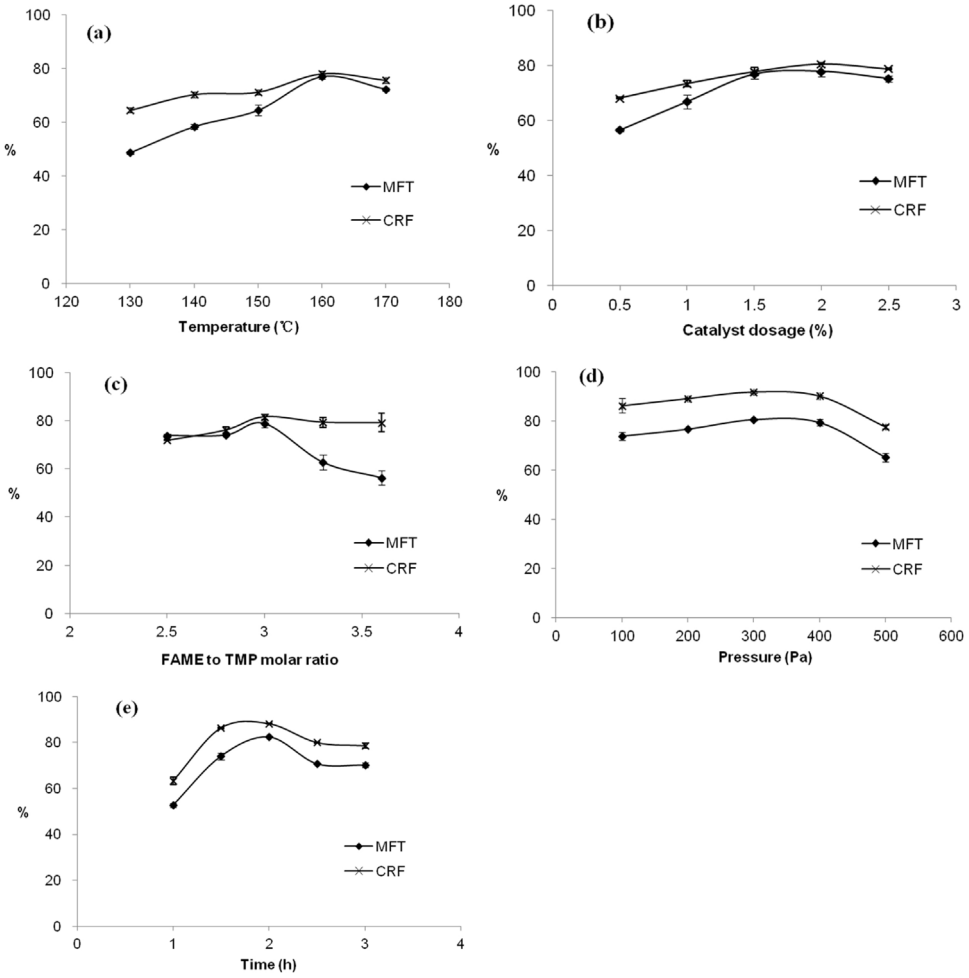

Fig. 2. The single effect of reaction parameters on mass fraction of trimethylolpropane fatty acid triester (MFT) and conversion rate of FAME (CRF): (a) temperature (FAME to TMP molar ratio: 2.8:1, catalyst dosage: 1.5% w/w, 400 Pa and 2 h); (b) catalyst dosage(160 °C, FAME to TMP molar ratio: 2.8:1, 400 Pa and 2 h); (c) FAME to TMP molar ratio (160 °C, catalyst dosage: 2% w/w, 400 Pa and 2 h); (d) pressure (160 °C, FAME to TMP molar ratio: 3:1, catalyst dosage: 2% w/w and 2 h); (e) time (160 °C, FAME to TMP molar ratio: 3:1, catalyst dosage: 2% w/w and 300 Pa).

Table 1
The composition of fatty acid methyl esters (FAME) transformed from waste cooking oils.

Retention time (min)	FAME	Relative content (%)
8.8	Methyl myristate	0.82 ± 0.08
10.9	Methyl palmitate	31.87 ± 1.10
11.1	Methyl palmitoleate	1.10 ± 0.11
12.8	Methyl stearate	6.19 ± 0. 56
13.0	Methyl oleate	36.11 ± 1.58
13.6	Methyl linoleate	21.71 ± 1.06
14.2	Methyl linolenate	1.53 ± 0.35
14.8	Methyl arachidate	0.35 ± 0.03
15.0	Methyl eicosenoate	0.32 ± 0.01

Values are presented as means ± standard deviation of triplicate.

where X is nine, $m_{1,2,\ldots,x}$ and $M_{1,2,\ldots,x}$ stand for weight in 100 g of WCO-based FAME and molecular weight, respectively, corresponding to nine identified FAMEs.

3.2. The single-factor effect on the TFATE production

Fig. 2 illustrated earlier increase and later decrease trend for all five operating parameters in the HT/K_2CO_3-catalyzed transesterification of TMP and WCO-FAME. Temperature was investigated first while other reaction parameters were set as FAME to TMP molar ratio of 2.8:1, catalyst dosage of 1.5%, time of 2 h and pressure of 400 Pa. The upward trend of MFT was similar to that of previous study [25], but in this case, the MFT and CRF increased quickly to their peak at first ranging from 130 to 160 °C, followed by a slight decline as the temperature continued to increase (Fig. 2a). It is known that higher temperatures are preferred for the endothermic transesterification. However, the elevated temperatures may induce more TMP evaporation and side reactions like saponification and partial carbonization, which lead to a reduced TFATE yield and product quality. Thus, 160 °C was selected as the optimal temperature for subsequent reactions.

As shown in Fig. 2b, the increased catalyst dosage could accelerate the reaction, from which the highest MFT and CRF were obtained using 2% w/w of catalyst dosage and they gradually decreased afterwards. This may be due to the limited solubility of HT/K_2CO_3 in TMP and the lack of catalyst substrates. Considering the costing and the difficulty in post-treatments, 2.0% was considered the optimal catalyst dosage. MFT and CRF rose up to their maximum when FAME to TMP molar ratio of 3:1 was used in Fig. 2c. However, a further increase of FAME loading caused a sharp decline in the MFT, which could be explained by the excessive addition of FAME that adversely affected the reaction equilibrium in the TFATE synthesis. Moreover, the recovery of unreacted FAME would consume more energy and cost. Therefore, the FAME to TMP molar ratio of 3:1 was chosen.

A significant increase in MFT and CRF was found as the pressure decreased from 500 to 300 Pa (Fig. 2d). The further decrease of

pressure would let both FAME and TMP boil at a lower temperature, resulting in an evaporation loss of raw reactants required for the TFATE synthesis. Hence, 300 Pa was selected as the optimal. Time also had significant effect as it went up from 1 to 2 h. Both MFT and CRF dropped down afterwards but the extension of time had little effect on the further TFATE synthesis. Meanwhile, the prolonged time also require more energy. Consequently, 2 h has been used to ensure the efficiency of TFATE production.

According to the single-factor experimental results above, the operating parameters for subsequent experiments were determined with the consideration of both costing and efficiency. The highest MFT (82.5%) and CRF (88.2%) could be attained under the optimal conditions as follows: FAME to TMP molar ratio of 3:1, catalyst dosage of 2% w/w, 160 °C, 300 Pa and 2 h.

3.3. Optimization of prepared HT/K_2CO_3 catalyst

The preparation of HT/K_2CO_3 catalyst was optimized based on the optimal transesterification obtained before. As described in Table 2, the CRF kept rising at a constant calcination temperature (600 °C) as the K_2CO_3 dosage increased, in which an insignificant difference in the CRF change was found as the K_2CO_3 dosage increased from 15 to 25% whereas the CRF went dramatically up to its peak (87.1%) when the K_2CO_3 dosage reached 30%. The CRF change was significant when 30% of K_2CO_3 dosage was fixed at different calcination temperatures, among which 500 °C performed the best. Therefore, 30% of K_2CO_3 dosage at 500 °C of calcination temperature was determined for the preparation of HT/K_2CO_3 catalysts.

3.4. HT/K_2CO_3 characterization

3.4.1. FT-IR spectra

Owing to the stretching vibration of hydroxyls in the hydrated surface layer formed by water molecules [26], the absorbance ranging from 3800 to 3250 cm^{-1} was observed, as well as a similar absorption around 3199.35 cm^{-1} in the spectra of 400 °C. As illustrated in Fig. 3a, the band at about 3459.96 cm^{-1} associated with stretching vibrations is due to the water absorption onto the surface of the catalyst, and it could also be partly attributed to the stretching vibration of the Al–O–K groups, which is considered to be active sites [27,28]. A δ-OH bending vibration at 1636.89 cm^{-1} may be resulted in the water absorption from the air as well, which might also greatly affect the XRD spectra [29]. The absorbance of CO_3^{2-} bonding K^+ was commonly in the range of 1722–1160 cm^{-1} [30], in which the absorbance around 1477 cm^{-1} could be attributed to the symmetric and asymmetric stretching vibrations of mono-dentate carbonates at the surface of the K_2CO_3 [31], and the HT/K_2CO_3 calcinate exhibited the co-existence of weak absorption peaks around 1410 cm^{-1}. Moreover, the absorption at 487 cm^{-1} was probably caused by the lattice vibration of metal oxide (KO_x) [32]. In Fig. 3b, the absorption peaks of HT/K_2CO_3 calcinates at 500 °C were stronger as the K_2CO_3 dosage increased, and absorptions around 861 and 670 cm^{-1} were found in all HT/K_2CO_3 calcinates, which could be assigned to the stretching vibration of Al–O active sites [33]. In the case of 30% of K_2CO_3 dosage used (Fig. 3c), the HT/K_2CO_3 calcinate at 500 °C gave a stronger absorption band around 1477 cm^{-1} due to the presence of carbonate [25]. The absorption peaks around 3427 cm^{-1} for higher calcination temperatures were very similar to hydroxy absorption band around 3412 cm^{-1} reported for irreversible structures like $KAl(CO_3)(OH)_2$ and $Mg(Al)O_x$, which could also exhibit its absorptions at 1105 cm^{-1} [34]. This means that irreversible structures generated at 600 or 700 °C could reduce the surface area and alkalinity of catalysts. Notwithstanding, no irreversible structures were found for HT/K_2CO_3 calcinated at 400 and 500 °C, in which inconspicuous absorption peaks around 860 and 670 cm^{-1} indicated less active sites on the HT/K_2CO_3 calcinated at 400 °C. Based on the above, it could be concluded that only calcination induced the formation of active sites (i.e., K and Al oxides) on the HT/K_2CO_3, in which one with 30% of K_2CO_3 addition at 500 °C calcination seems to have better characteristic peaks in accordance with the obtained optimal conditions for the HT/K_2CO_3 preparation.

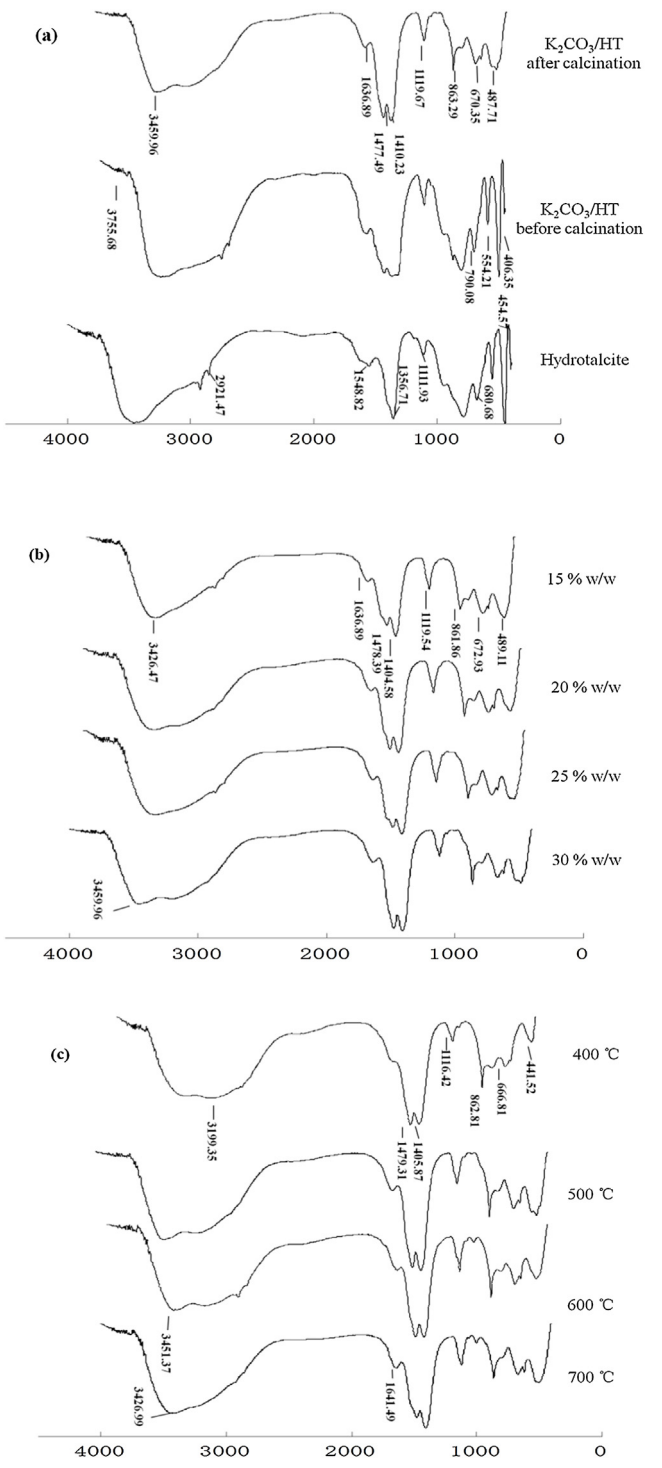

Fig. 3. FT-IR spectrum: (a) Hydrotalcite (HT), HT/K_2CO_3 before and after calcination; (b) HT/K_2CO_3 catalyst with different K_2CO_3 dosages at the calcination temperature of 600 °C; (c) HT/K_2CO_3 catalyst with the K_2CO_3 dosage of 30% w/w under different calcination temperatures.

Table 2
The performance of HT/K_2CO_3 catalyst under various conditions regarding the yield of trimethylolpropane fatty acid mono-, di-, tri- esters and the conversion rate of FAME (CRF).

Preparation condition	TFAME[a]	TFADE[b]	TFATE[c]	CRF[d]
15% K_2CO_3 at 600 °C	0.16 ± 0.28	7.75 ± 0.13	68.42 ± 0.54	76.53 ± 0.37
20% K_2CO_3 at 600 °C	0.12 ± 0.21	2.94 ± 0.17	75.82 ± 1.48	79.25 ± 1.60
25% K_2CO_3 at 600 °C	0.00 ± 0.00	2.00 ± 0.08	77.78 ± 0.57	80.20 ± 0.66
30% K_2CO_3 at 600 °C	0.00 ± 0.00	2.09 ± 0.03	84.32 ± 0.44	87.12 ± 0.47
30% K_2CO_3 at 400 °C	0.00 ± 0.00	6.72 ± 0.46	77.02 ± 2.66	84.29± 3.20
30% K_2CO_3 at 500 °C	0.00 ± 0.00	2.58 ± 0.22	93.89 ± 0.44	97.71 ± 0.49
30% K_2CO_3 at 700 °C	0.00 ± 0.00	4.52 ± 0.13	78.88 ± 0.03	83.95± 0.12

Values are presented as means ± standard deviation of triplicate.
[a] TFAME: trimethylolpropane fatty acid monoester.
[b] TFADE: trimethylolpropane fatty acid diester.
[c] TFATE: trimethylolpropane fatty acid trimester.
[d] CRF: conversion rate of FAME.

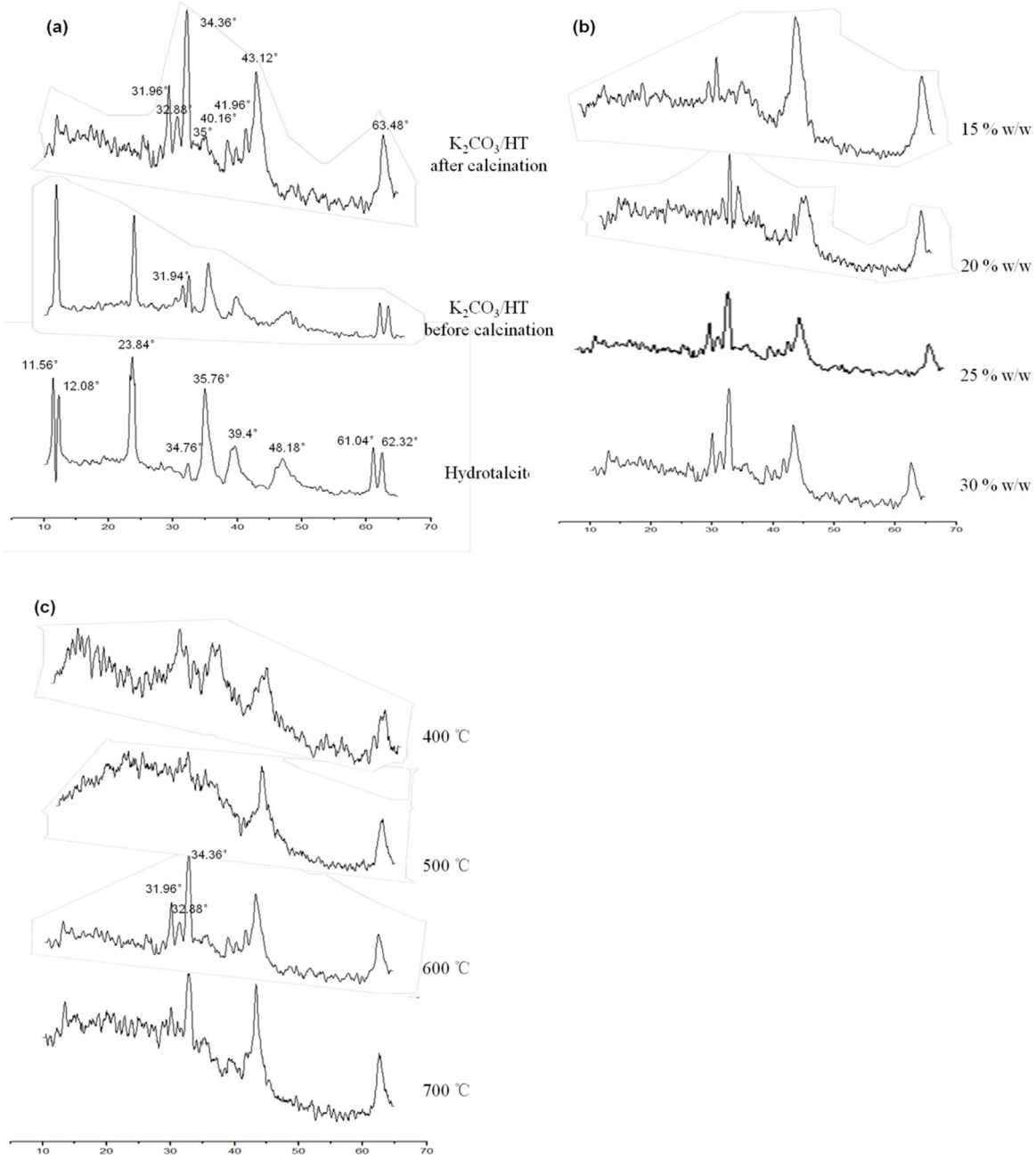

Fig. 4. X-ray diffractogram: (a) HT, HT/K_2CO_3 before and after calcination; (b) HT/K_2CO_3 catalyst with different K_2CO_3 dosages at the calcination temperature of 600 °C; (c) HT/K_2CO_3 catalyst with the K_2CO_3 dosage of 30% w/w under different calcination temperatures.

3.4.2. XRD diffractograms

As can be seen in Fig. 4a, the XRD diffraction pattern of HT displayed typical characteristic peaks at 11.56°, 12.08°, 23.84°, 34.76°, 35.76°, 39.4°, 48.18°, 61.04° and 62.32° [35], among which the peaks at 11.56° and 23.84° could be used to calculate the basal spacing between the layers whilst the peak at 61.04° could used for calculating the unit-cell dimension [36]. However, the peaks at 11.56° and 12.08° were replaced by a new peak at 11.96° when adding K_2CO_3 into HT, as well as the new peak at 31.94° instead of the peak at 34.76°, indicating the layered basal spacing changed. After calcination, the HT layered structure was destroyed, and the characteristic peaks at 31.96°, 32.88°, 34.36°, 35°, 40.16°, 41.96° 43.12° and 63.48° were exhibited [33], in which Al—O—K ($2\theta = 43°$) and K_2O ($2\theta = 63°$) active sites were observed corresponding to their FT-IR absorbance [37,38]. These newly-formed crystals consisting of multiple metal oxides may explain the excellent catalytic activity of HT/K_2CO_3. The XRD diffractogram of HT/K_2CO_3 calcinates with different K_2CO_3 dosages at 600 °C showed no significant difference in Fig. 4b whereas HT/K_2CO_3 calcinates at 600 and 700 °C with K_2CO_3 dosage of 30% presented the characteristic peaks at 31.99°, 32.88°, 34.36° in Fig. 4c corresponding to spinelle-like irreversible structures, which is in consistency with FT-IR spectra.

3.4.3. Thermal analysis

HT/K_2CO_3 before and after calcination ranging from 0–950 °C was traced by TG-DTA. Before calcination (Fig. 5a), endothermic peaks at about 75 and 110 °C were found accompanying with a total mass loss of 6.23%, which may be because of the elimination of interlayer and weakly bound water on the surface of MgO structures without disruptions [39]. The endothermic peak at around 230 °C involving a mass loss of 11.77% was attributed to the K_2CO_3 decomposition, which might lead to the carbonate ion and further decomposition in the brucite-like layers [40]. The mass loss of approximately 21.62% ranging from 300 to 510 °C was caused by the K_2O decomposition resulting in the anionic hydroxyls between brucite-like layers [27], in which the endothermic peak at around 450 °C represented the formation of K_2O and Al–O–K during the K_2CO_3 decomposition as the main active sites required for the transesterification [41]. The last mass loss of 10.13% happened in the range of 510–900 °C, suggesting the newly-formed substances in line with both FT-IR and XRD results. The catalytic activity decreased since K_2O species and Al—O—K groups began to decompose when the calcination temperature increased over 510 °C [42]. HT/K_2CO_3 after calcination performed a good thermostability (Fig. 5b), in which the mass loss of 18.67% occurred only throughout the whole temperature range, corresponding to the loss of surface moisture.

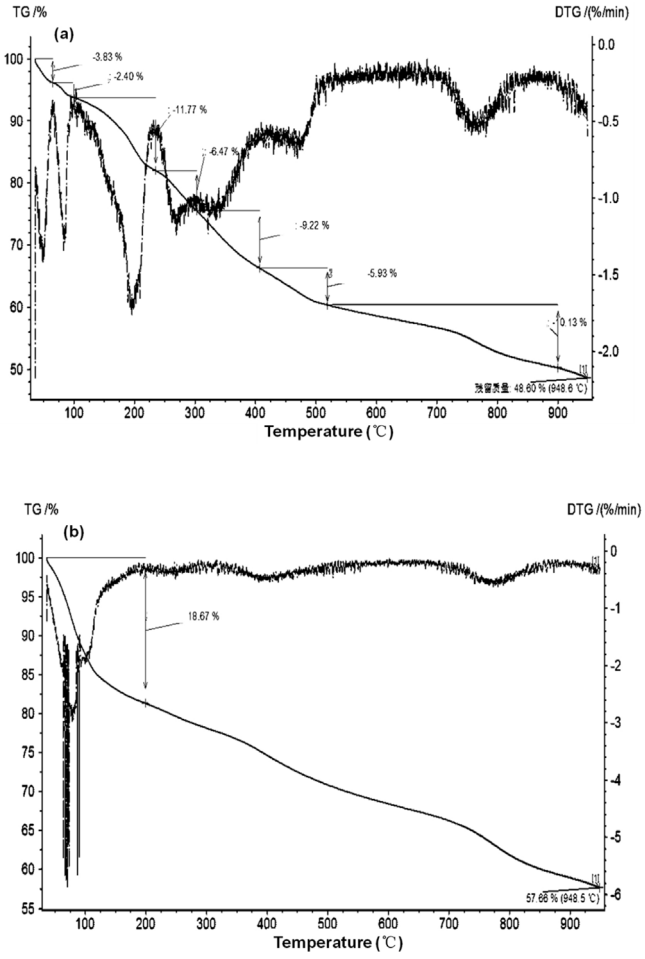

Fig. 5. Thermogravimetry/differential thermal analytical results for HT/K_2CO_3 catalysts: (a) before calcination; (b) after calcination.

Table 3
The property of HT/K_2CO_3 catalysts prepared under different conditions.

Preparation condition	Special surface area (m^2/g)	Average pore size (nm)	Total pore volume (cm^3/g)
15% K_2CO_3 at 600 °C	4.15	327.76	4.25
30% K_2CO_3 at 600 °C	16.58	38.80	16.16
30% K_2CO_3 at 500 °C	24.69	35.18	23.96

3.4.4. BET analysis

BET special surface area is recognized an important characterization of solid catalysts due to its direct relation to the catalytic activity. In Table 3, the prepared HT/K_2CO_3 catalyst under optimal conditions had a special surface area of 24.69 m^2/g with an average pore size of 35.18 nm corresponding to mesoporous (2 50 nm), which could have a better catalytic efficiency for absorbing organic macromolecules in transesterifications [43]. As the calcination temperature rose up to 600 °C, both special surface area and pore volume dramatically decreased due to the generation of metal oxides, which accords with IR, XRD and TG-DTG results. Such significant decline was also observed as the K_2CO_3 dosage decreased.

3.4.5. FESEM micrographs

The surface of HT appeared as a smooth laminated structure before and after adding K_2CO_3 (Fig. 6a, b) whereas the double-layered structures were significantly changed after calcination with numerous pores and spiculate substances on the surface (Fig. 6c). These typical needle/pillar-like structures are different from clustered spinel-like oxides formed on the calcined HT without the impregnation of metal carbonates [44], which are potential active sites or irreversible structures caused by excessive calcinations in accordance with FT-IR, XRD and TG-DTG results. On the whole, the larger special surface area and pore volume of HT/K_2CO_3 prepared under optimal conditions could improve the K^+ absorption onto the HT surface, which helped to enhance alkalinity and catalytic active sites [20]. The layered porous structure could also increase the contact area between catalysts and reactants in the catalysis. However, such structure got looser with an increased pore number as the calcination temperature rose up. The HT/K_2CO_3 calcinated at 700 °C presented a large number of compact spiculate structures on its surface due to the excessive calcinations, which led to the reduction of specific surface area closely related to the catalytic efficiency. The increasing K_2CO_3 dosage could also increase the number of pores and active sites on the HT/K_2CO_3 surface resulting in the higher

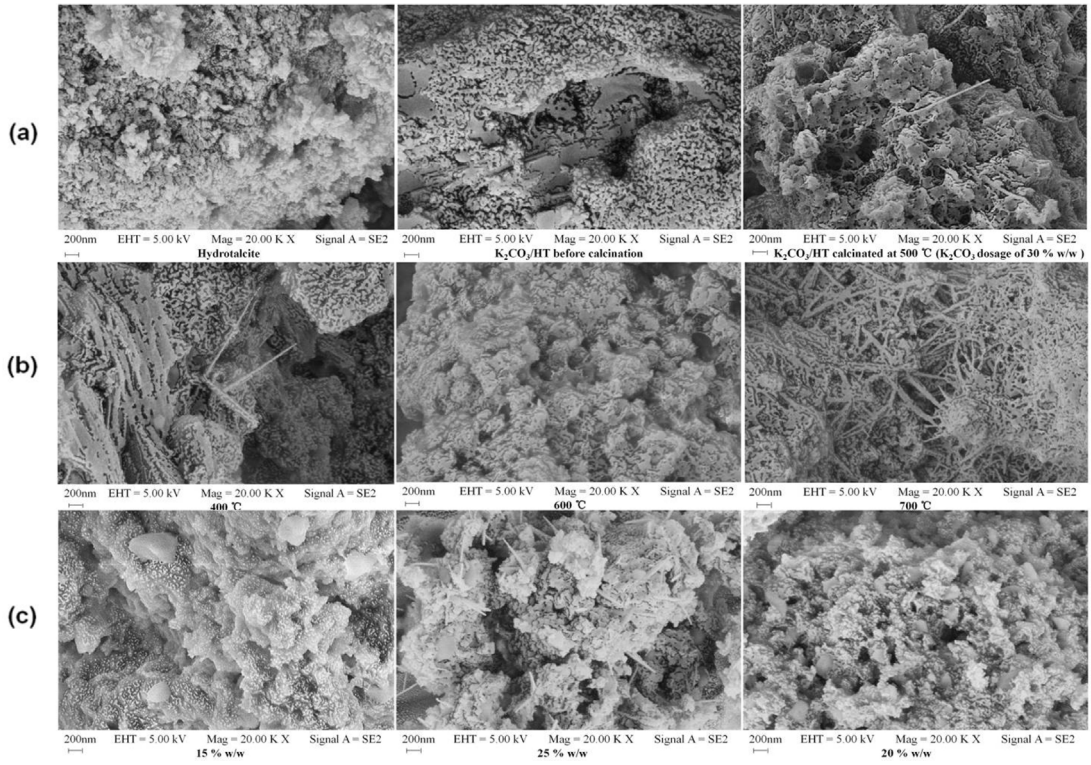

Fig. 6. Field emission scanning electron microgram: (a) HT, HT/K_2CO_3 before and after calcination; (b) HT/K_2CO_3 catalyst with K_2CO_3 dosage of 30% w/w under different calcination temperatures; (c) HT/K_2CO_3 catalyst with different K_2CO_3 dosages at the calcination temperature of 600 °C.

MFT and CRF. Nonetheless, the HT/K_2CO_3 surface began to appear spiculate structures when K_2CO_3 dosage was beyond 25%.

3.4.6. Metal ion leaching in the TFATE

The metal ion leaching of the HT/K_2CO_3 in the TFATE, potassium ion in particular, increased certainly as the K_2CO_3 dosage increased from 25 to 30% when the calcination temperature was fixed at 600 °C (Table 4). However, this ion leaching significantly decreased since the HT/K_2CO_3 catalyst prepared under optimal conditions. In the case of fixed K_2CO_3 dosage (30%), potassium ion immediately dropped from 177.4 at 600 °C to 26.9 mg/L at 500 °C, which accounts for 2.7% of total potassium ions in the HT/K_2CO_3 catalyst. As previously mentioned, potassium leaching was relevant to the hydroxyl in methanol and the solubility of potassium ion increased with the number of alcohol groups [30,43]. Hence, the dissolution of potassium ions in TMP with three hydroxyl groups is easier than that in methanol. As compared to the conventional transesterification of triglyceride with methanol, the cleaner transesterification of TMP with FAME is less destructive to catalytic active sites thus resulting in reduced ion leaching.

Table 4
The content of metal ions in the trimethylolpropane fatty acid trimesters (TFATE).

	K^+	Mg^{2+}	Al^{3+}	Na^+
25% K_2CO_3 at 600 °C	131.90 ± 0.47	54.70 ± 0.31	11.30 ± 0.28	7.49 ± 0.11
30% K_2CO_3 at 600 °C	177.40 ± 0.68	69.60 ± 0.42	10.60 ± 0.33	8.61 ± 0.15
30% K_2CO_3 at 500 °C	26.92 ± 0.13	3.60 ± 0.10	0.31 ± 0.07	0.78 ± 0.02

Values are presented as means ± standard deviation of triplicate.

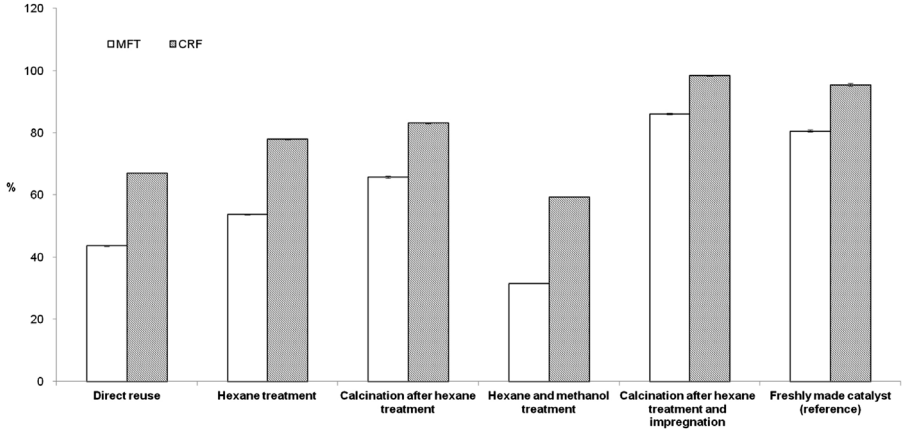

Fig. 7. The effect of different reactivation methods on the efficiency of recycled HT/K_2CO_3 catalyst regarding mass fraction of trimethylolpropane fatty acid triester (MFT) and conversion rate of fatty acid methyl ester (CRF).

3.5. Recycling of HT/K_2CO_3 catalysts

As depicted in Fig. 7, the HT/K_2CO_3 catalyst after hexane treatment obtained 10.89% higher CRF than direct reuse of the recycled catalysts, in which residual TFATE and soap could block catalytic active sites. The calcinated recycled catalyst after hexane treatment increased the CRF by 5.16% as compared to that without calcination. The high-temperature calcination could not only eliminate side products and water that negatively affect the catalyst, but also reactivate the active sites so as to increase the catalytic efficiency. The recycled catalyst after hexane and methanol treatment had the poorest MFT and CRF that may attribute to more potassium leaching caused by methanol washing, residual water in methanol, CO_2 and moisture reacted with $KHCO_3$ [30,42]. The catalyst reactivated by impregnation and calcinations after hexane treatment performed the best overall with MFT of 86.12% and CRF of 98.4%, which was even better than freshly made catalyst. This could be explained by the fact that the impregnation of more K_2CO_3 to the HT with some remaining active sites after hexane washing implies the formation of more catalytic active sites after calcination. For reactivation by calcinating the washed catalyst, the MFT increased from 22.21 to 42.58% in comparison with the reactivated catalysts by washing only without calcination (10.13%).

4. Conclusion

HT/K_2CO_3 catalyst, prepared with 30% of K_2CO_3 dosage at 500 °C under the optimal transesterification conditions, has been proved as a promising heterogeneous solid base catalyst for biolubricant base oil production from waste cooking oils accompanying with the highest MFT (93.9%) and CRF (97.7%) and the lowest potassium leaching. Furthermore, active sites and irreversible structures on the surface of HT/K_2CO_3 catalysts in various states were characterized for better understanding the catalytic mechanism. Besides, calcination was investigated to be necessary to reactivate catalysts for obtaining a satisfactory recycling.

Conflict of interest

The authors have declared no conflict of interest.

Acknowledgements

This work was supported by the Program for New Century Excellent Talents in University (Grant NECT-12-0675), Guangdong Provincial Department of Science and Technology (Grant 2012A03230016 and 2012B050600005) and the Fundamental Research Funds for the Central Universities (Grant 21612434).

References

[1] S.Z. Erhan, B.K. Sharma, Z. Liu, A. Adhvaryu, Lubricant base stock potential of chemically modified vegetable oils, J. Agric. Food. Chem. 56 (2008) 8919–8925.
[2] Global Market for Lubricating Oils and Greases to Reach 10.9 Billion Gallons by New Reports by Global Industry Analysts, Inc., 2012, http://www.prweb.com/releases/lubricatingoils/lubricants reases/prweb9351336.htm, (Accessed 29 November 2016).
[3] H.A. Hanmid, R. Yunus, U. Rashid, T.S.Y. Choong, A.H. Al-Muhtaseb, Synthesis of palm oil-based trimethylolpropane ester as potential biolubricant: chemical kinetics modelling, Chem. Eng. J. 200 (2012) 532–540.
[4] S. Gryglewicz, M. Muszynski, J. Nowicki, Enzymatic synthesis of rapeseed oil-based lubricants, Ind. Crop. Prod. 45 (2013) 25–29.
[5] P. Nagendramma, S. Kaul, Development of ecofriendly/biodegradable lubricants: an overview, Renew. Sust. Energy Rev. 16 (2012) 764–774.
[6] B. Wilson, Lubricants and functional fluids from renewable sources, Ind. Lubr. Tribol. 50 (1998) 6–15.
[7] J.R. Steven, Synthetics, mineral oils, and bio-based lubricants: chemistry and technology, in: R.L. Rudnick (Ed.), Chemical Industries, CRC Press, Boca Raton, 2006, pp. 47–74.
[8] R. Yunus, A. Fakhru'l-Razi, T.L. Ooi, D.R.A. Biak, S.E. Iyuke, Kinetics of transesterification of palm-based methyl esters with trimethylolpropane, J. Am. Oil Chem. Soc. 81 (2004) 497–503.
[9] Y.Y. Linko, X.Y. Wu, Biocatalytic production of useful esters by two forms of lipase from *candida rugose*, J. Chem. Technol. Biotechnol. 56 (1996) 163–170.
[10] E. Uosukainen, Y.Y. Linko, M. Lämsä, T. Tervakangas, P. Linko, Transesterification of trimethylolpropane and rapeseed oil methyl ester to environmentally acceptable lubricants, J. Am. Oil Chem. Soc. 75 (1998) 1557–1563.
[11] M. Di Serio, R. Tesser, M. Dimiccoli, F. Cammarota, M. Nastasi, E. Santacesaria, Synthesis of biodiesel via homogeneous lewis acid catalyst, J. Mol. Catal. A: Chem. 239 (2005) 111–115.
[12] M.H. Zong, Z.Q. Duan, W.Y. Lou, T.J. Smith, H. Wu, Preparation of a sugar catalyst and its use for highly efficient production of biodiesel, Green Chem. 9 (2007) 434–437.
[13] Z.Z. Yang, W.L. Xie, Y. Zuo, Application in transesterification of oil and fat via heterogeneous base catalysts, Cereal Oil 7 (2006) 13–16.
[14] L.J. Gao, G.Y. Teng, G.M. Xiao, R.P. Wei, Biodiesel from palm oil via loading KF/Ca-Al hydrotalcite catalyst, Biomass Bioenergy 34 (2010) 1283–1288.
[15] X. Deng, Z. Fang, Y.H. Liu, C.L. Yu, Production of biodiesel from jatropha oil catalyzed by nanosized solid basic catalyst, Energy 36 (2011) 777–784.
[16] H. Liu, L.Y. Su, F.F. Liu, C. Li, U.U. Solomon, Cinder supported K_2CO_3 as catalyst for biodiesel production, Appl. Catal. B: Environ. 106 (2011) 550–558.
[17] W.L. Xie, L.L. Zhao, Heterogeneous CaO–MoO_3–SBA-15 catalysts for biodiesel production from soybean oil, Energy Convers. Manag. 79 (2014) 34–42.
[18] M. Farooq, A. Ramli, D. Subbarao, Biodiesel Production from waste cooking oil using bifunctional heterogeneous solid catalysts, J. Clean Prod. 59 (2013) 131–140.
[19] N.P. Asri, S. Machmudah, Suprapto Wahyudiono, K. Budikarjono, A. Roesyadi, M. Goto, Palm oil transesterification in sub- and supercritical methanol with heterogeneous base catalyst, Chem. Eng. Process. 72 (2013) 63–67.
[20] G. Teng, L. Gao, G. Xiao, H. Liu, J. Lv, Biodiesel preparation from jatropha curcas oil catalyzed by hydrotalcite loaded with K_2CO_3, Appl. Biochem. Biotechnol. 162 (2010) 1725–1736.
[21] Z. Zhang, X. Ma, Y. Wang, R.A. Yan, M.M. Liu, Production of monoacylglycerols from fully hydrogenated palm oil catalyzed by hydrotalcite loaded with K_2CO_3, Chem. Eng. Commun. 202 (2015) 585–592.
[22] Y. Wang, S. Ma, L.L. Wang, S.Z. Tang, W.W. Riley, M.J.T. Reaney, Solid superacid catalyzed glycerol esterification of free fatty acids in waste cooking oil for biodiesel production, Eur. J. Lipid Sci. Technol. 114 (2012) 315–324.
[23] E.P. Wang, X. Ma, S.Z. Tang, R.A. Yan, Y. Wang, W.W. Riley, M.J.T. Reaney, Synthesis and oxidative stability of trimethylolpropane fatty acid triester as a biolubricant base oil from waste cooking oil, Biomass Bioenergy 66 (2014) 371–378.
[24] Y. Wang, E.P. Wang, S.Z. Tang, Z. Zhang, M.J.T. Reaney, Synthesis of trimethylolpropane fatty acid triester as biolubricant from palm-based methyl esters and trimethylolpropane, J. Chin. Cereals Oils Assoc. 28 (2013) 27–32.
[25] T.S. Chang, H. Masood, R. Yunus, U. Rashid, T.S.Y. Choong, D.R.A. Biak, Activity of calcium methoxide catalyst for synthesis of high oleic palm oil based trimethylolpropane triesters as lubricant base stock, Ind. Eng. Chem. Res. 51 (2012) 5438–5442.
[26] I. Alexandra, I.Z. Mohamed, K. Charles, Interfacial chemistry in the preparation of catalytic potassium-modified, J. Chem. Soc. Faraday Trans. 89 (1993) 2527–2536.
[27] W.L. Xie, H. Peng, L.G. Chen, Transesterification of soybean oil catalyzed by potassium loaded on alumina as a solid-base catalyst, Appl. Catal. A: Gen. 300 (2006) 67–74.
[28] I. Lukic, J. Krstic, D. Jovanovic, D. Skala, Alumina/silica supported K_2CO_3 as a catalyst for biodiesel synthesis from sunflower oil, Bioresour. Technol. 100 (2009) 4690–4696.
[29] W.L. Xie, H.T. Li, Alumina-supported potassium iodide as a heterogeneous catalyst for biodiesel production from soybean oil, J. Mol. Catal. A: Chem. 255 (2006) 1–9.
[30] D.M. Alonso, R. Mariscal, R. Moreno-Tost, M.D.Z. Poves, M.L. Granados, Potassium leaching during triglyceride transesterification using K/c-Al_2O_3 catalysts, Catal. Commun. 8 (2007) 2074–2080.
[31] G. Busca, V. Lorenzelli, Infrared spectroscopic identification of species arising from reactive adsorption of carbon oxides on metal oxide surfaces, Mater. Chem. 7 (1982) 89–126.
[32] H.A. Al-Abadleh, H.A. Al-Hosney, V.H. Grassian, Oxide and carbonate surfaces as environmental interfaces: the importance of water in surface composition and surface reactivity, J. Mol. Catal. A: Chem. 228 (2005) 47–54.
[33] F.F. Chen, F. Yang, G.H. Wang, W. Li, Calcined Zn/Al hydrotalcites as solid base catalysts for glycolysis of poly (ethylene terephthalate), J. Appl. Polym. Sci. 131 (2014).
[34] I.Z. Alexandra, Formation of carboxy species at CO/Al_2O_3 interfaces. Impacts of surface hydroxylation, potassium alkalization and hydrogenation as assessed by in situ FTIR spectroscopy, Phys. Chem. Chem. Phys. 6 (2004) 2502–2512.
[35] F. Cavani, F. Trifiro, A. Vaccari, Hydrotalcite-type anionic clays: preparation, properties and applications, Catal. Today 11 (1991) 173–301.
[36] D.G. Cantrell, L.J. Gillie, A.F. Lee, K. Wilson, Structure-reactivity correlations in MgAl hydrotalcite catalysts for biodiesel synthesis, Appl. Catal. A: Gen. 287 (2005) 183–190.
[37] M.G. Alvarez, A.M. Segarra, S. Contreras, J.E. Sueiras, F. Medina, F. Figueras, Enhanced use of renewable resources: transesterification of glycerol catalyzed by hydrotalcite-like compounds, Chem. Eng. J. 161 (2010) 340–345.

[38] J.F.P. Gomes, J.F.B. Puna, L.M. Goncalves, J.C.M. Bordado, Study on the use of MgAl hydrotalcites as solid heterogeneous catalysts for biodiesel production, Energy 36 (2011) 6770–6778.
[39] T. Wan, P. Yu, S. Gong, Q. Li, Y. Luo, 2008. Application of KF/MgO as a heterogeneous catalyst in the production of biodiesel from rapeseed oil, Korean J. Chem. Eng. 25 (2008) 998–1003.
[40] Y.H. Li, F.X. Qiu, D.Y. Yang, X.H. Li, P. Sun, Preparation, characterization and application of heterogeneous solid base catalyst for biodiesel production from soybean oil, Biomass Bioenergy 35 (2011) 2787–2795.
[41] M. Tu, J. Shen, Y. Chen, Microcalorimetric studies of Zn-Al mixed oxides obtained from hydrotalcite-type precursors, J. Therm. Anal. Calorim. 58 (1999) 441–446.
[42] C.J. Sun, F.X. Qiu, D.Y. Yang, B. Ye, Preparation of biodiesel from soybean oil catalyzed by Al-Ca hydrotalcite loaded with K_2CO_3 as heterogeneous solid base catalyst, Fuel Proces. Technol. 126 (2014) 383–391.
[43] L. Čapek, M. Hájek, P. Kutálek, L. Smoláková, Aspects of potassium leaching in the heterogeneously catalyzed transesterification of rapeseed oil, Fuel 115 (2014) 443–451.
[44] P. Liu, M. Derchi, E.J.M. Hense, Promotional effect of transition metal doping on the basicity and activity of calcined hydrotalcite catalysts for glycerol carbonate synthesis, Appl Catal. B: Environ. 144 (2014) 135–143.

APPENDIX B

Pradhan, S, J Shen, S Emami, P Mohanty, SN Naik, AK Dalai, MJT Reaney (2017) Synthesis of potassium glyceroxide catalyst for sustainable green fuel (biodiesel) production. *Journal of Industrial and Engineering Chemistry* 46, 266–272.

Journal of Industrial and Engineering Chemistry 46 (2017) 266–272

Contents lists available at ScienceDirect

Journal of Industrial and Engineering Chemistry

journal homepage: www.elsevier.com/locate/jiec

Synthesis of potassium glyceroxide catalyst for sustainable green fuel (biodiesel) production

Subhalaxmi Pradhan[a,b], Jianheng Shen[a], Shahram Emami[a], Pravakar Mohanty[c,d,*], S.N. Naik[b], Ajay K. Dalai[d], Martin J.T. Reaney[a,e,**]

[a] Department of Plant Sciences, University of Saskatchewan, Saskatoon, Saskatchewan S7N 5A8, Canada
[b] Centre for Rural Development and Technology, Indian Institute of Technology, Delhi, Hauz Khas, New Delhi 110016, India
[c] Department of Chemical Engineering, Indian Institute of Technology, Delhi, Hauz Khas, New Delhi 110016, India
[d] Department of Chemical and Biological Engineering, University of Saskatchewan, Saskatoon, Saskatchewan S7N 5A9, Canada
[e] Guangdong Saskatchewan Oilseed Joint Laboratory, Department of Food Science and Engineering, Jinan University, 601 Huangpu Avenue West, Guangzhou, Guangdong 510632, China

ARTICLE INFO

Article history:
Received 24 December 2015
Received in revised form 4 September 2016
Accepted 27 October 2016
Available online 2 November 2016

Keywords:
Potassium hydroxide
Glycerol
Potassium glyceroxide
Response surface methodology
Biodiesel

ABSTRACT

Metal hydroxides and alkoxides are used as base catalysts for biodiesel production. When metal hydroxides are dissolved in alcohol, they produce water, which can react with triglycerides (TGs) and produce free fatty acids (FFAs) rather than the desired fatty acid alkyl esters. Metal alkoxides are more expensive to produce and their transportation is hazardous. In this study, potassium alkoxide catalysts were synthesized from potassium hydroxide (KOH) solution and glycerol, which is by-product of biodiesel production process, by heating 50% KOH solution and glycerol at different mole ratios, temperatures and vacuum pressures. These operating parameters were optimized and their interactive effect on catalyst synthesis was studied by using response surface methodology (RSM). This study also focused on the development of a correlation relating the effects of these variables with drying behavior of reagents during catalyst synthesis.

The results indicated that KOH to glycerol mole ratio and vacuum pressure had the most significant effects ($P < 0.0001$) on free water mass loss during catalyst synthesis. The optimum reaction condition was KOH to glycerol mole ratio of 2:1, reaction temperature 130 °C and vacuum pressure 113 mbar. X-ray powder diffraction showed that glycerol derived alkoxide compounds were predominantly mono-potassium substituted alkoxides that occur as adducts with potassium hydroxide. The glyceroxide catalyst prepared at 3:1 mole ratio of KOH:glycerol has improved biodiesel yield to that of conventional potassium methoxide ($KOCH_3$) catalyst.

Introduction

Biodiesel is a monoalkyl ester of long chain fatty acids, produced from renewable feed stocks, such as vegetable oil or animal fats by reactions with an alcohol in the presence of a base catalyst. This alternative fuel has received favorable attention due to its origin from renewable liquids and its decreased environmental impact when compared to conventional diesel fuel.

Metal alkoxides and hydroxides are used by the biodiesel industry to produce fatty acid esters of lower alkanols by transesterification. However, hydroxides produce water when dissolved in an alcohol. In turn, water molecules react with triglycerides (TGs) to produce free fatty acids (FFA) instead of producing fatty acid ester. In this case, the FFA reacts quickly with the base catalyst to produce soap and, thereby, reduce product yield [1,2]. Alkoxides do not participate in ester hydrolysis and are, therefore, preferred to hydroxides. The major drawback of alkoxide catalysts is that they are more expensive, and their production and transportation is hazardous.

* Corresponding author at: Department of Chemical Engineering, Indian Institute of Technology, Delhi, Hauz Khas, New Delhi 110016, India. Fax: +91 11 26591121.
** Corresponding author at: Department of Plant Sciences, University of Saskatchewan, Saskatoon, Saskatchewan S7N 5A8, Canada. Fax: +1 306 966 5015.
E-mail addresses: pravakar.mohanty@gmail.com, p.mohanty@serb.gov.in (P. Mohanty), martin.reaney@usask.ca (M.J.T. Reaney).

http://dx.doi.org/10.1016/j.jiec.2016.10.038
1226-086X/

Glycerol is produced in large amounts as a co-product of biodiesel synthesis processes. In a biodiesel manufacturing plant, ~10 wt.% of triglyceride is released as the co-product glycerol that can be utilized further for value-added products. The oleochemical industry is also a major source of glycerol production, where it is obtained from splitting of triglycerides to produce fatty acids [3]. The utilization of glycerol contributes to biodiesel production economics [4]. There is a global need for technologies that efficiently convert glycerol into various value-added products. Kapicak and Schreck [5] have reported synthesis of an anhydrous basic metal salt of glycerol and used as catalysts for biodiesel production. They reported 90–98% conversion of TG to biodiesel using glycerol metal salts. Reaney and Westcott [6] have produced alkoxide catalysts by reacting aqueous metal hydroxide solutions (40–50% w/v) with polyether alcohols (polyethylene glycol and polypropylene glycol). The resulting alkoxide compounds were effective in isomerization of linoleic and linolenic acid alkyl esters to fatty esters with conjugated double bonds. This process was used for commercial synthesis of conjugated linoleic acid [7]. Reaney et al. [8] have synthesized different metal alkoxide catalysts from a series of non-toxic and non-volatile polyols. Production of potassium alkoxide catalyst from KOH solution and glycerol is not reported. The present study describes potassium glyceroxide catalyst production from low cost starting materials, i.e. 50% KOH solution and glycerol mixed at different mole ratios under different vacuum pressures and temperatures. A statistical experimental design was used to optimize reaction parameters [9,10]. In this study, reaction parameters were optimized using response surface methodology (RSM). The RSM approach was selected as it is effective for designing statistically valid experiments, building models and investigating complex processes and optimization of target values [11–13]. The objective of this study was to optimize potassium alkoxide base catalysts production from low cost starting materials including potassium hydroxide and glycerol so that optimum conditions could be used to prepare these alkoxide catalysts in biodiesel production facilities. Potassium glyceroxide catalysts were then used for fatty acid methyl ester production. It was found that the transesterification reaction rate using this catalyst was high in comparison to other base catalysts [14].

Materials and methods

Catalyst production

Alkoxide catalysts were synthesized using KOH solution and glycerol by a two-stage vacuum dehydration process. KOH solution (50 wt.%) was prepared by dissolving 2 g (0.0357 mol) of potassium hydroxide pellets (EMD Chemicals, Gibbstown, NJ, USA) in distilled water (2 g). Glycerol (EMD Chemicals) which was mixed in three different mole ratios of glycerol to produce KOH to glycerol at 1:1, 2:1 and 3:1 mole ratios. Moles of KOH were held constant (2 g or 0.0357 mol) while glycerol was added at different mole amounts of 0.0357 mol (3.287 g), 0.01785 mol (1.6438 g) and 0.0119 mol (1.0965 g) to create the desired mole ratios 1:1, 2:1 and 3:1, respectively.

Mixtures were added to a round bottom flask and the reaction was conducted in a Kugelrohr short path distillation apparatus (GKR-50, Büchi®, Flawil, Switzerland) fitted to a vacuum pump (Model V-700; Büchi) for 2 h. The reaction was carried out at different vacuum pressures (200, 113, 50 and 25 mbar) and temperatures (120, 130 and 140 °C) for 2 h to evaporate free water added in the reaction mixture with the KOH as well as water released during the formation of alkoxide catalyst. The reaction temperatures used were above the boiling point of water but below than that of glycerol. After 2 h of reaction the flask was weighed to calculate the loss of weight, which is due to water loss during the reaction of KOH and glycerol and free water added to KOH. The % of free water loss was calculated as follows:

$$\textit{free water loss}\ (\%) = \frac{\textit{Total water released}}{\textit{Free water added to}\ \mathrm{KOH}} \times 100 \quad (1)$$

Solids obtained after 2 h reaction time were further dried in a vacuum oven (Model 280A; Fischer Scientific, St. Louis, MO) at 120 °C under vacuum gauge pressure of 94.8 kPa for an additional 24 h.

Experimental design and statistical analysis

Response surface methodology (RSM) was employed to evaluate the effects of various parameters on free water mass loss during the reaction of glycerol and KOH to prepare potassium glycerolate catalyst. The experimental design for this reaction was conducted utilizing a central composite design. The total experiment number was 20 ($=2^n+2n+6$) where n is the number of independent variables. Six axial and eight factorial experimental runs were conducted with six replications at the center point to evaluate the error. The three independent variables were KOH to glycerol mole ratio (1:1–3:1) (*A*), temperature (120–140 °C) (*B*) and vacuum pressure (200–25 mbar) (*C*). All variables at zero level constitute the center point. Therefore, the lowest and the highest levels are assigned to be −1 and +1 respectively.

A second-order polynomial equation (Eq. (2)) was fitted to the experimental data using RSM (Design Expert 8.0.6) to determine the relationship between response variable (free water mass) and independent variables.

$$Y = b_{o'} + \sum_{i=1}^{n} bi \times Xi + \sum_{i=1}^{n} bii \times Xi^2 + \sum_{i=1}^{n} \sum_{j>1}^{n} bij \times XiXj \quad (2)$$

where Y is the free water mass loss; b_o, b_i, b_{ii}, b_{ij} are intercept, linear, quadratic and interaction constant coefficients, respectively; n is the number of variable factors studied and optimized in the experiment; X_i, X_j are the encoded independent variables. The Design Expert version 8.0.6 software was used for regression and graphical analysis of the experimental data. Response surfaces and contour plots were developed using fitted quadratic polynomial equations obtained from regression analysis, holding one independent variable at a constant value corresponding to the stationary point and changing the other two variables.

Catalyst characterization by powder X-ray diffraction

Dried products obtained after two-stage vacuum dehydration were analyzed by X-ray powder diffraction (XRD) [15] using a Bruker-D8 Advance, II series®, Germany equipment having a vertical diffractometer (Cu Kα radiation λ = 0.154 nm) equipped with a PW Bragg–Brentano (BB) goniometer ($\theta/2\theta$), operated at 45 kV and 40 mA. The X-ray diffractometer control stage enabled both atmosphere and temperature control, where all samples were scanned with Bragg angles between 10° and 90° using a step size (θ) of 0.046° per step having scan step time 177 s and the goniometer at a radius of 240 mm. Data were collected at ambient temperature using a Lynxeye® detector. The sample was placed in a sample holder of 2.5 cm diameter and 0.5 cm depth. The total run time for each sample was 1 h. XRD JCPDS® software was used for identifying peaks with its corresponding phases. The powder diffraction patterns of potassium glyceroxide catalysts obtained from KOH solution and glycerol were compared with those of dried powders of KOH obtained by KOH solution dehydration without glycerol. Microsoft Office Excel 2007 and Systat software Sigma Plot Version 11.2 were used to generate these diffraction patterns.

Nuclear Magnetic Resonance (NMR) spectroscopy

The dried powder samples were diluted in deuterated water, and proton Nuclear Magnetic Resonance (NMR) spectra were recorded. A known amount of each catalyst was taken and trimethylol propane (TMP) was added as an internal standard. Proton NMR spectra were recorded with a 500 MHz Avance NMR spectrometer (Bruker BioSpin Corporation, Billerica, MA) equipped with a 5 mm ^{1}H NMR probe (spectral width: 10,330.58 Hz; data points: 32,768; pulse width: 6.05 μs at 90°; pulse delay: 1.79 s and number of scans: 128) [16]. The unprocessed free induction decay (fid) data were then converted into frequency domain by Fourier transform (ACD Labs version 11).

Results and discussion

Potassium glyceroxide catalyst synthesis

Solid products obtained after the first stage of vacuum dehydration were hygroscopic white powders. During catalyst synthesis, glycerol dehydration occured in the presence of KOH to produce potassium glyceroxide catalyst. About 2.75 g of water was released during the 2 h reaction between KOH (2 g) and glycerol (3.29 g). Total water released by reaction of 50% KOH solution and glycerol was more than the water (2 g) added to the reaction with the KOH solution. Additional H_2O (0.75 g) was released by the reaction of hydroxyl groups in glycerol with KOH. Brönsted acid–base theory may be used to describe this alkoxide producing reaction. In this reaction, glycerol served as an acid (proton donor); whereas, —OH of KOH served as base (proton acceptor). Lawrance et al. [17] stated that polyols compete with water molecules to dissolve cations in neutral aqueous solution. However, the alkaline medium enables alcoholic hydroxyl group deprotonation. After reaction, polyols behave as a much stronger base with the ability to bind with metal ions to afford metal alkoxide [18]. Mono substituted carbohydrate alkoxides were formed by reaction of lithium, sodium, potassium and caesium hydroxides with simple non-acidic sugar alcohols at room temperature in anhydrous alcoholic media. The metal ion attached to the deprotonated hydroxyl moiety is chelated to neighboring donor groups such as vicinal hydroxyl moieties within the same sugar alcohol structure.

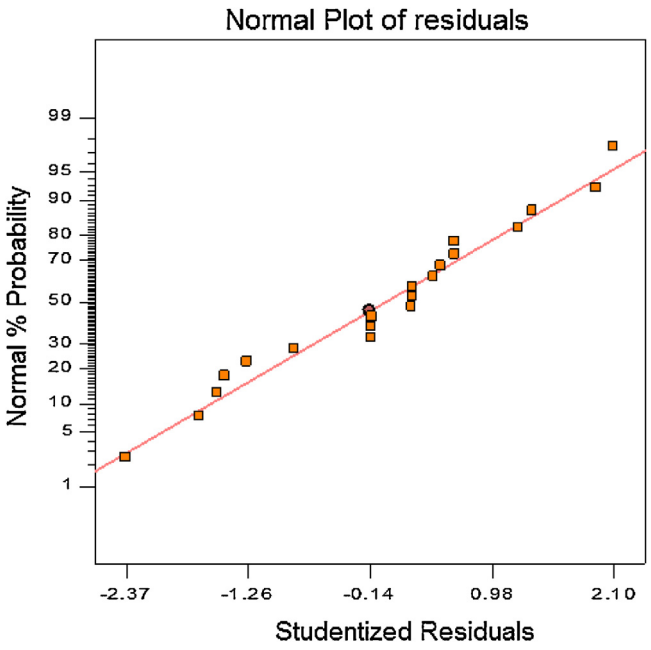

Fig. 1. Normal plot of residuals for free water mass loss.

So chelation increases metal alkoxide stability and, subsequently, acts as a driving force to enhance alkoxide formation [19]. Since glycerol has three adjacent hydroxyl donor groups, metal alkoxide compound formation is promoted by intermolecular metal chelation.

Response surface methodology and regression analysis

Table 1 presents free water loss at different mole ratios, temperatures and vacuum pressure. Normal probability of the residuals was determined by a normal probability plot (Fig. 1).

A quadratic polynomial equation was obtained from the experimental data and the following equation was generated to

Table 1
Experimental design matrix and results.

Std.	Run	Factor 1 A: mole ratio of KOH to glycerol	Factor 2 B: temperature (°C)	Factor 3 C: vacuum pressure (mbar)	Response 1 Free water loss (%)
3	1	1	140	25	98.1
1	2	1	120	25	97.4
9	3	1	130	113	94.2
5	4	1	120	200	87.5
17	5	2	130	113	85.6
16	6	2	130	113	86.2
14	7	2	130	200	65.6
11	8	2	120	113	84.5
12	9	2	140	113	86.8
4	10	3	140	25	89.5
2	11	3	120	25	88.3
10	12	3	130	113	78.4
19	13	2	130	113	85.4
8	14	3	140	200	69.6
7	15	1	140	200	94.3
20	16	2	130	113	84.8
6	17	3	120	200	51.6
13	18	2	130	25	92.7
15	19	2	130	113	84.7
18	20	2	130	113	86.5

Table 2
Analysis of variance (ANOVA) for response surface quadratic model [12,13,23].

Source of variation	Sum of squares	Degree of freedom (DF)	Mean square	F value	P-value
Model	2326.5	9	258.5	33.4	<0.0001
Mole ratio of KOH to glycerol (A)	902.5	1	902.5	116.7	<0.0001
Temperature (B)	84.1	1	84.1	10.9	0.0080
Vacuum pressure (C)	960.4	1	960.4	124.2	<0.0001
A^2	19.8	1	19.8	2.6	0.1409
B^2	7.8	1	7.78	1.0	0.3396
C^2	63.8	1	63.8	8.3	0.0166
AB	15.1	1	15.1	2.0	0.1922
AC	231.1	1	231.1	29.9	0.0003
BC	66.1	1	66.1	8.6	0.0152
Residual	77.3	10	7.7		
Lack of fit	73.3	5	14.7	18.3	0.0031
Pure error	4	5	0.8		
Cor total	2403.8	19			

C.V. = 3.3%, R^2 = 0.9678, Adj R^2 = 0.9388.

predict free water mass loss, as shown below (in terms of the code factors):

$$\textit{Free water loss} = 84.3272 - 9.5A + 2.9B - 9.8C + 2.6818A^2 + 1.6818B^2 - 4.81818C^2 + 1.375AB - 5.375AC + 2.875BC \quad (3)$$

The results of ANOVA based fitting of the second order response surface model are summarized in Table 2. The high F-value (F_{model} = 33.4) with very low probability value ($P < 0.0001$) indicates a high significance of the fitted model. The significance of each of the coefficients are determined from *P*-values (probability of error value), which also indicate the interaction strength of each parameter. In linear terms, mole ratio, temperature and vacuum pressure (*P*-value ≤ 0.0001) and in quadratic terms, squared vacuum pressure (*P*-value = 0.0166) made most significant contribution to the fitted model. The first order interaction of mole ratio × vacuum pressure (*P*-value = 0.0003) and temperature × vacuum pressure (*P*-value = 0.02) are statistically significant. The smaller the *P* value for a parameter the more significant it is, hence reflecting the relative importance of the term attached to that parameter [20]. The effects of A, B, C, C^2, AC ($P < 0.01$) and BC ($P < 0.02$) were statistically significant in the model. The quality of the model fit was evaluated by the coefficient of determination (R^2), this value being calculated to be 0.97 for the response. Fig. 2 represents predicted values versus actual values for free water mass loss. The responses predicted from the empirical model were close to experimental data, indicating that the model was successful in capturing correlations between reaction variables and free water mass loss. As the fitted model Eq. (3) provides a good approximation to experimental data, the model was employed to find process variable values for maximum free water mass loss.

Model analysis and influence of parameters on free water loss

Regression analysis indicated that water loss during the reaction was affected by KOH to glycerol mole ratio (A), temperature (B), vacuum pressure (C) and its respective highest order term (C^2). The interaction effects of mole ratio × vacuum pressure (A × C) and temperature × vacuum pressure (BC) are found to be more significant than mole ratio × temperature (A × B). The plots representing the effects of independent and dependent variables for different fixed parameters are shown in Figs. 3–5 . It is found that at lower KOH to glycerol mole ratios the free water loss increased with increasing temperature. However, increasing the mole ratio from 1:1 to 3:1 resulted in a decrease in free water mass loss with increase in temperature (Fig. 3). Therefore, the greatest dehydration is obtained at lowest KOH to glycerol mole ratio and at

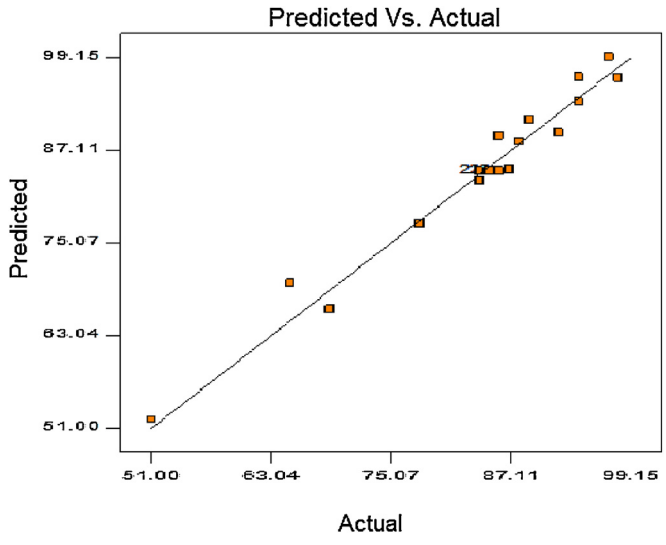

Fig. 2. Predicted versus actual free water mass loss.

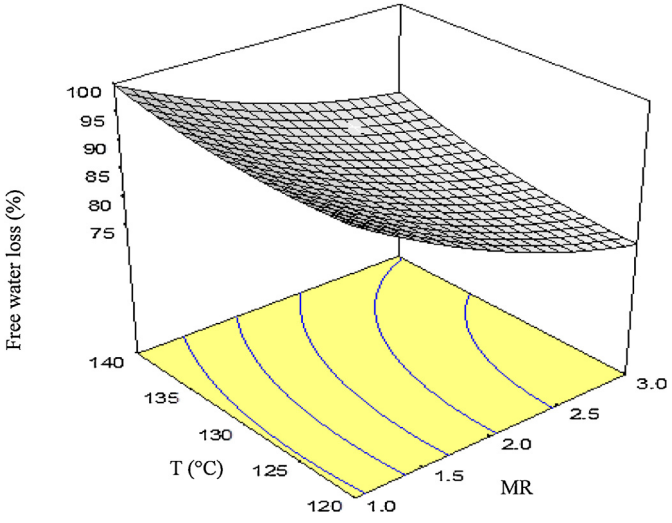

Fig. 3. Combined effects of mole ratio (MR) and temperature (T, °C) on free water mass loss during reaction of KOH and glycerol under vacuum at constant pressure of 113 mbar at reaction time of 2 h.

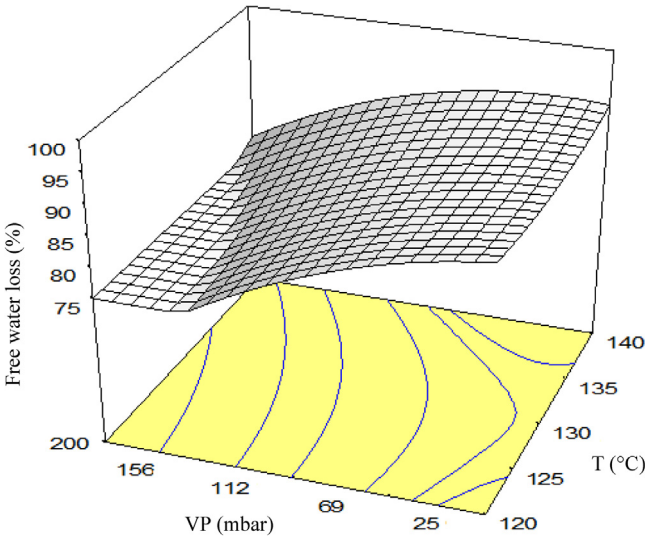

Fig. 4. Combined effects of vacuum pressure (VP, mbar) and temperature (T, °C) on free water mass loss during reaction of KOH and glycerol at constant mole ratio of 2:1 (KOH:glycerol) at reaction time of 2 h.

highest temperature of 140 °C. This trend indicates that the presence of greater amounts of glycerol improved catalyst dehydration. Multiple hydroxyl moieties in glycerol have the enable water removal by providing multiple metal-binding sites. The catalyst prepared from 1:1 mole ratio of base:polyol had relatively lower reaction rates during transesterification in comparison with those prepared with 2:1 and 3:1 ratios and may not be preferred for biodiesel synthesis [21]. The authors have produced biodiesel using potassium glyceroxide catalysts prepared at three different mole ratios and catalyst transesterification reactivity follows the order KOH:Gly (1:1) <KOH:Gly (2:1) <KOH: Gly (3:1) [14]. Dehydration rates for different mole ratios of aqueous KOH to glycerol solution were in the order of 1:1 > 2:1 > 3:1. Though the catalyst prepared at high mole ratio of glycerol and KOH (KOH:Gly (1:1)) is a dried catalyst but

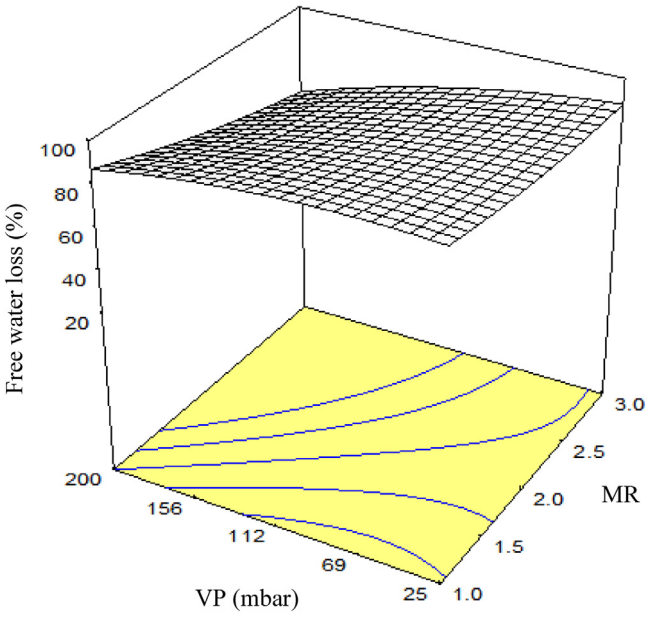

Fig. 5. Combined effects of mole ratio (MR) and vacuum pressure (VP, mbar) on free water mass loss during reaction of KOH and glycerol at constant temperature of 130 °C at reaction time of 2 h.

decreases the reactivity toward biodiesel production due to formation of glycerol esters at initial stage of the reaction. Therefore, catalyst prepared at 2:1 mole ratio is efficient as it enhances the reaction rate during biodiesel production and produces better dried catalyst during synthesis.

Effects of temperature and vacuum pressure and their combined interaction on free water mass loss during reaction at a constant mole ratio of 2:1 (KOH:glycerol) are provided in Fig. 4. At lower vacuum pressure (200 mbar) water loss increased with increasing temperature. A similar pattern was noted with increasing reaction temperature and vacuum pressure. Therefore, increasing temperature and vacuum improves the dehydration rate, indicating that interactions of temperature and vacuum pressure are significant factors.

Effects of mole ratio and vacuum pressure and their combined interactions on free water loss during reaction at 130 °C is depicted in Fig. 5. Water loss increased at a constant temperature as mole ratio decreased and vacuum pressure increased. At vacuum pressure water boiling point decreases and removal of free water added to the reaction medium as well as the binding water produced from the reaction is more efficient resulting in more free water loss.

Process optimization

Optimal values of the selected variables were obtained by solving the regression equation (Eq. (3)). A predicted optimal value obtained from the model equation was a KOH to glycerol mole ratio of 2:1, a reaction temperature of 130 °C and vacuum pressure of 113 mbar. The model predicted that the maximum free water loss that can be obtained under these optimum conditions is 84.3%. To verify the model predictions, the optimum response variables were tested under the following conditions; KOH to glycerol mole ratio of 2:1, reaction temperature of 130 °C and vacuum pressure of 113 mbar. The free water mass loss from the experiment is 85.4%, which is very close to the model prediction.

Potassium glyceroxide catalyst powder diffraction

Powder diffraction patterns of three catalysts prepared at different mole ratios (1:1, 2:1 and 3:1) of KOH to glycerol were compared with that of KOH (Fig. 6). The catalyst XRD patterns obtained at three different mole ratios were comparable and the respective patterns matched closely. Catalyst XRD patterns also shared some peaks observed in the KOH powder diffraction

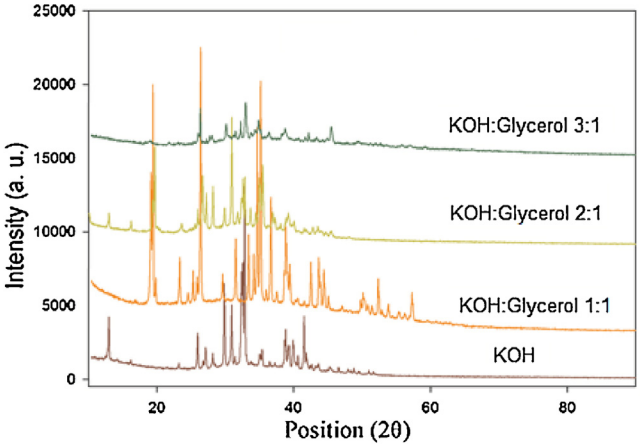

Fig. 6. X-ray powder diffraction patterns of KOH and potassium glycerolate catalyst obtained at different KOH to glycerol mole ratios.

spectrum. Therefore the compounds contain potassium glyceroxide [CH_2(OH)–CH(OH)–CH_2OK] and varying amounts of KOH. Additional peaks observed might be attributed to potassium glyceroxide derivatives, di or tripotassium glyceroxide, or KOH × *n* H_2O compounds. In case of 1:1 mole ratio, deprotonation of glycerol occurs with the loss of an —OH group from KOH forming mono potassium glyceroxide [CH_2(OH)–CH(OH)–CH_2OK] [22] and releasing a molecule of water. At the end of the reaction free water added to the reaction and the binding water formed from the reaction are lost. But in case of 2:1 and 3:1 mole ratios, the product formed contains potassium glyceroxide, varying amount of potassium hydroxide and some water, as KOH binds with water molecule due to hygroscopic nature of KOH.

NMR analysis

^{1}H NMR spectra of the catalyst prepared at 1:1 mole ratio is shown in Fig. 7. The —CH_3 proton of TMP appeared as a triplet at 0.75 ppm and —CH_2 proton at 1.21 ppm (quartet). The resonance at 3.5 ppm represented —CHO proton of glycerol. Two other proton resonances attributed to glycerol appear at 3.4 ppm and 3.3 ppm. The —CHOH proton of glycerol is integrated with both —CH_2 and —CH_3 protons of TMP. The NMR spectra of all the three different catalysts are similar but the integration value of —CHOH proton of glycerol was different. The glycerol amount in each catalyst was calculated by NMR integration of the NMR spectra. It is found that residual glycerol was present in the products.

Activity of potassium glyceroxide catalyst for biodiesel production and industrial importance

Potassium glyceroxide catalyst 0.36 wt.% efficiently produced biodiesel at a yield comparable with potassium methoxide catalyst at 0.5 wt.% [14]. The glyceroxide catalyst prepared at 3:1 mole ratio of KOH:glycerol achieved superior biodiesel yield to that of conventional potassium methoxide ($KOCH_3$) catalyst under the same reaction conditions. At 120 s after adding catalyst, the reactions achieved a yield of 74.3%–78.9%, which was similar to that catalyzed by $KOCH_3$ catalyst (77.9%). Potassium glyceroxide catalysts prepared from 2:1 and 3:1 mole ratios of KOH and glycerol have similar reaction rates when compared with reactions catalyzed by $KOCH_3$ and reaction yields are comparable. Similar biodiesel yield was recorded for all catalysts (94–96%) after 1.5 h of reaction but the rate of the reaction is high in first two minutes. In this study, low cost potassium alkoxide base catalysts were synthesized from 50 wt.% potassium hydroxide solution and non-toxic glycerol using an alternative route which is less expensive and hazardous. The catalyst production process is convenient and safer and glyceroxides can be easily prepared at the site of biodiesel production. The glycerol-derived potassium alkoxide catalyst has promising qualities for use by the biodiesel industry. This catalyst may serve as an alternative solution to lower the cost of biodiesel plant operation without compromising production efficiency.

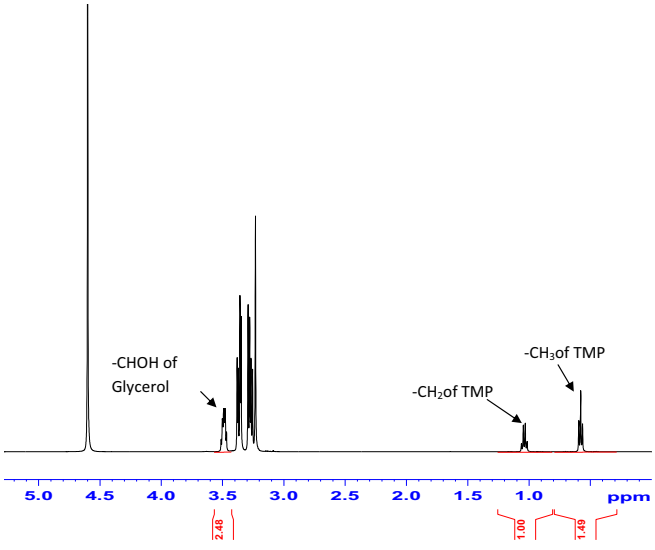

Fig. 7. ^{1}H NMR spectra of the catalyst prepared from KOH and glycerol at 1:1 mole ratio.

Conclusions

Glycerol derived alkoxide base catalysts were prepared by heating aqueous potassium hydroxide solutions with glycerol at different mole ratios under vacuum pressure. The interaction effects of mole ratio of KOH to glycerol and vacuum pressure on free water loss were more significant than interaction effect of temperature and vacuum pressure. Temperature has significant effect at lower vacuum pressure, and at higher vacuum pressure, temperature has negligible effect on free water loss of the reaction. Quadratic polynomial models were obtained to predict free water mass loss during the reaction. An optimized condition for catalyst synthesis is a KOH to glycerol mole ratio of 2:1, a temperature of 130 °C and vacuum pressure of 113 mbar. Powder diffraction analysis of the catalyst confirmed that catalyst prepared at 1:1 mole ratio contained mono-potassium glyceroxide while products produced at higher mole ratios contained mono-potassium glyceroxide with varying amounts of KOH. The synthetic method presented in this study was an efficient way to produce strong alkoxide base catalysts from the by-product glycerol derived from biodiesel production process. This process would addition value to glycerol as well as reduce the cost of biodiesel production.

Acknowledgments

Authors thank financial support provided by the Canadian Bureau for International Education (CBIE), on behalf of the Dept. of Foreign Affairs and International Trade Canada (DFAIT). The grant was given under Graduate Student Exchange Program (GSEP) Fellowship to Subhalaxmi Pradhan. Presently P. Mohanty is working as Scientist at Science and Engineering Research Board (Statutory Body Established Through an Act of Parliament: SERB Act 2008), Department of Science and Technology, Government of India, whereas this work was carried out during GSEP Fellowship period.

References

[1] H.N. Basu, M.E. Norris, US Patent 5, 1996, 525:126.
[2] K.S. Liu, J. Am. Oil. Chem. Soc. 71 (1994) 1179.
[3] L.R. Morrison, in: R.E. Kirk, D.F. Othmer (Eds.), Encyclopedia of Chemical Technology, John Wiley & Sons, Inc., New York, 2000.
[4] E. Engelhaupt, Environ. Sci. Technol. 41 (2007) 5175.
[5] L.A. Kapicak, D.J. Schreck, US Patent 2010/0048941 A1, 2008.
[6] M.J.T. Reaney, N.D. Westcott, WO 2007/022621 A2.
[7] M.J.T. Reaney, Y.D. Liu, N.D. Westcott, US Patent 6, 2002, 414:171.
[8] M.J.T. Reaney, J. Shen, D.W. Soveran, US 2010/0305344 A1.
[9] G.T. Jeong, D.H. Park, Appl. Biochem. Biotechnol. 156 (2009) 431.
[10] E. Ryantin, M.B. Mohd, B.A. Rahman, A.B. Salleh, R.N.Z.A. Rahman, Enzym. Microb. Technol. 37 (2005) 739.
[11] S. Demirkol, H.A. Aksoy, M. Tuter, G. Ustum, D.A. Sasmaz, J. Am. Oil. Chem. Soc. 83 (2006) 929.
[12] U. Rashid, F. Anwar, T.M. Ansari, M. Arif, M. Ahmad, J. Chem. Technol. Biotechnol. 84 (2009) 1364–1370.
[13] S. Pradhan, C.S. Madankar, P. Mohanty, S.N. Naik, Fuel 97 (2012) 848.
[14] S. Pradhan, J. Shen, S. Emami, S.N. Naik, M. Reaney, Eur. J. Lipid Sci. Technol. 116 (2014) 1590.

[15] S.K. Das, P. Mohanty, S. Majhi, K.K. Pant, Appl. Energy 111 (2013) 267.
[16] S. Nanda, P. Mohanty, J.A. Kozinski, A.K. Dalai, Energy Environ. Res. 4 (2014) 21.
[17] G.A. Lawrance, M.J. Robertson, Sutrisno, E.I. von Nagy-Felsobuki, Inorg. Chim. Acta 328 (2002) 159–168.
[18] M. Pospĺsilová, M. Polásek, J. Procházka, J. Chromatogr. A 772 (1997) 277.
[19] J.A. Rendleman, J. Org. Chem. 31 (1996) 1839.
[20] A.I. Khuri, J.A. Cornell, Response Surfaces: Design and Analysis, Marcel Dekker, New York, 1987.
[21] H.Y.F. Gok, S. Emami, J. Shen, M.J.T. Reaney, J. Am. Oil Chem. Soc. 90 (2013) 299.
[22] G. Schatte, J. Shen, M. Reaney, R. Sammynaiken, Acta Cryst. Sect. E 67 (2011) m141.
[23] G.J. Myung, K.K. Deog, C.P. Soon, S.L. Jin, W.K. Seung, Renew. Energy 42 (2012) 99.

APPENDIX C

Dhabhai, R, E Ahmadifeijani, AK Dalai, MJT Reaney (2016) Purification of crude glycerol using a sequential physico-chemical treatment, membrane filtration, and activated charcoal adsorption. *Separation and Purification Technology* 168, 101-106.

Separation and Purification Technology 168 (2016) 101–106

Contents lists available at ScienceDirect

Separation and Purification Technology

journal homepage: www.elsevier.com/locate/seppur

Purification of crude glycerol using a sequential physico-chemical treatment, membrane filtration, and activated charcoal adsorption

Ravi Dhabhai [a], Elahe Ahmadifeijani [a,b], Ajay K. Dalai [a,*], Martin Reaney [c,d]

[a] Department of Chemical and Biological Engineering, University of Saskatchewan, SK S7N 5AN, Canada
[b] School of Chemistry, College of Science, University of Tehran, Tehran 14174, Iran
[c] Department of Plant Sciences, University of Saskatchewan, SK S7N 5AN, Canada
[d] Guangdong Saskatchewan Oilseed Joint Laboratory, Department of Food Science and Engineering, Jinan University, 601 Huangpu Avenue West, Guangzhou, Guangdong 510632, China

ARTICLE INFO

Article history:
Received 3 March 2016
Received in revised form 25 May 2016
Accepted 26 May 2016
Available online 27 May 2016

Keywords:
Crude glycerol
Glycerol purification
Physico-chemical treatment
Membrane filtration

ABSTRACT

The presence of impurities decreases the economic value of glycerol. Thus, glycerol impurities must be greatly reduced if it is to be used as a fuel or feedstock for chemicals. A sequential procedure for crude glycerol refining that includes saponification, acidification, neutralization, membrane filtration, solvent extraction, and activated charcoal adsorption was investigated in the present work. Membrane filtration was studied at temperature and pressure ranges of 25–60 °C and 50–350 kPa, respectively. A range of ultra-filtration (UF) and fine ultra-filtration (UFF) ceramic membranes (molecular weight cut off 1, 3, 5, 8, and 15 kDa) were utilized to obtain highly enriched glycerol. Membrane filtration at 60 °C and 350 kPa using 1 kDa membrane, followed by solvent and water evaporation, and activated charcoal treatment produced the maximum glycerol content (97.5 wt%). Acid value and free fatty acid (FFA) content of all treated samples were found to be <1.1 and <0.6 wt%, respectively. Crude, enriched crude (purified), and ACS grade glycerol were characterized using FTIR and bomb calorimeter which further confirmed the glycerol purity. The present study shows the potential of this treatment for crude glycerol purification.

1. Introduction

Over the last few years, global increase in biodiesel production due to strong governmental policies and incentives has also led to increased production of the main by-product of the process - glycerol [1,2]. Glycerol, also called as glycerine, 1,2,3- propanetriol, glyceritol, glycyl alcohol and 1,2,3-trihydroxypropane, is an organic substance with molecular formula $C_3H_8O_3$. It is a biodegradable, colorless, hygroscopic, nontoxic, odorless, transparent, and viscous liquid [3].

Glycerol is obtained as a co-product of four different processes-transesterification (biodiesel production); saponification (manufacture of soap); hydrolysis for fatty acid production; and microbial fermentation [1,4,5]. Most glycerol produced, is obtained from homogenous catalytic transesterification reactions and glycerol arising from this source is termed crude glycerol. It typically contains, (in addition to glycerol), matter organic non glycerol (MONG), inorganic salts due to unspent catalyst, and water [6]. MONG might contain free fatty acids (FFA), residual fatty acid methyl ester (FAME), glycerides, and alcohol (generally methanol or ethanol) [6].

Crude glycerol has limited applications and is inexpensive compared to pure glycerol. Pure glycerol has more than a thousand uses as an important industrial feedstock in food, pharmaceutical, and chemical products [3]. Other promising uses are as fuel or fuel additive [7]. Applications of crude glycerol might be limited due to the presence of salt and impurities and its fuel value is also marginal [4]. Purification increases its value and helps to improve economic viability of the biodiesel production [1,5]. During the last 10–15 years, with increased glycerol production, crude glycerol prices have declined significantly (~$0.1/kg), while pure glycerol prices are more stable (~$1/kg) [5]. Furthermore, it has been predicted that by 2024, global glycerol production will be about 6 million tons i.e. triple of that of 2013 [8].

Abbreviations: AC, activated carbon; ACS, American Chemical Society; FAME, fatty acid methyl ester; FCC, Food Chemical Codex; FFA, free fatty acid; FID, flame ionization detector; FTIR, Fourier transform infrared; GC, gas chromatography; MONG, matter organic non glycerol; MWCO, molecular weight cut off; SFA, saponified fatty acid; USP, United States Pharmacopeia.

* Corresponding author.
E-mail address: Ajay.Dalai@usask.ca (A.K. Dalai).

http://dx.doi.org/10.1016/j.seppur.2016.05.030
1383-5866/

Glycerol quality is defined by the grade (by wt%). Glycerol of 95% concentration is called technical grade, a term most commonly used in industries for variety of chemical products that are not employed for food uses. USP (United States Pharmacopeia) grade (96–99%) glycerol can be used for food or pharmaceuticals production, while USP/FCC (Food Chemical Codex) Kosher glycerol (99.7%) is mainly used for kosher foods [8]. Crude glycerol is purified by distillation, ion-exchange, and physico-chemical treatments such as filtration, saponification, acidification, neutralization, extraction and adsorption [9]. Simple distillation cannot be used for glycerol, as it is prone to thermal degradation (polymerization, dehydration, or oxidation at varying high temperature conditions) [1]. However, due to the high specific heat of glycerol and its heat of vaporization, vacuum distillation is an energy-intensive process that leads to high-energy input requirements for elevating temperature and evaporating the glycerol [10]. Furthermore, the high salt content of biodiesel glycerol makes ion-exchange an uneconomical process [11]. Chemical treatment (acidification) at low pH is a better option, as it can increase the glycerol content and reduce the ash content in the recovered glycerol. However, it might lead to a higher MONG content in the enriched glycerol [12].

Membrane technology has a great potential as it can provide solutions for many environmental problems by recovering valuable products as well as treating effluents and minimizing their harm to the atmosphere [13]. A combination of physico-chemical process and membrane filtration can enhance glycerol purification efficiency. Ceramic membranes are potential alternatives to conventional membranes due to their high thermal, chemical and mechanical stability [14]. The use of ultrafiltration ceramic membranes for glycerol purification is relatively new and offers some potential advantages such as - ease of operation, robustness, and efficiency over other methods.

Saifuddin et al. [11] combined physico-chemical treatments followed by adsorption onto dead yeast cells immobilized on chitosan. The final glycerol concentration was 93.1–94.2% (w/w). Another study reported a glycerol content of 95.7% (wt) with the sequential acidification to pH 2.5 with H_3PO_4 and phase separation, followed by extraction with propanol as a solvent: crude glycerol ratio of 2:1 (v/v) [10]. Kongjao et al. [15] reported a glycerol concentration of >93 wt% with 5.2 wt% MONG and almost no ash with physico-chemical treatments at low pH using 1.19 M H_2SO_4. Recently, a continuous-effect membrane distillation process was employed to concentrate 10 g/l aqueous glycerol solution to 400 g/l with a rejection efficiency greater than 99.9% [16].

In the present work, crude glycerol was purified using a sequential physico-chemical treatment, membrane filtration, solvent removal, and activated charcoal adsorption. Membrane filtration was studied at different membrane module temperature (25–60 °C), trans-membrane pressure (50–350 kPa) for different pore size ceramic membranes (1–15 kDa molecular weight cut off). The aim of this work was to obtain technical grade glycerol (~95 wt% purity). To the best of our knowledge, no systemic purification study has been conducted using membranes for producing technical grade glycerol from crude glycerol.

2. Experimental

2.1. Materials

Crude glycerol samples were obtained from Milligan Biofuels, Foam Lake, SK, Canada, while ACS grade glycerol (99.5% wt% purity) was purchased from Fisher scientific, Canada. Ceramic membrane discs DISRAM™ (diameter 47 mm; area 13.1 cm^2) composed of ZrO_2—TiO_2 with TiO_2 support and membrane disc holder were purchased from Tami industries, France. The molecular weight cut off (MWCO) of the ceramic membranes was in the range of 1–15 kDa (kg/mol). All other chemicals were analytical grade, unless otherwise stated.

2.2. Physico-chemical treatment of crude glycerol (step 1)

Physico-chemical treatments included sequential saponification, acidification, phase separation, and extraction. Crude glycerol was first diluted to about 10 wt% glycerol using methanol to reduce viscosity and improve the ease of operation. Then, KOH (12.5 M) was added to convert FFA to soaps (saponification) at 60 °C for 30 min with constant stirring till pH 12.0. Subsequently the alkaline mixture was acidified to pH 1.0 by addition of concentrated HCl. After acidification, samples were stirred for 30 min at room temperature (25 °C) then left overnight in a separatory funnel to allow time for phase separation. Separation produced two phases with the upper layer being primarily FFA. The upper layer was decanted and bottom, glycerol rich, layer was extracted by equal volumes of petroleum ether to remove residual FFAs. This was followed by neutralization of the glycerol rich layer with 12.5 M KOH. This treated feed was used for all membrane filtration experiments.

2.3. Membrane filtration of treated feed (step 2)

For membrane filtration of treated crude glycerol, a membrane filtration assembly was employed. The schematic of the setup is presented in Fig. 1.

The apparatus consisted of a feed tank connected with the membrane module (dead-end filtration) and a by-pass. Flow of treated feed in the stainless steel tubing was controlled by ball valves. Temperature control was achieved using a type K thermocouple (Omega) placed between the tubing and heating tape wrapped around the tubing. Temperature and pressure inside the feed tank and membrane module were monitored constantly and controlled by thermocouples (K type, Omega) and pressure transducers (Honeywell) connected to temperature and pressure monitors which were connected to PC using interface LabVIEW software via USB. The feed tank was connected to the nitrogen tank to maintain positive flow of feed in the line and to maintain the desired trans-membrane pressure to pass the filtered product. In order to ensure constant feed tank temperature, a circulatory bath was also connected to the feed tank *via* a flow through a U tube. To study membrane filtration of treated feed, transmembrane temperature and pressure were varied in the range of 25–60 °C and 50–350 kPa, respectively (as the maximum pressure holding capacity of membrane module was 400 kPa). The details of membrane filtration experiments are presented in Table 1.

The treated feed (obtained after step 1) was filled into about two-thirds of feed tank capacity (about 300–350 ml) and the tank was heated and pressurized. As the feed solution reached the desired temperature, valves were opened and feed was introduced to the membrane module. A fixed volume of filtrate (15 mL) was collected. It took about 5–30 min to collect the samples at different process conditions. The flow was faster with higher MWCO membrane, temperature, and pressure. As dead end filtration enhances membrane fouling, membranes were cleaned periodically with methanol.

2.4. Solvent and water evaporation and activated charcoal treatment (step 3 and 4)

Methanol and water were removed from all treated and filtered samples using vacuum evaporation in a rotary evaporator (Rotavapor®) for a fixed time (about 4 min) at 90 °C to obtain about 3 mL of final purified sample. Samples were clear, did not scatter light, and light brown in color. Color and other impurities were removed by activated charcoal treatment by mixing with

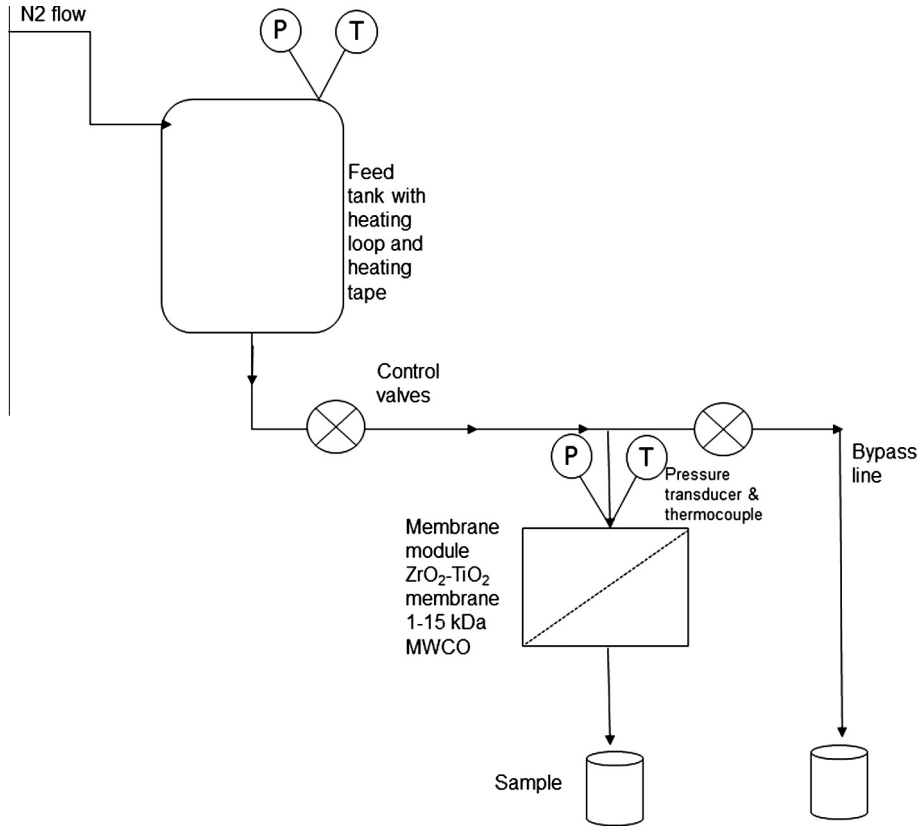

Fig. 1. Schematic of the membrane filtration setup.

Table 1
Experimental conditions for membrane filtration.

Experiments	Pressure (kPa)	Temperature (°C)
1	100	25.0
2	225	42.5
3	225	42.5
4	350	42.5
5	100	60.0
6	225	42.5
7	225	60.0
8	225	25.0
9	50	42.5
10	350	60.0
11	225	42.5
12	225	42.5
13	350	25.0

commercial granulated activated carbon at a ratio of 1:10 (100 g/L) with constant stirring for 30 min at room temperature.

2.5. Analytical methods

Glycerol and methanol content (in wt%) were determined by gas chromatography (Agilent 7890A series) on a StabilWax column (30 m × 250 μm × 0.5 μm; Restek Corp., USA) at 250 °C, an FID detector at 300 °C, nitrogen at 23 psi, and helium as the carrier. Water content was determined by an automated Karl-Fischer coulometric titrator (Mettler Toledo DL32) using methanol for dilution as the titrator is sensitive to water content of maximum 5 wt%. Ash content was determined by burning 1 g of sample in muffle furnace at 750 °C for 3–4 h. FFA (wt%) and acid value were determined by acid base titration according to the Lubrizol test procedure (TP-TM-001C). Fourier transform infrared (FTIR) spectra were generated using a FTIR spectrometer (Bruker Vertex 70, MA, USA) with an ATR module. Each spectrum was the average of 16 co-addition scans with a total scan time of 15 s in the IR range of 400–4000 cm^{-1} at 4 cm^{-1} resolution. Gross calorific (heating) value was determined by an oxygen bomb calorimeter (Parr bomb calorimeter 6400) by burning 1 g sample in a high pressure oxygen atmosphere within a stainless steel pressure vessel or bomb.

3. Results and discussions

3.1. Composition of crude glycerol and treated feed

Crude glycerol obtained from the supplier was a dark brown liquid with a high pH (10–11) that was less viscous than pure glycerol. Its composition (as obtained from the supplier) was as follows (on wt% basis): glycerol 40.0; matter organic non glycerol (MONG) 55.0; and moisture 5.0. MONG consisted of free fatty acid (FFA) as saponified fatty acids (SFA) 15%; fatty acid methyl ester (FAME) 10%; and methanol 30%. The ash content of crude glycerol is 4.9% due to salts from unspent catalyst (KOH) which is a component of SFA, while the water content might be due to the washing/rinsing to remove catalyst during biodiesel production [15]. Some water could also be present in the oil feed that was used to produce biodiesel and glycerol [17]. Crude glycerol samples were diluted with methanol to a final glycerol concentration of about 10 wt% (confirmed by GC) for ease of operation.

3.2. Purification of glycerol by physico-chemical treatment

Saponification of free fatty acids with excess of strong alkali (KOH) resulted in the formation of saponified fatty acids (SFA) [18] according to the following Eq. (1)

$$R - COOCH_3 + KOH \rightarrow R - COOK + CH_3OH \quad (1)$$

When HCl was added to saponified crude glycerol, it formed two distinct layers or phases – a FFA layer and a glycerol rich layer. As the FFA phase has lower density than the glycerol phase [19], it forms the upper layer and there is well defined separation of the two layers. Mineral acid (H^+ ions) converted soaps (saponified fatty acids; SFA) to insoluble FFA. After this was removed, excess acid in the crude glycerol was neutralized with base to form salts [10]. In the present case, H^+ ions from HCl reacted with the basic soap to produce FFA. The Cl^- originating from ionized HCl combined with the K^+ arising from KOH and soaps, forming water soluble KCl. The reaction is presented in Eq. (2):

$$R - COOK + H^+ \rightarrow R - COOH + K^+ \quad (2)$$

Inorganic salt might precipitate during acidification depending on the acid used [15], if the salt is insoluble or sparingly soluble in water. However, in the present case, as KCl is water soluble (342 g/L at 20 °C), no third layer was formed.

Herein separations of FFA and glycerol rich phases is conducted by gravity sedimentation in separatory funnels and the glycerol rich phase is neutralized with KOH after acidification. Any residual FFA and FAME entrained in the glycerol layer might be converted to soaps by reacting with KOH. Residual soap would increase MONG and ash content of final enriched ('purified') glycerol while SFA would contribute to MONG content only. This phenomenon has also been observed in previous studies [10,15] and might limit the enrichment possible with physico-chemical treatments alone. Compositions of glycerol-rich layers and MONG content are highly dependent on acid used and pH of acidification [10]. Kongjao et al. [15] reported that acidification to pH 1 favors glycerol content and eliminates most contaminants. They further reported, that decreasing pH during acidification step leads to increased amount of the glycerol-rich layer and decreased inorganic salts and the FFA phase [15]. After physico-chemical treatments, glycerol content of treated feed was 88.6 wt%, while water content, acid value, and FFA was 2.9 wt%, 1.1 and 0.6 wt%, respectively (shown in Table 2 in Section 3.5). The rest of the components may be the residual salt, di- and triglycerides or FAME which were not separated completely during the physico-chemical treatment. In a similar study, after physico-chemical treatment of crude glycerol, Manosak et al. [10] obtained a glycerol content of 82.9%, ash 7%, water 8.5%, and 1.6% MONG (in wt%). The glycerol obtained in the present study was more enriched than that reported by Manosak et al. [10].

Table 2
Glycerol compositional analysis after the treatment.

Experimental conditions[a]	Glycerol concentration (wt%)	Water content (wt%)	Acid value	FFA (wt %)	Gross calorific value (kJ/kg)
ACS grade glycerol	99.7	<0.1	ND	ND	17,678
1 kDa, 25 °C, 350 kPa	92.7	2.9	0.6	0.3	16,865
1 kDa, 42.5 °C, 350 kPa	96.6	2.2	0.6	0.3	16,980
1 kDa, 60 °C, 350 kPa	97.5	2.2	0.6	0.3	16,949
3 kDa, 60 °C, 350 kPa	84.7	3.6	1.1	0.6	16,870
5 kDa, 42.5 °C, 350 kPa	91.1	2.7	0.6	0.3	16,786
8 kDa, 42.5 °C, 350 kPa	90.5	2.9	0.6	0.3	16,876
15 kDa, 60 °C, 350 kPa	88.3	2.9	1.1	0.3	16,408
Treated feed	88.6	2.9	1.1	0.6	16,808

[a] ND – Not determined.

3.3. Effect of membrane filtration of treated feed (obtained from step 1)

Ceramic membranes offer many advantages over polymeric membranes such as resistance to chemical, mechanical and thermal degradation, combined with higher permeability rates and easier cleaning. Membrane performance is affected by several parameters including; membrane composition and porosity, temperature and pH of feed solution, pressure, tangential flow velocity, and physical/chemical interactions between feedstock components and the membrane surface, such as – shape of the particle (straight or coiled), attraction or repulsion [13,20].

The parameters studied in the present work were membrane module temperature, pressure, and MWCO. However, membrane fouling due to cake resistance limits the performance of UF [21]. Angelis et al. [22] found a strong dependence between foulant concentration and solution pH for iron oxide ceramic membrane. However, in the present work, solution pH was not studied and all the experiments were carried out at a neutral pH (~7).

Temperature effects (25–60 °C) were studied at a fixed pressure (350 kPa). Temperatures of <25 °C were not chosen due to the significant increase in viscosity at lower temperature. Temperatures higher than 60 °C were also not employed as it might lead to methanol evaporation which is undesirable. It was assumed that even with the smallest membrane pores (1 kDa or 1 kg/mol), glycerol (molecular weight 92.1 g/mol) and oleic acid (molecular weight 282.5 g/mol) would not be retained by the membrane. Impurities with molecular weight higher than the MWCO of the membrane (such as oil droplets and colloidal particles) will be retained by the membrane. The effects of temperature on membrane filtration of treated feed were determined (Fig. 2). At 25 °C, least glycerol was obtained after membrane filtration. Highest glycerol content was obtained at 60 °C though, the glycerol at 42 °C was comparable. Lower glycerol content is likely due to higher glycerol viscosity at lower temperature (Fig. 3).

At a temperatures from 40 to 60 °C, the glycerol viscosity curve reaches a plateau for 10 wt% glycerol which suggests that the change in glycerol viscosity at 10 wt% concentration can be considered non-significant at this temperature range. The similar glycerol content at 42.5 and 60 °C might arise from the relatively small viscosity differences between these samples. Flow through the membrane would be faster for glycerol solutions with higher viscosity. This also explains inferior membrane performance at 25 °C as the viscosity of glycerol is comparatively higher (~1.2 mPa s) at 42.5 °C, as compared to that at 25 °C (~0.8 mPa s) [23]. In experiments conducted at the same temperature, it can be seen in Fig. 3 that 1 kDa membranes lead to greater glycerol enrichment than other membranes. With increased membrane pore size,

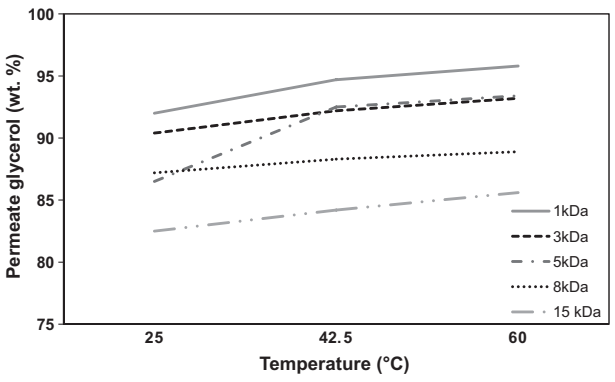

Fig. 2. Effects of temperature of membrane filtration on permeate glycerol (wt%) at fixed pressure of 350 kPa.

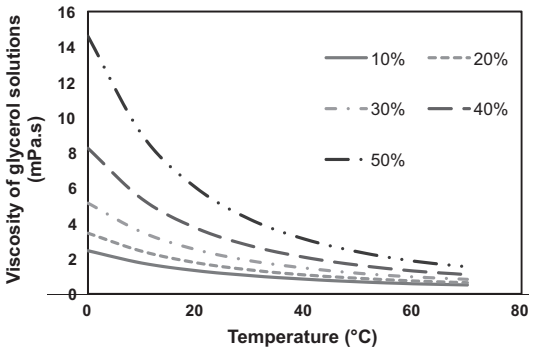

Fig. 3. Viscosity of aqueous glycerol solutions with increased temperature. Drawn from the data. Source: [23].

decreased glycerol content was obtained. This might be due to the incomplete filtration with increased pore size leading to impurities in filtrate and lesser relative glycerol content.

Pressure is the driving force in membrane separation processes such as MF and UF [24]. The effect of pressure was studied at 100 and 350 kPa at a fixed temperature of 25 °C. Due to the limitations of the membrane module (400 kPa maximum) pressure exceeding 350 kPa was not employed in the present work. Lower pressure of 50 kPa was not successful in purifying glycerol. Fig. 4 shows the data related to the effect of pressure on membrane filtration of treated feed.

At a pressure of 100 kPa, a higher glycerol content was obtained than at 350 kPa with the exception of 1 kDa membrane. Lower pressure also led to reduced transmembrane flux compared to 350 kPa. However, flux was not determined in the present study as the focus of the study was to obtain higher content of glycerol. With increased membrane pore size at a fixed pressure, permeate glycerol decreased, due to the increased trans-membrane flow of impurities. As higher glycerol content was obtained at 60 °C, 350 kPa and using 1 kDa MWCO membrane, these conditions can be considered most suitable for membrane filtration of treated feed. Further research is required to study membrane flux and fouling.

3.4. Reduction in color and other impurities by activated charcoal treatment

Adsorption on activated charcoal can remove residual water, methanol and salt [9]. The glycerol content has been reported to remain unaffected by charcoal treatment, as the size of glycerol molecule (~0.3 nm) is larger than the pore size of activated carbon (AC) (0.1–0.3 nm) used in this study [10]. In the present study, the color of crude glycerol was dark brown which improved to light brown after the physico-chemical treatment and clear (colorless) solution similar to ACS grade glycerol was obtained after the treatment.

Improvement in relative glycerol content after membrane filtration and AC adsorption might have been achieved due to adsorption of residual MONG on AC. It has been reported that color and impurity removal increases with increased activated carbon dosage. Manosak et al. [10] reported that increasing the activated carbon dose from 65 to 100 g/L glycerol, led to the largest decrease in ash content and at 200 g/L glycerol, almost all color was removed from glycerol. Decrease in ash content was observed as the residual salt and methanol were bound to the residual MONG and it is adsorbed by AC. In addition, AC treatment may also have removed a portion of the fatty acids such as lauric acid and myristic acid as reported in other similar studies [10]. In the present work, a fixed AC dose of 100 g/L was employed for treatment.

3.5. Characterization of crude and enriched (purified) glycerol

After treatment enriched (purified) glycerol samples were characterized by FTIR which were compared with those of pure and crude glycerol (Fig. 5). Similar FTIR spectra were obtained for ACS grade and enriched (purified) glycerol samples while there were clear distinctions in spectra for crude glycerol owing to the impurities present in crude glycerol. A broad peak at 3200–3400 cm^{-1} present in all three glycerol samples is a characteristic of —OH stretching. For crude glycerol, a relatively smaller peak was obtained. Peaks at 2880 and 2930 cm^{-1} were due to —CH stretching, the later was more intense for crude glycerol. Some smaller peaks due to —COH bending were obtained at 1400–1460 cm^{-1}. Another group of peaks were due to —CO stretching at 1450 cm^{-1} (primary alcohol), an intense peak at 1100 cm^{-1} (secondary alcohol) and —OH bond bending at 920 cm^{-1} [12,15].

Small peaks for ACS grade and enriched (purified) glycerol at about 1550 and 1700 cm^{-1} are due to —C=O bond indicating the presence of carboxylic acid or fatty acid ester of in purified and ACS grade glycerol while a strong peak was obtained for crude glycerol [12]. Peaks at 2900, 1550, and, 1740 cm^{-1} indicate impurities in crude glycerol. The sharp absorbance at 1550 cm^{-1} represented the presence of soap COO^- [6]. The small absorbance at about 2900 cm^{-1} indicated the presence of unsaturated C=C compound(s). The sharp peak at 1740 cm^{-1} indicated the presence of C=O compound(s) of an ester or carboxylic acid of fatty acid [15]. These latter peaks were either below detection limits or were very small for enriched (purified) and ACS grade glycerol samples.

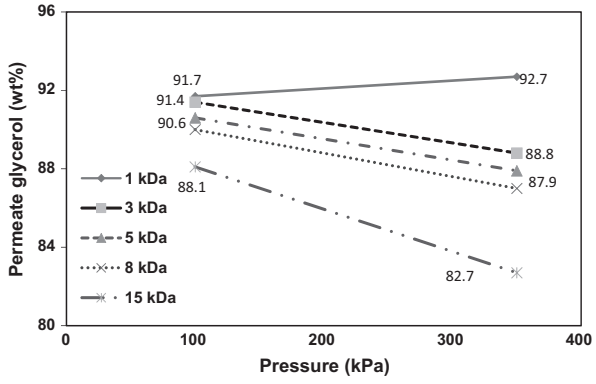

Fig. 4. Effect of pressure of membrane filtration on permeate glycerol (wt%) at fixed temperature of 25 °C.

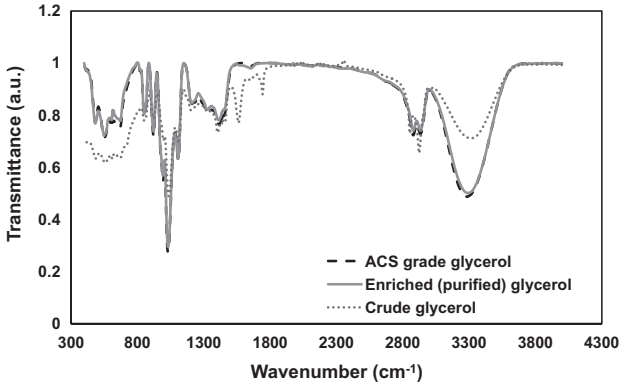

Fig. 5. Comparative FTIR spectra of crude, enriched (purified), and ACS grade glycerol samples.

Table 2 presents the comparison of physico-chemical properties between treated feed, ACS grade glycerol, and enriched (purified) glycerol. It shows the effects of physico-chemical treatment alone (treated feed) and in combination with membrane filtration and activated charcoal adsorption. Only representative samples are presented in Table 2.

Residual water content of samples after treatments was in the range of 2.2–3.6 wt%, which was lower than that of crude glycerol (5.5 wt%). Acid value and free fatty acid content of all treated samples were in the range of 0.6–1.1 and 0.3–0.6%, respectively. The most important parameter, glycerol content, was 88.6 wt%, after physico-chemical treatment alone, and increased to 97 wt% after membrane filtration and activated charcoal adsorption. As glycerol is also a fuel, its calorific value is an important characteristic for determining its purity. The calorific value of ACS grade glycerol was found to be 17,678 kJ/kg, while the calorific value of enriched (purified) glycerol was found to be as close as 95–96% of that of ACS grade glycerol (16,408–16,980 kJ/kg). These values are slightly lower than those obtained by Thompson and He [25] for pure glycerol (~18,000 kJ/kg). However, calorific value of purified glycerol is not an absolute indicator of the glycerol purity. The physico-chemical treatment alone was successful in producing 88.6% glycerol from the initial 40.0% crude glycerol solution (the feed was diluted prior to use to 10 wt%).

The ash content in all treated samples was <1%. It has been reported that chemical treatment at a low pH is a better option as it can increase the glycerol content and reduce ash content in recovered crude glycerin [12]. In the present study technical grade glycerol (>95%) was produced. The enriched glycerol can be used as feedstock for the production of value-added chemicals such as glycerol carbonate and glycerol ethers.

4. Conclusions

In this work, glycerol purification was conducted using combined physico-chemical treatments, membrane filtration, and activated charcoal treatment. Process that combined physico-chemical treatment, membrane filtration and charcoal adsorption was studied to increase glycerol content. Sequential treatment of saponification, acidification, neutralization, phase separation, solvent removal, membrane filtration (1 kDa MWCO, 60 °C and 350 kPa), and activated charcoal treatment, a maximum of 97.5% glycerol was obtained with very low residual FFA, water and ash content. This work highlights the importance of membrane purification in conjunction with physico-chemical treatment and showed a promise for crude glycerol purification. However, it needs to be studied further at continuous/semi-continuous mode.

Conflict of interest

The authors declare no competing financial interests.

Acknowledgments

This work was supported by the Agriculture Development fund (ADF), Saskatchewan Ministry of Agriculture, Canada [award no. 20130289] and Mitacs. Authors also thank Rlee Prokopishyn and Heli Eunike for their generous technical support.

References

[1] M.S. Ardi, M.K. Aroua, N.A. Hashim, Progress, prospect and challenges in glycerol purification process: a review, Renew. Sust. Energy Rev. 42 (2015) 1164–1173, http://dx.doi.org/10.1016/j.rser.2014.10.09.

[2] M. Ayoub, A.Z. Ahmad, Critical review on the current scenario and significance of crude glycerol resulting from biodiesel industry towards more sustainable renewable energy industry, Renew. Sust. Energy Rev. 16 (5) (2012) 2671–2686, http://dx.doi.org/10.1016/j.rser.2012.01.054.

[3] M. Pagliaro, M. Rossi, The Future of Glycerol, Royal Society of Chemistry, 2010, http://dx.doi.org/10.1039/9781849731089. PDF eISBN: 978-1-84973-108-9 2010 1-28.

[4] H.W. Tan, A.R. Aziz, M.K. Aroua, Glycerol production and its applications as a raw material: a review, Renew. Sust. Energy Rev. 27 (2013) 118–127, http://dx.doi.org/10.1016/j.rser.2013.06.035.

[5] C.A.G. Quispe, C.J.R. Coronado, J.A. Carvalho Jr., Glycerol: Production, consumption, prices, characterization and new trends in combustion, Renew. Sust. Energy Rev. 27 (2013) 475–493, http://dx.doi.org/10.1016/j.rser.2013.06.017.

[6] W.N.R.W. Isahak, M. Ismail, M.A. Yarmo, J.M. Jahim, J. Salimon, Purification of crude glycerol from transesterification RBD palm oil over homogeneous and heterogeneous catalysts for the biolubricant preparation, J. Appl. Sci. 10 (21) (2010) 2590–2595, http://dx.doi.org/10.3923/jas.2010.2590.2595.

[7] F. Yang, M.A. Hanna, R. Sun, Value-added uses for crude glycerol – a byproduct of biodiesel production, Biotechnol. Biofuels 5 (2012) 13, http://dx.doi.org/10.1186/1754-6834-5-13.

[8] R. Ciriminna, C. Della Pina, M. Rossi, M. Pagliaro, Understanding the glycerol market, Eur. J. Lipid Sci. Technol. 116 (10) (2014) 1432–1439, http://dx.doi.org/10.1002/ejlt.201400229.

[9] I. Contreras-Andrade, E. Avella-Moreno, J. Fabián Sierra-Cantor, C.A. Guerrero-Fajardo, J.R. Sodré, Purification of glycerol from biodiesel production by sequential extraction monitored by 1H NMR, Fuel Process. Technol. 132 (2015) 99–104, http://dx.doi.org/10.1016/j.fuproc.2014.12.016.

[10] R. Manosak, R. Limpattayanate, M. Hunsom, Sequential-refining of crude glycerol derived from waste used-oil methyl ester plant via a combined process of chemical and adsorption, Fuel Process. Technol. 92 (2011) 92–99, http://dx.doi.org/10.1016/j.fuproc.2010.09.002.

[11] N. Saifuddin, H. Refal, P. Kumaran, Rapid purification of glycerol by-product from biodiesel production through combined process of microwave assisted acidification and adsorption via Chitosan immobilized with yeast, Res. J. Appl. Sci. Eng. Technol. 7 (3) (2014) 593–602.

[12] C. Tianfeng, L. Huipeng, Z. Hua, L. Kejian, Purification of crude glycerol from waste cooking oil based biodiesel production by orthogonal test method, China Petrol. Process. Petrochem. Technol. 15 (1) (2013) 48–53.

[13] R.W. Baker, Membrane Technology and Applications, second ed., John Wiley & Sons Ltd., 2000. ISBN: 0-470-85445-6.

[14] M. Peyravi, A. Rahimpour, M. Jahanshahi, Developing nanocomposite PI membranes: morphology and performance to glycerol removal at the downstream processing of biodiesel production, J. Membr. Sci. 473 (1) (2015) 72–84, http://dx.doi.org/10.1016/j.memsci.2014.08.009.

[15] S. Kongjao, S. Damronglerd, M. Hunsom, Purification of crude glycerol derived from waste used-oil methyl ester plant, Korean J. Chem. Eng. 27 (3) (2010) 944–949, http://dx.doi.org/10.1007/s11814-010-0148-0.

[16] K. Zhang, Y. Qin, F. He, J. Liu, Y. Zhang, L. Liu, Concentration of aqueous glycerol solution by using continuous-effect membrane distillation, Sep. Purif. Technol. 144 (2015) 186–196, http://dx.doi.org/10.1016/j.seppur.2015.02.034.

[17] M.C.S. Gomes, P.A. Arroyob, N.C. Pereira, Influence of oil quality on biodiesel purification by ultrafiltration, J. Membr. Sci. 496 (15) (2015) 242–249, http://dx.doi.org/10.1016/j.memsci.2015.09.004.

[18] M. Házek, F. Skopal, Treatment of glycerol phase formed by biodiesel production, Bioresour. Technol. 101 (2010) 3242–3245, http://dx.doi.org/10.1016/j.biortech.2009.12.094.

[19] R.W.M. Pott, C.J. Howe, J.S. Dennis, The purification of crude glycerol derived from biodiesel manufacture and its use as a substrate by *Rhodopseudomonas palustris* to produce hydrogen, Bioresour. Technol. 152 (2014) 464–470, http://dx.doi.org/10.1016/j.biortech.2013.10.094.

[20] I.M. Atadashi, M.K. Aroua, A.R. Abdul Aziz, N.M.N. Sulaiman, Membrane biodiesel production and refining technology: a critical review, Renew. Sust. Energy Rev. 15 (2011) 5051–5062, http://dx.doi.org/10.1016/j.rser.2011.07.051.

[21] S.-K. Mah, C.-K. Chuah, W.P.C. Lee, S.-P. Chai, Ultrafiltration of palm oil–oleic acid–glycerin solutions: fouling mechanism identification, fouling mechanism analysis and membrane characterizations, Sep. Purif. Technol. 90 (2012) 419–431, http://dx.doi.org/10.1016/j.seppur.2012.07.020.

[22] L. De Angelis, M.M.F. de Cortalezzi, Ceramic membrane filtration of organic compounds: effect of concentration, pH, and mixtures interactions on fouling, Sep. Purif. Technol. 118 (2013) 762–775, http://dx.doi.org/10.1016/j.seppur.2013.08.016.

[23] Dow chemical company, 2016, <http://www.dow.com/optim/optim-advantage/physical-properties/viscosity.htm> (assessed 10.02.16).

[24] N. Sdrula, A study using classical or membrane separation in the biodiesel process, Desalination 250 (3) (2010) 1070–1072, http://dx.doi.org/10.1016/j.desal.2009.09.110.

[25] J.C. Thompson, B.B. He, Characterization of crude glycerol from biodiesel production from multiple feedstocks, Appl. Eng. Agricult. 22 (2) (2006) 261–265.

APPENDIX D

Jacome-Sosa, MM, C, Vacca, R Mangat, A Diane, RC Nelson, MJT Reaney, J Shen, JM Curtis, DF Vine, CJ Field, M Igarashi, D Piomelli, S Banni, SD Proctor (2016) Vaccenic acid suppresses intestinal inflammation by increasing anandamide and related *N*-acylethanolamines in the JCR:LA-cp rat. *Journal of Lipid Research* 57(4), 638-649.

✤ *Author's Choice*

Vaccenic acid suppresses intestinal inflammation by increasing anandamide and related *N*-acylethanolamines in the JCR:LA-cp rat[S]

Miriam Jacome-Sosa,* Claudia Vacca,† Rabban Mangat,* Abdoulaye Diane,* Randy C. Nelson,* Martin J. Reaney,§ Jianheng Shen,§ Jonathan M. Curtis, Donna F. Vine,* Catherine J. Field,** Miki Igarashi,†† Daniele Piomelli,§§ Sebastiano Banni,† and Spencer D. Proctor[1],***

Metabolic and Cardiovascular Disease Laboratory,* Group on Molecular and Cell Biology of Lipids, Alberta Diabetes and Mazankowski Heart Institutes, University of Alberta, Edmonton, AB, Canada; Department of Biomedical Sciences,† University of Cagliari, Cittadella Universitaria, Monserrato, Cagliari, Italy; Department of Plant Science,§ University of Saskatchewan, Saskatoon, SK, Canada; Department of Agricultural Food and Nutritional Science,** University of Alberta, Edmonton, AB, Canada; Laboratory for Medical Homeostasis,†† RIKEN Center for Integrative Medical Sciences, Kanagawa, Japan; and Departments of Anatomy and Neurobiology, Pharmacology, and Biological Chemistry,§§ University of California, Irvine, CA

Abstract Vaccenic acid (VA), the predominant ruminant-derived *trans* fat in the food chain, ameliorates hyperlipidemia, yet mechanisms remain elusive. We investigated whether VA could influence tissue endocannabinoids (ECs) by altering the availability of their biosynthetic precursor, arachidonic acid (AA), in membrane phospholipids (PLs). JCR:LA-*cp* rats were assigned to a control diet with or without VA (1% w/w), *cis*-9, *trans*-11 conjugated linoleic acid (CLA) (1% w/w) or VA+CLA (1% + 0.5% w/w) for 8 weeks. VA reduced the EC, 2-arachidonoylglycerol (2-AG), in the liver and visceral adipose tissue (VAT) relative to control diet ($P < 0.001$), but did not change AA in tissue PLs. There was no additive effect of combining VA+CLA on 2-AG relative to VA alone ($P > 0.05$). Interestingly, VA increased jejunal concentrations of anandamide and those of the noncannabinoid signaling molecules, oleoylethanolamide and palmitoylethanolamide, relative to control diet ($P < 0.05$). This was consistent with a lower jejunal protein abundance (but not activity) of their degrading enzyme, fatty acid amide hydrolase, as well as the mRNA expression of TNFα and interleukin 1β ($P < 0.05$). The ability of VA to reduce 2-AG in the liver and VAT provides a potential mechanistic explanation to alleviate ectopic lipid accumulation. The opposing regulation of ECs and other noncannabinoid lipid signaling molecules by VA suggests an activation of benefit via the EC system in the intestine.—Jacome-Sosa, M., C. Vacca, R. Mangat, A. Diane, R. C. Nelson, M. J. Reaney, J. Shen, J. M. Curtis, D. F. Vine, C. J. Field, M. Igarashi, D. Piomelli, S. Banni, and S. D. Proctor. **Vaccenic acid suppresses intestinal inflammation by increasing anandamide and related *N*-acylethanolamines in the JCR:LA-cp rat. *J. Lipid Res.* 2016.** 57: **638–649.**

Supplementary key words vaccenic acid • endocannabinoids • *N*-acylethanolamines • intestinal inflammatory diseases • anandamide

Trans-11 18:1 [vaccenic acid (VA)] is the most abundant ruminant-derived *trans* fatty acid (rTFA) in the food chain and has sparked major interest due to mandatory labeling of all *trans* fat on foods in North America. This interest has also been simulated by the recent announcement by the Food and Drug Administration to retract the generally recognized as safe (GRAS) status of "artificial" *trans* fatty acids (1). VA is also the precursor to endogenous synthesis of conjugated linoleic acid (CLA), the first rTFA to be recognized as having numerous health-related effects. Interestingly, a growing body of evidence from studies in animal models has suggested a bioactivity for VA independent of its conversion to CLA. More specifically, VA has been shown to attenuate complications observed in the metabolic

This research was supported in part by Dairy Farmers of Canada, Canadian Institutes of Health Research, Alberta Livestock Industry Development Fund, and Alberta Livestock and Meat Agency. M.J-S. was supported by a scholarship from the National Council of Mexico for Science and Technology (CONACyT). S.D.P. was supported by a New Investigator Award from the Heart and Stroke Foundation of Canada and the Natural Science and Engineering Research Council of Canada. All authors have declared no financial conflicts of interest.

Manuscript received 6 January 2016 and in revised form 15 February 2016.

Published, JLR Papers in Press, February 17, 2016
DOI 10.1194/jlr.M066308

Abbreviations: AA, arachidonic acid; AEA, anandamide; 2-AG, 2-arachidonoylglycerol; CB, cannabinoid; CLA, conjugated linoleic acid; EC, endocannabinoid; ECS, endocaccanabinoid system; FAAH, fatty acid amide hydrolase; FAME, fatty acid methyl ester; IL-1β, interleukin 1β; LPS, lipopolysaccharide; NF-κB, nuclear factor κB; OEA, oleoylethanolamide; PEA, palmitoylethanolamide; PL, phospholipid; rTFA, ruminant-derived *trans* fatty acid; VA, vaccenic acid; VAT, visceral adipose tissue.

[1]To whom correspondence should be addressed.
e-mail: spencer.proctor@ualberta.ca

[S] The online version of this article (available at http://www.jlr.org) contains a supplement.

syndrome, including dyslipidemia, fatty liver disease, and low-grade inflammation (2–5). It has been proposed that the lipid-lowering and anti-inflammatory effects of VA may be partially associated with its ability to ligand activate PPARγ-regulated pathways (6, 7) by acting directly in the intestine (6) and adipose tissue (5). In general, bioactive long chain fatty acids also act by modifying the composition of membrane phospholipids (PLs) and potentially replacing or interfering with the synthesis of PL-derived lipid signaling molecules, including endocannabinoids (ECs) (8, 9). However, the incorporation of VA into membrane PLs and potential effects on EC pathways remains unknown.

ECs, the endogenous ligands for cannabinoid (CB) receptors, are lipid-derived messengers that have emerged as key regulators of appetite behavior, energy metabolism, and intestinal inflammation. The most common ECs include arachidonoylethanolamide [anandamide (AEA)] and 2-arachidonoylglycerol (2-AG); and are derivatives of the PUFA, arachidonic acid (AA; C20:4, n-6), in PLs and can be modulated in response to dietary PUFA intake (10–13). Increased plasma EC concentrations, due to alterations in the activity/expression of enzymes regulating their biosynthesis and degradation, are associated with abdominal obesity, dyslipidemia, and insulin resistance in humans (14–16). Intriguingly, CB receptor over-activity can result in tissue-specific metabolic effects. For instance, central and hepatic CB receptor activation leads to hyperphagia (17), hepatic de novo lipogenesis, and insulin resistance (18–20). In contrast, in animal models of experimental colitis, increased CB receptor signaling has been shown to ameliorate smooth muscular irritation (21) and the T cell-mediated aberrant immune response (22); thus, counteracting the excessive inflammatory responses/signs in intestinal disease conditions. Therefore, nutritional interventions that target tissue-specific EC pathways could be used as potential therapeutic strategies for treatment of obesity-associated metabolic diseases.

A recent study in hypercholesterolemic subjects provided the first evidence that a dairy product naturally enriched with VA and CLA decreases plasma concentrations of AEA in a dose-dependent manner (23). However, the direct effect of VA on EC regulation was not able to be determined in this study. Furthermore, given the bioactive properties of VA to favorably modulate whole body energy metabolism and low-grade inflammation (5, 24), we proposed to explore novel regulatory effects of VA on tissue ECs as a potential mechanism of action for these metabolic effects. In order to address the specific role of dietary VA alone or in combination with CLA in EC metabolism, we supplemented the diets of an established rodent model of metabolic syndrome (the JCR:LA-*cp* rat) with these bioactive long chain fatty acids, and examined tissue concentrations of CB receptor ligands, AEA and 2-AG, and the biosynthetic precursor, AA, in membrane PLs. We also analyzed two noncannabinoid lipid signaling molecules, oleoylethanolamide (OEA) and palmitoylethanolamide (PEA), which only differ from AEA by their acyl chain and have been shown to induce satiety (25, 26) and exert anti-inflammatory effects through activation of the PPARα receptor (27).

MATERIALS AND METHODS

Animals and diets

Rats of the JCR:LA-*cp* strain that are homozygous for the corpulent trait (*cp/cp*) have a complete absence of the leptin receptor in the plasma membrane and spontaneously develop symptoms associated with the metabolic syndrome and the prediabetic state typically observed in humans; including obesity, insulin resistance, and dyslipidemia (28). Male JCR:LA-*cp* rats were raised in our established breeding colony at the University of Alberta, as previously described (29). At 8 weeks of age, rats (n = 5) were randomized and assigned to one of four diets (control and experimental diets) for 8 weeks and had free access to food and water.

The control diet was prepared by adding 1% cholesterol and 15% w/w of fat to an 85% basal mix diet (Harlan Laboratories; TD.06206) that contained 42% of energy from carbohydrate, 23.7% of energy from protein, and 34% of energy from fat, as previously described (5). Experimental diets were prepared by adjusting the fatty acid composition (replacing oleic acid with VA, CLA, or VA+CLA) of the control diet to provide approximately 1% w/w of VA (VA), 1% w/w of *cis*-9, *trans*-11 CLA (CLA), or both 1% w/w of VA + 0.5% w/w of *cis*-9, *trans*-11 CLA (VA+CLA). The amount of VA in the diet (∼2% of total energy from VA) was chosen based on previously published studies (2–4) and was intended to be compared with health effects of moderate doses of rTFA previously examined in human clinical trials (30). The fat composition of the control and experimental diets is shown in supplementary Table 1. Control and experimental diets were isocaloric and had a constant PUFA to SFA ratio of 0.4 and a constant n6 to n3 PUFA ratio of 8. Purified VA was synthesized by chemical alkali isomerization from linoleic acid-rich vegetable oil (31). Semi-purified *cis*-9, *trans*-11 CLA (G-c9t11 80:20) containing 59.8% of *cis*-9, *trans*-11 CLA and 14.4% of *trans*-10, *cis*-12 CLA was kindly provided by Lipid Nutrition. The fatty acid composition of diets was confirmed by gas chromatograph analysis (32) of the fat blend samples (**Table 1**). After euthanization, samples of the hypothalamus, skeletal muscle, visceral adipose tissue (VAT), liver, and jejunal mucosa segments of the intestine were excised and snap-frozen at −80°C until analysis. Animal care and experimental procedures were conducted in accordance with the Canadian Council on Animal Care and approved by the University of Alberta Animal Care and Use Committee-Livestock.

Tissue lipid extraction

Tissues (0.2–0.3 g) were homogenized and total lipids extracted with chloroform/methanol (2:1, v/v) containing internal deuterated standards for AEA, 2-AG, OEA, and PEA to quantify for recovery efficiency ($[^2H]_8$-AEA, 20 ng/ml), ($[^2H]_5$-2-AG, 200 ng/ml), ($[^2H]_2$-OEA, 20 ng/ml), and ($[^2H]_4$-PEA, 20 ng/ml) (Cayman Chemical, Ann Arbor, MI). This mixture was washed with 0.25 vol of 0.9% KCl according to the Folch procedure (33) to separate the phases. Samples were centrifuged and the lipid-containing lower phase was transferred to clean tubes and evaporated to dryness under a stream of nitrogen at room temperature. After lipid extraction from tissue samples, lipid classes were separated by solid phase extraction using commercial silica cartridges, Strata SI-1 (Phenomenex, Torrance, CA). Samples were reconstituted in 500 μl of chloroform, vortexed, and loaded to the column followed by washing with 10 ml of chloroform to elute neutral lipids. The fractions containing ECs were then eluted with 10 ml chloroform/methanol (9:1, v/v), evaporated to dryness under nitrogen, and reconstituted in methanol until analysis by LC/MS. The fractions containing PLs were eluted with 10 ml methanol and stored at −20°C until further preparation

JOURNAL OF LIPID RESEARCH ASBMB JLR

TABLE 1. Fatty acid composition of control and experimental diets

Fatty Acid	Control Diet	VA Diet	CLA Diet	VA+CLA Diet
C12:0	1.0	1.2	1.2	2.1
C14:0	3.6	4.2	4.4	7.6
C14:1	0.3	0.4	0.4	0.7
C16:0	19.0	18.1	17.7	22.6
C16:1	1.2	1.0	1.0	1.1
C18:0	11.0	10.9	10.6	7.7
C18:1 *trans*-9	0.5	0.5	0.4	0.2
C18:1 *trans*-11 (VA)	1.3	8.8	1.0	8.8
C18:1 *cis*-9 (oleic acid)	35.6	27.9	26.3	17.3
C18:1 *cis*-11	1.9	1.4	1.3	0.8
C18:2 n6	13.7	13.9	13.6	12.7
C18:3 n3	1.7	1.7	1.7	1.7
cis-9, *trans*-11 CLA	0.2	0.3	8.8	4.1
Summaries				
∑SFA	37.5	37.6	37.3	45.2
∑C12:0, C14:0, C16:0	23.6	23.5	23.3	32.2
PUFA	15.6	15.8	15.4	14.4
*cis*MUFA	40.0	31.6	29.8	20.5
*trans*MUFA	4.2	11.4	3.0	10.7
n6	13.8	13.8	13.8	13.8
n3	1.7	1.7	1.7	1.7
n6:n3 ratio	7.9	7.9	7.9	7.9
PUFA:SFA ratio	0.4	0.4	0.4	0.3

Values are expressed as percentage of fatty acids.

for fatty acid analysis. Recovery of ECs in the chloroform/methanol (9:1, v/v) eluates was confirmed by LC/MS and estimated to be higher than 90%. Purity of the PL fraction was confirmed by TLC using heptane/isopropyl ether/acetic acid (60:40:4, by volume) as previously described (34).

Analysis of ECs and AEA analogs

Samples were analyzed by LC-ESI-MS using an Agilent 1200 series HPLC coupled to a 3200 QTRAP mass spectrometer (AB SCIEX, Concord, ON, Canada). LC separation was performed through an Ascentis Express C18 column (7.5 cm × 2.1 mm, 2.7 μm particle size) at a flow rate of 0.3 ml/min. Two mobile phases were used: mobile phase A, methanol with 0.2% formic acid; and mobile phase B, 50 mM ammonium formate (pH 3). The gradient elution method started at 85% A from 0 to 0.1 min; then the mobile phase A linearly increased to 95% from 0.1 to 2 min and was held for an additional 2 min (from 2.1 to 4 min). Then, the mobile phase was returned to 85% A and was held at this composition for 6 min equilibrium time prior to the next injection. The mass spectrometer was operated in the multiple reaction monitoring scan mode under positive ionization. Nitrogen was used as curtain gas, for drying, and as nebulizing gas. AEA, 2-AG, and the two *N*-acylethanolamines (OEA and PEA) in their protonated forms $[M+H]^+$ were identified as peaks with the appropriate *m/z* values and quantified by comparison with their external synthetic standards that were run under the same conditions. The multiple reaction monitoring transitions monitored were as follows: AEA *m/z* 348→62 (35 eV); AEA-d8 *m/z* 356→62 (35 eV); 2-AG *m/z* 379→287 (18 eV); 2-AG-d5 *m/z* 384→287 (18 eV); PEA *m/z* 300→62 (30 eV); PEA-d4 *m/z* 304→62 (30 eV); OEA *m/z* 326→62 (30 eV); OEA-d2 *m/z* 328→62 (30 eV). The linear range for the calibration (standard) curves for AEA, PEA, and OEA was 5–500 ng/ml and for 2-AG was 0.1–10 μg/ml. Because 2-AG and 1-AG undergo rapid isomerization (35), results for 2-AG were reported as the sum of the individual peaks of 2-AG + 1-AG.

Fatty acid analysis in PLs

PL fractions were transesterified using 0.5 N methanolic base (metallic sodium in methanol) (Sigma-Aldrich) at 80°C for 15 min forming fatty acid methyl esters (FAMEs). The FAMEs were flushed with N_2 and stored at −35°C until analysis and fatty acids were separated by GC with flame ionization detector (Varian 3900; Varian Inc., Mississauga, ON) using a 100 m CP-Sil 88 fused-silica capillary column [100 m × 0.25 mm i.d. × 0.2 μm film thickness (Varian Inc.)] as previously described (32). The FAMEs were identified by comparison with retention times of commercial GC reference FAME standards (FAME mix #463 and CLA FAME #UC-59M) from Nu-Chek Prep Inc.

Measurement of fatty acid amide hydrolase protein expression in the jejunum

Samples of the jejunum were washed with phosphate-buffered saline, and a 2 cm segment was cut from 10 cm below the pyloric sphincter. Mucosal samples were then scraped from jejunal segments. Proteins from jejunal mucosa homogenates were separated by SDS-PAGE on Tris-acetate polyacrylamide gels (3–8%; Invitrogen), transferred to a polyvinylidene difluoride membrane, and incubated with anti-fatty acid amide hydrolase (FAAH)1 rabbit polyclonal antibody (1:1,000; catalog number 9179; Cell Signaling Technology®) and anti-β-actin mouse polyclonal antibody (1:5,000; catalog number ab8226; Abcam®, St Louis, MO), as previously described (36). Detection was achieved using anti-rabbit and anti-murine secondary antibodies and the ECL advance detection system (Amersham Biosciences). Results are expressed as a ratio of target protein:β-actin protein.

Enzyme activity assays

The activity of FAAH and *N*-acylphosphatidylethanolamine phospholipase type D in jejunal mucosa was measured by standard assays, as previously described (37).

Measurement of pro-inflammatory genes in the jejunum

Total RNA was isolated from frozen segments of jejunal mucosa using TRIzol® (Invitrogen, Canada), as described in the manufacturer's protocol, and reversed transcribed into cDNA using MultiScribee reverse transcriptase (high-capacity cDNA reverse transcription kit; Applied Biosystems, Foster City, CA). The expression of CB1, FAAH, and the pro-inflammatory cytokines, TNFα

and interleukin 1β (IL-1β) relative to the housekeeping gene, *Actb* (β-actin), was assessed by quantitative real-time PCR, using the StepOne™ Plus real-time PCR system (Applied Biosystems) and StepOne™ software (version 2). The PCR contained cDNA template, 100 nM of commercially available premixed target-specific primers, and TaqMan® FAM™-labeled probe (Applied Biosystems) for CB1, FAAH, TNFα, IL-1β, and *Actb*. Thermal cycling conditions were as follows: 95°C for 20 s, followed by 40 cycles of 95°C for 1 s and 60°C for 20 s. Relative mRNA expression for each target gene was normalized to *Actb* mRNA and quantified using the comparative cycle threshold (Ct) method. Data were expressed as the ratio of target mRNA expression relative to β-actin. All assays were performed in triplicate.

Caco2 cell culture and measurement of FAAH inhibition on inflammatory cytokines

Caco2 cells (ATCC) were cultured in MEM (M4655; Sigma) with 10% fetal bovine serum and 1% penicillin/streptomycin and kept at 37°C in 5% CO_2 and 95% humidity. Cells were grown in 6-well plates and seeded at 10^6 cells per insert (24 mm diameter, 0.4 μm pore polycarbonate inserts). Cells at passages 15–25 were grown for a minimum of 18 days and used for experimentation between 18 and 21 days. Cells were maintained for 12 h in 1% fatty acid-free BSA after which they were treated with vehicle control, VA (100 μM), or VA (100 μM) + URB597 (FAAH inhibitor; Cedarlane) (1 μM) in the presence or absence of OEA (10 μM) for 24 h. Following this, the cells were challenged with lipopolysaccharide (LPS) (1 μg/μl) for 24 h. During this time, fresh vehicle control or VA (100 μM), URB597 (1 μM), OEA (10 μM) in 0.5% BSA was added. Total RNA was isolated from Caco2 cells and reversed transcribed into cDNA. The expression of TNFα relative to the housekeeping gene, GAPDH, was assessed by quantitative real-time PCR using SYBR Green (Applied Biosystems).

Statistical analysis

All results are expressed as mean ± SEM. Statistical comparisons between dietary groups were analyzed using one-way ANOVA followed by Tukey's post hoc test. The level of significance was set at $P < 0.05$ (Graph Pad Prism 5.0, USA).

RESULTS

Supplementation with VA alone or in combination with CLA does not affect EC concentrations in plasma, brain, or skeletal muscle

Contrary to our hypothesis, dietary supplementation with VA, CLA, or VA+CLA for 8 weeks did not affect EC concentrations in plasma (**Table 2**), the hypothalamus (data not shown), or skeletal muscle (**Fig. 1**) relative to control diet ($P > 0.05$). All dietary treatments (VA, CLA, and VA+CLA) significantly reduced ($P < 0.01$) the concentrations of OEA (−20, −19, and −17%, respectively) while only VA reduced the concentration of PEA (21%, $P < 0.05$) in the skeletal muscle relative to control (Fig. 1).

Dietary supplementation with VA alone or in combination with CLA decreases the concentration of 2-AG and AEA analogs (OEA and PEA) in the liver and VAT

Supplementation with VA, CLA, or VA+CLA significantly reduced 2-AG concentrations in the liver (83%, $P < 0.001$; 47.6%, $P < 0.05$; and 74%, $P < 0.001$, respectively) relative to control diet. Interestingly, the VA diet (but not the VA+CLA diet) lowered liver 2-AG concentrations by 68% as compared with the CLA-fed group ($P < 0.05$). In addition, VA or VA+CLA supplementation (but not CLA) resulted in decreased ($P < 0.001$) concentrations of the *N*-acylethanolamines, OEA (to not detectable levels) and PEA (−57 and −56%, respectively) in this tissue as compared with control (**Fig. 2**). AEA was not detected in the liver of JCR:LA-*cp* rats.

VA and VA+CLA (but not CLA) significantly ($P < 0.05$) reduced the concentrations of 2-AG (−86 and −87%, respectively) and OEA (−59%, $P < 0.05$ and −74%, $P < 0.01$, respectively) in VAT as compared with control (**Fig. 3**).

Collectively, results from this study suggest that there were no additive effects of combining VA with CLA on reducing EC concentrations in liver and VAT.

Supplementation with VA increases the concentration of AEA and AEA analogs (OEA and PEA) in the jejunum

Unexpectedly, dietary supplementation with VA (but not CLA or VA+CLA) significantly increased jejunal concentrations of the EC, AEA (3.8-fold, $P < 0.05$), and its analogs, OEA (1.7-fold, $P < 0.05$) and PEA (1.9-fold, $P < 0.01$) (**Fig. 4**). It is important to note that VA did not alter food intake in the present study (data not shown) or in previous studies using different animal models (2, 3, 38, 39). Therefore, it is unlikely that increased AEA concentrations in the jejunum (following VA treatment) would result in an appetite stimulatory effect as a result of CB receptor activation.

Effects of dietary supplementation with VA, CLA, or their combination on tissue PL fatty acid composition

We analyzed tissue PL fatty acid composition to determine whether changes in tissue EC and *N*-acylethanolamine concentrations were due to alterations in the availability of their biosynthetic precursors in membrane PLs (**Table 3**).

TABLE 2. EC and *N*-acylethanolamine concentrations in plasma of JCR:LA-*cp* rats fed control or experimental diets for 8 weeks

	Control		VA		CLA		VA+CLA	
	Mean	SEM	Mean	SEM	Mean	SEM	Mean	SEM
2-AG[a]	ND	—	ND	—	ND	—	ND	—
AEA[a]	8.9	4.1	5.6	0.6	7.9	0.4	6.4	1.9
PEA[a]	145.9	11.1	145.2	2.5	144.1	6.0	146.9	3.3
OEA[a]	62.1	6.8	59.3	1.8	59	6.5	57.9	3.1

Values are mean ± SEM, n = 3. Means did not differ, $P > 0.05$. ND, not detectable.
[a]Nanomoles per milliliter of plasma.

JOURNAL OF LIPID RESEARCH ASBMB JLR

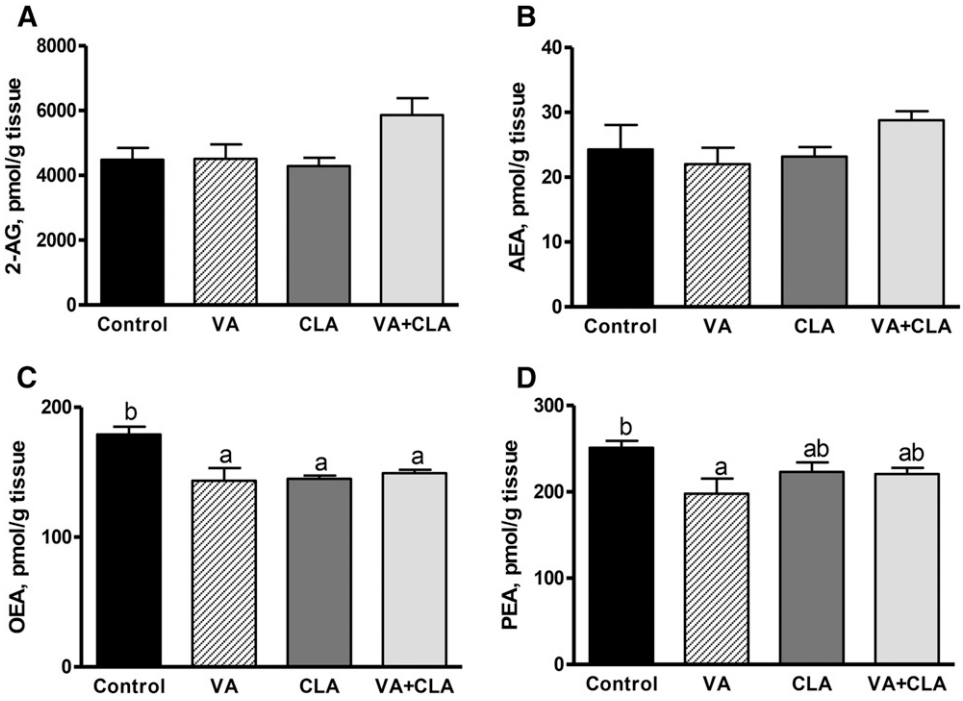

Fig. 1. EC (A, B) and *N*-acylethanolamine (C, D) concentrations in the skeletal muscle of JCR:LA-*cp* rats following dietary supplementation with VA, CLA, or VA+CLA. Values are mean ± SEM, represented by vertical bars (n = 5). Means without a common letter differ ($P < 0.05$).

Interestingly, we found that VA supplementation increased the EC precursor, AA, in liver (30%, $P < 0.001$) and skeletal muscle (11%, $P < 0.05$) PLs compared with control diet. VA+CLA-fed rats also had increased amounts of AA (20%) in liver PLs relative to control rats ($P < 0.01$). The incorporation of AA in VAT, jejunal, and hypothalamus PLs was not affected by any experimental diet (VA, CLA, or VA+CLA) relative to control ($P > 0.05$). VA- and VA+CLA-fed rats had lower concentrations of the OEA precursor, oleic acid (−35 and −40%, respectively), while VA-fed rats only had lower amounts of the PEA precursor, palmitic acid (−21%), in liver PLs relative to control rats ($P < 0.001$).

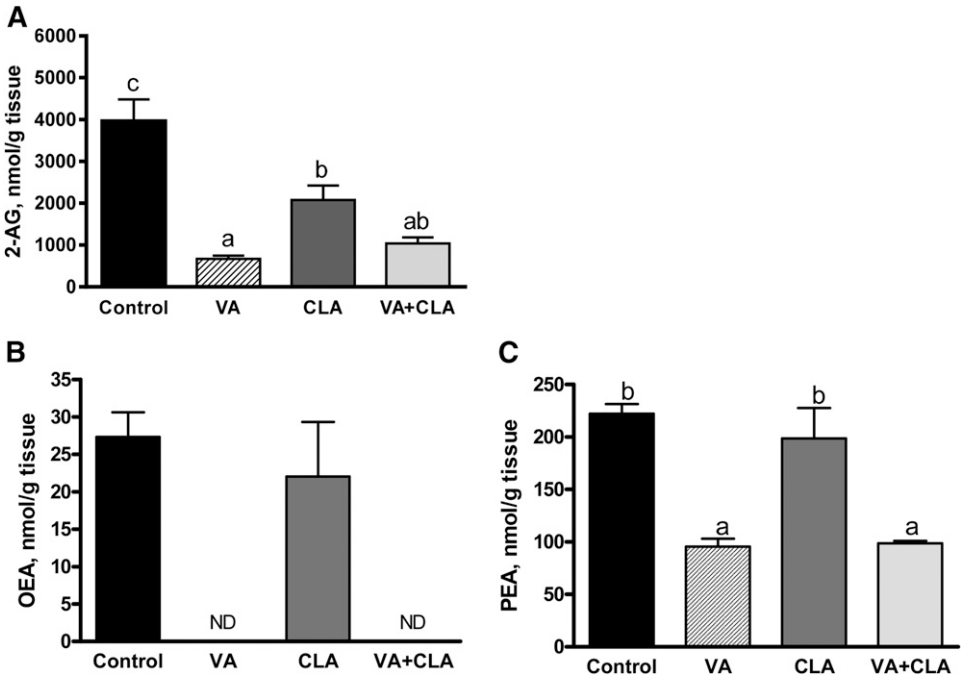

Fig. 2. EC (A) and *N*-acylethanolamine (B, C) concentrations in the liver of JCR:LA-*cp* rats following dietary supplementation with VA, CLA, or VA+CLA. Values are mean ± SEM, represented by vertical bars (n = 5). Means without a common letter differ ($P < 0.05$). ND, not detectable

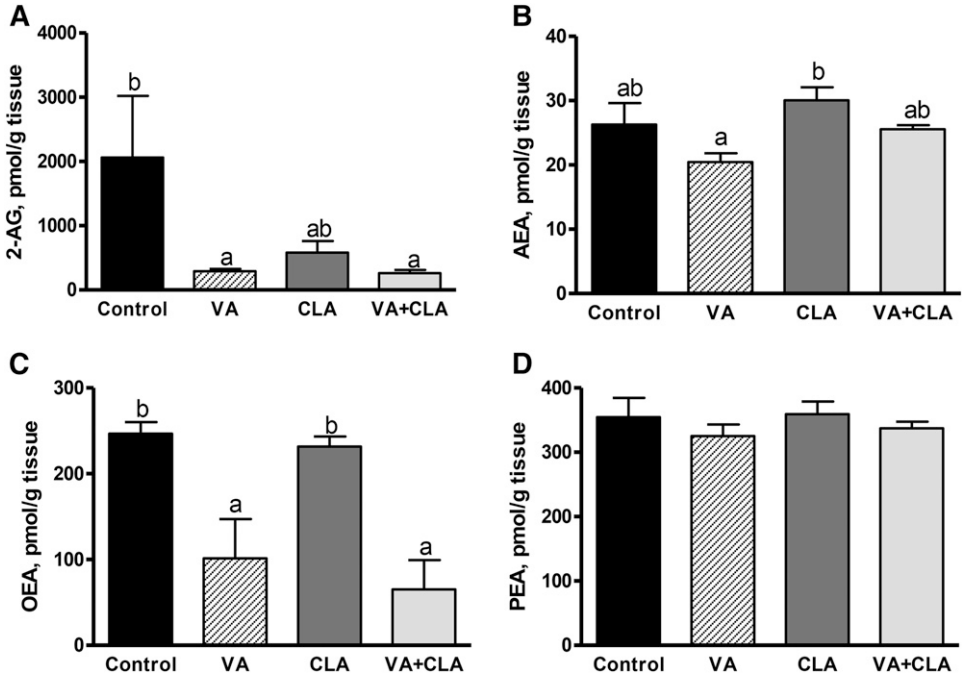

Fig. 3. EC (A, B) and *N*-acylethanolamine (C, D) concentrations in VAT of JCR:LA-*cp* rats following dietary supplementation with VA, CLA, or VA+CLA. Values are mean ± SEM, represented by vertical bars (n = 5). Means without a common letter differ ($P < 0.05$).

CLA- and VA+CLA-fed rats had lower ($P < 0.001$) amounts of oleic acid (−15 and −17%, respectively) in VAT PLs, while only VA+CLA rats had lower concentrations of oleic acid (−33%, $P < 0.01$) in jejunal PLs relative to control rats. Collectively, findings from fatty acid analysis in tissue PLs suggest that the regulatory effect of VA on tissue ECs could not be explained by changes in their biosynthetic membrane PL precursor (AA).

We also assessed the PL incorporation of VA and CLA in all tissues analyzed. As expected, VA- and VA+CLA-fed rats had higher ($P < 0.001$) concentrations of VA in liver (8-fold), VAT (4.5-fold), skeletal muscle (10-fold), and

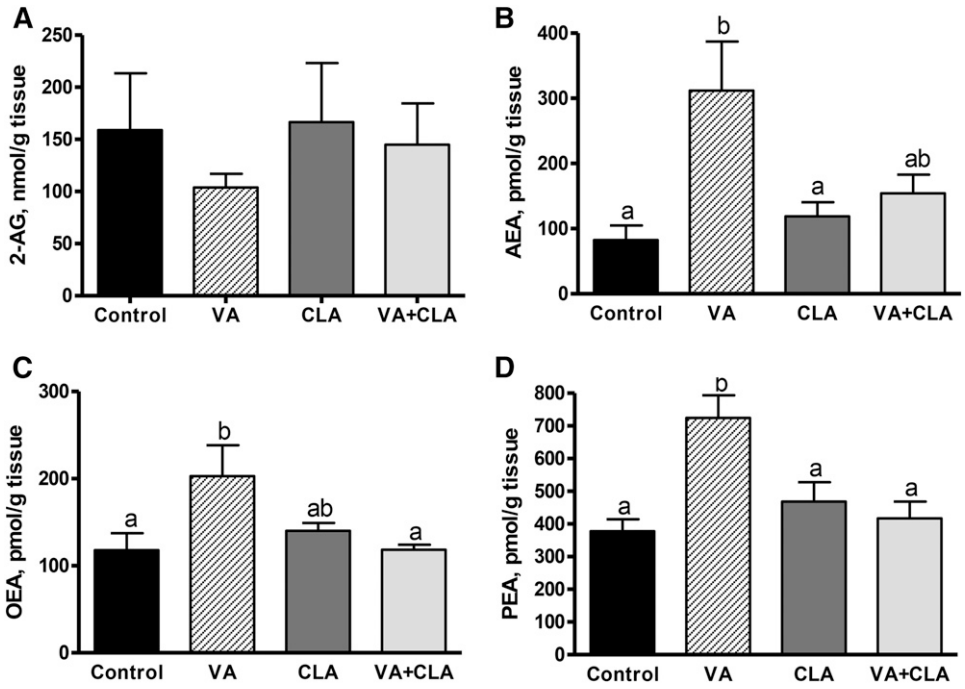

Fig. 4. EC (A, B) and *N*-acylethanolamine (C, D) concentrations in the jejunal mucosa of JCR:LA-*cp* rats following dietary supplementation with VA, CLA, or VA+CLA. Values are means ± SEM, represented by vertical bars (n = 5). Means without a common letter differ ($P < 0.05$).

JOURNAL OF LIPID RESEARCH
ASBMB

TABLE 3. PL fatty acid composition in tissues of JCR:LA-*cp* rats fed control or experimental diets for 8 weeks

	Control		VA		CLA		VA+CLA	
Fatty Acids[a]	Mean	SEM	Mean	SEM	Mean	SEM	Mean	SEM
Liver								
16:0	16.4^{b}	0.7	12.9^{a}	0.3	15.7^{b}	0.4	14.6^{ab}	0.5
cis-9 18:1 (OA)	6.0^{b}	0.3	3.9^{a}	0.1	5.2^{b}	0.2	3.6^{a}	0.1
trans-11-VA	0.2^{a}	0.1	1.6^{c}	0.0	0.7^{b}	0.0	1.6^{c}	0.1
cis-9, *trans*-11 CLA	ND	—	ND	—	0.6^{b}	0.0	0.3^{a}	0.0
20:4 *n*6 (AA)	19.7^{a}	0.7	25.2^{b}	0.5	18.5^{a}	0.7	24.2^{b}	0.6
VAT								
16:0	10.8	1.2	9.5	0.1	11.3	1.3	10.3	0.1
cis-9 18:1 (OA)	11.8^{b}	0.3	11.6^{b}	0.2	10.0^{a}	0.2	9.8^{a}	0.2
trans-11 VA	0.4^{a}	0.1	1.8^{c}	0.0	0.7^{b}	0.1	1.9^{c}	0.0
cis-9, *trans*-11 CLA	ND	—	ND	—	0.8^{b}	0.1	0.6^{a}	0.0
20:4 *n*6 (AA)	15.0	1.3	13.9	0.2	14.5	0.9	14.1	0.3
Hypothalamus								
16:0	17.6	0.3	17.1	0.3	17.2	0.4	18.2	0.4
cis-9 18:1 (OA)	21.4	0.3	21.9	0.2	21.0	0.7	20.7	0.6
trans-11 VA)	ND	—	0.1^{b}	0.0	0.04^{a}	0.0	0.1^{b}	0.0
cis-9, *trans*-11 CLA	ND	—	ND	0.0	0.1^{c}	0.0	0.08^{b}	0.0
20:4 *n*6 (AA)	9.9	0.2	9.6	0.2	10.2	0.5	10.3	0.6
Muscle								
16:0	19.8	1.9	21.3	0.7	21.0	0.6	17.1	0.8
cis-9 18:1 (OA)	5.3	0.4	5.3	0.4	5.7	0.4	4.6	0.4
*trans*11 VA	0.1^{a}	0.1	1.0^{b}	0.0	0.1^{a}	0.1	1.2^{b}	0.1
cis-9, *trans*-11 CLA	ND	—	ND	—	ND	—	ND	—
20:4 *n*6 (AA)	11.7^{a}	0.3	13.0^{b}	0.3	11.8^{ab}	0.4	10.8^{a}	0.3
Jejunal mucosa								
16:0	13.2	0.5	11.6	0.3	13.0	0.3	12.5	0.8
cis-9 18:1 (OA)	8.3^{b}	0.1	7.2^{ab}	0.4	7.7^{b}	0.6	5.6^{a}	0.4
trans-11 VA	0.4^{a}	0.0	1.5^{c}	0.1	0.6^{b}	0.1	1.4^{c}	0.1
cis-9, *trans*-11 CLA	ND	—	ND	—	0.5^{b}	0.0	0.2^{a}	0.0
20:4 *n*6 (AA)	14.5	0.6	18.3	1.5	14.7	1.5	20.0	1.6

Values are mean ± SEM, n = 5. Means in a row with superscripts without a common letter differ, $P < 0.05$. OA, oleic acid; ND, not detectable.

[a]Grams per 100 grams total fatty acids.

jejunal (3.8-fold) PLs compared with rats fed the control diet. The incorporation of VA into the hypothalamus of JCR:LA-*cp* rats was found to be at trace amounts (0.1 g/100 g total fatty acids).

CLA was not detected in tissues of VA-fed rats, suggesting limited incorporation of CLA (produced from VA desaturation) into tissue PLs. Furthermore, CLA was only incorporated in the liver, VAT, hypothalamus, and jejunal PLs of CLA-fed rats (<1 g/100 g total fatty acids) and to a lesser extent in tissue PLs of rats fed the VA+CLA diet ($P < 0.05$).

The magnitude of incorporation of VA in membrane PLs is tissue dependent

To associate the tissue-specific effects of VA with its magnitude of incorporation, we conducted a comparison of VA in tissue membrane PLs (**Fig. 5**). VA was incorporated in VAT (1.8 g/100 g fatty acids), followed by the liver (1.6 g/100 g fatty acids), jejunum (1.5 g/100 g fatty acids), skeletal muscle (1.0 g/100 g fatty acids), and hypothalamus (0.1 g/100 g fatty acids).

Dietary supplementation with VA alters the mRNA and protein expression of FAAH, but does not affect the mRNA expression of CB1 receptor in the jejunum

To determine whether selective increase of AEA, OEA, and PEA in the jejunal mucosa by VA could be associated with synthetic or degradative pathways, we first measured the mRNA expression and protein activity of jejunal *N*-acylphosphatidylethanolamine phospholipase type D, one of the key enzymes responsible for the synthesis of these *N*-acylethanolamines, but no differences were found between groups (data not shown, $P > 0.05$). We then measured the expression of FAAH, their primary hydrolyzing enzyme. Interestingly, while VA- and VA+CLA-fed rats had higher jejunal mRNA expression of FAAH compared with the control group (1.4-fold, $P < 0.05$ and 1.6-fold, $P < 0.01$, respectively), the protein abundance of this enzyme was reduced in VA-fed rats only (−34%, $P < 0.05$) (**Fig. 6A–C**). However, the protein activity of jejunal FAAH did not differ between groups (Fig. 6E, $P > 0.05$). We also found that VA tended to lower jejunal mRNA expression of CB1 relative

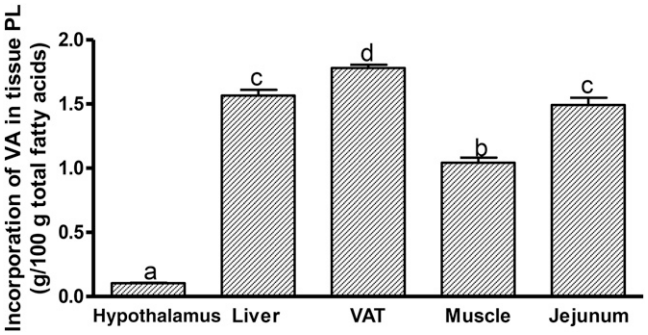

Fig. 5. Incorporation of VA in tissue PLs in JCR:LA-*cp* rats supplemented with VA for 8 weeks. Values are mean ± SEM, represented by vertical bars (n = 5). Means without a common letter differ, $P < 0.05$.

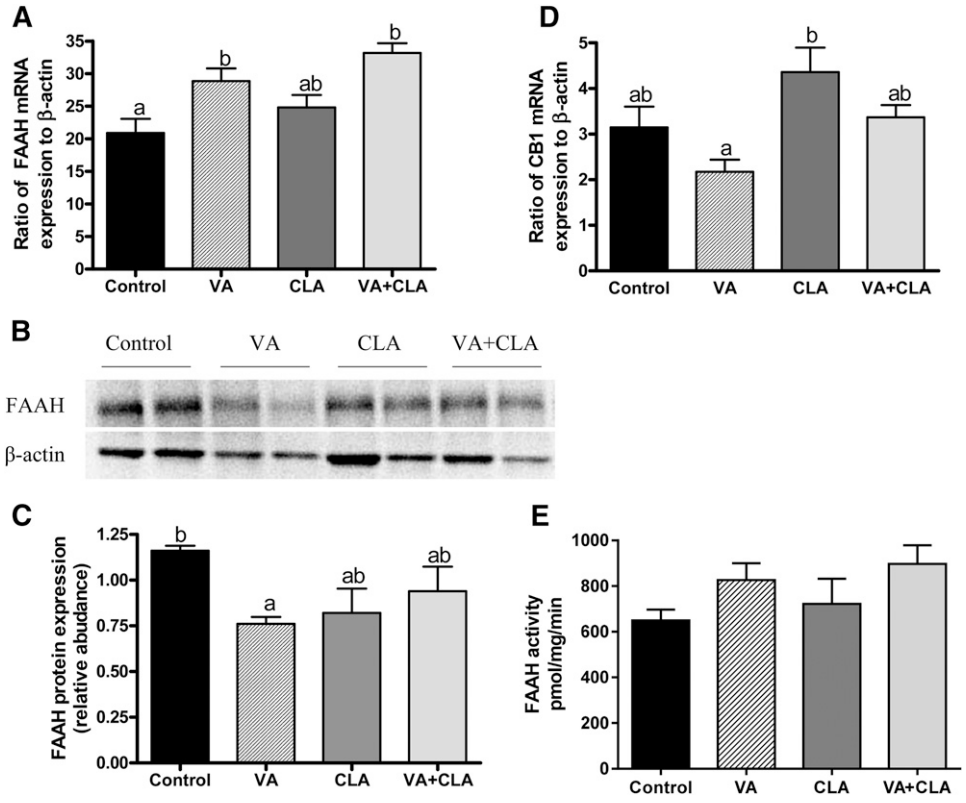

Fig. 6. Jejunal mucosal mRNA expression of FAAH and CB1 and protein abundance and activity of FAAH in JCR:LA-*cp* rats fed control or experimental diets for 8 weeks. The mRNA expression for FAAH (A) and CB1 (D) is relative to the housekeeping gene, β-actin. A representative blot (B) and graph (C) for FAAH relative protein abundance are shown. FAAH activity (E) was not significant within groups. Values are mean ± SEM, represented by vertical bars (n = 5). Means without a common letter differ, $P < 0.05$.

to the other diets; however, this did not reach statistical significance ($P > 0.05$) (Fig. 6D).

Dietary supplementation with VA reduced the mRNA expression of pro-inflammatory cytokines in the jejunum

The EC system (ECS) is upregulated in human inflammatory bowel diseases and experimental models of colitis and colorectal cancer growth (21, 40–42). During these conditions, an overactive ECS is proposed to be an adaptive response to counteract the consequences of inflammation, such as T cell-mediated aberrant immune response (41). Therefore, we explored whether the increase in jejunal AEA, OEA, and PEA that we observed was associated with intestinal inflammation. Indeed, the expression of pro-inflammatory cytokines [TNFα (**Fig. 7A**) and IL-1β (Fig. 7B)] in the intestine was significantly lower in rats fed the VA-supplemented diet compared with the control rats (−80 and −64%, respectively; $P < 0.05$).

Caco2 cell culture to verify VA action on anti-inflammatory pathways

We tested the anti-inflammatory properties of VA alone or in combination with the FAAH inhibitor, URB597, in the presence or absence of the FAAH substrate, OEA, in the Caco2 cell model of human intestinal epithelial cells. Treatment with VA alone reduced the LPS-induced mRNA expression of TNFα by 64%, while addition of URB597 did not result in reduction in Caco2 cells (**Fig. 8**). The mRNA expression of TNFα was not reduced by VA in the absence of OEA ($P > 0.05$), suggesting that OEA is required for the observed anti-inflammatory properties of VA in this cell model.

DISCUSSION

Dietary supplementation with VA reduces liver and VAT 2-AG without altering the availability of PL biosynthetic precursor

Increased plasma EC concentrations have been found to be positively correlated with visceral fat mass and waist circumference in humans (14–16). Consequently, the ECS has been proposed as a critical target for the treatment of abdominal obesity and associated metabolic abnormalities in the metabolic syndrome. While pharmacological blockade of the CB1 receptor with rimonabant has shown some clinical success, the adverse psychiatric side effects associated with this drug have led to its withdrawal as a treatment option (43). Given that the ECS can be modulated in response to dietary fat (9), nutritional interventions with tissue-specific effects could be an attractive alternative approach to clinically target the systemic ECS during metabolically abnormal conditions.

To our knowledge, this is the first report to demonstrate that despite a lack of a direct effect on either the plasma or

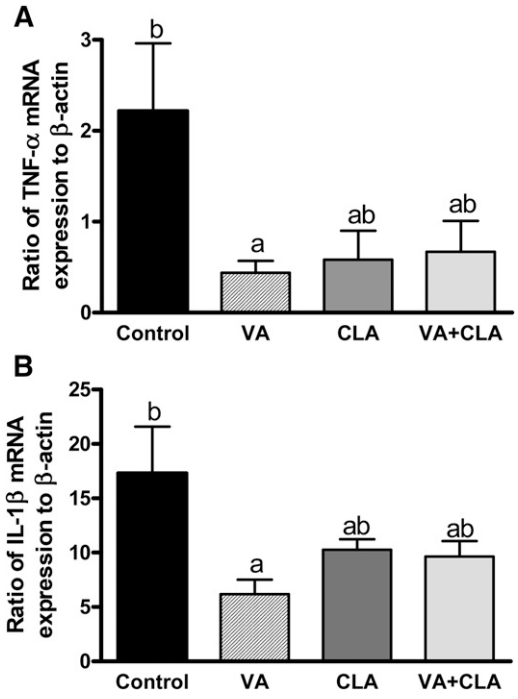

Fig. 7. Jejunal mucosa mRNA expression of pro-inflammatory cytokines in JCR:LA-*cp* rats fed control or experimental diets for 8 weeks. The expression of TNFα (A) and IL-1β (B) is relative to the housekeeping gene, β-actin. Values are mean ± SEM, represented by vertical bars (n = 5). Means without a common letter differ, $P < 0.05$.

the brain ECs, dietary supplementation with VA can effectively decrease liver and VAT 2-AG concentrations in a rat model of metabolic syndrome. Our findings resemble those reported for n3 long chain PUFA (in the form of krill oil) in the Zucker *fa/fat* rat (44) and may also suggest a putative mechanism of action for the ability of VA to decrease ectopic lipid accumulation and hepatic TG secretion (5). The rationale for this hypothesis is that CB receptor activation in the liver and VAT can lead to increased de novo lipogenesis and visceral adiposity (18, 19, 45), both of which are attenuated by VA (3, 5). Interestingly, effects of VA on liver and VAT 2-AG concentrations cannot be explained by changes in AA levels in membrane PLs, but

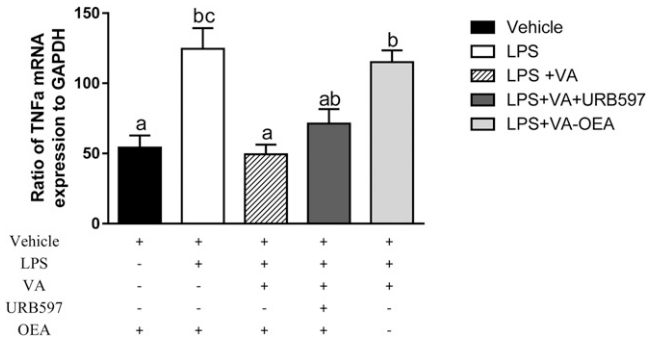

Fig. 8. Effect of VA in the presence or absence of OEA and the FAAH inhibitor, URB597, in the intestinal Caco2 cell model of inflammation. The expression of TNFα is relative to the housekeeping gene, GAPDH. Values are mean ± SEM, represented by vertical bars (n = 5). Means without a common letter differ, $P < 0.05$.

rather due to incorporation of VA into PLs. Thus, it is plausible that an increased incorporation of VA (relative to AA) into the lipid precursor of 2-AG (i.e., diacylglycerol) may occur during PL remodeling. This modification would result in the synthesis of a VA-derived glycerol compound instead of synthesis of 2-AG, thereby leading to decreased concentrations of 2-AG, but this requires further investigation.

Effects of VA on tissue EC concentrations are associated with its incorporation into tissue PLs

Previous studies in the JCR:LA-*cp* rat have shown that the lipid-lowering effects of CLA are enhanced by the addition of VA when compared with dietary supplementation with CLA alone (24). In this study, we provide evidence that VA per se can independently reduce tissue 2-AG concentrations corresponding with its magnitude of incorporation into tissue PLs when compared with CLA (Table 3). Our findings also reveal that effects of VA on EC concentrations may be tissue-specific and parallel the extent of VA incorporation into respective tissue membrane PLs (Fig. 5). We note that while the incorporation of VA in peripheral tissues (VAT, liver, and jejunal mucosa) is within the same general level, the lower hypothalamic incorporation of VA suggests a decreased active transport of VA across the blood brain barrier, but this requires further investigation. Further studies are also needed to determine the mechanism of how the incorporation of VA into tissue PLs mediates a lowering of EC concentrations in liver and VAT.

Increased jejunal AEA, OEA, and PEA by VA is associated with downregulation of FAAH protein expression and may explain the anti-inflammatory properties of VA

We have observed that VA re-equilibrates intestinal and hepatic lipid homeostasis while exerting differential transcriptional regulation in both organs, as reflected in mRNA levels of sterol regulatory element-binding protein 1 (SREBP1) and FAS (5). In this study, we found a consistent effect of VA to decrease 2-AG concentrations in the liver and VAT. In contrast, jejunal concentrations of AEA and its analogs (OEA and PEA) were selectively increased following VA treatment alone. This selective increase of jejunal *N*-acylethanolamines by VA could not be explained by changes in their biosynthetic PL precursors, but associated with a reduction in protein expression of the enzyme, FAAH (known to hydrolyze AEA, OEA, and PEA). Notably, feeding n3 long chain PUFAs is associated with an increase in the FAAH inhibitor, arachidonoyl-serotonin (AA-5-HT), and other jejunal long chain PUFA-serotonins (also capable of inhibiting FAAH activity in vitro) in mice (46). Interestingly, in the present study, we found discordance between increased mRNA levels and reduced protein abundance of FAAH in the jejunal mucosa upon VA supplementation, which suggests a compensatory mechanism for the reduced protein and infers an active feedback pathway for the enzyme. Furthermore, the protein activity of FAAH was not different between groups (Fig. 6E). Although it is plausible that VA supplementation may stimulate the formation of lipid mediators that regulate FAAH

abundance, the factors that regulate FAAH abundance and/or activity are complex. For example, the literature describes a complex interaction of FAAH with appetite and sex hormones (47, 48), as well as preferential membrane stabilization of FAAH by sterols (49) that could potentially be involved.

Targeting the ECS (via inhibition of FAAH) has therapeutic potential in the treatment of intestinal inflammatory diseases (50–52). AEA is found to be increased in human intestinal inflammatory diseases and is proposed to be an adaptive response to counteract the inflammatory milieu during these conditions (40–42). In contrast to the pathological role of the ECS in the liver and VAT (13, 18, 53), activation of CB1 or CB2 receptors (via exogenous agonists or FAAH inhibition) has been shown to reduce macroscopic damage scores of colonic inflammation and to attenuate the activation of T-cells and the infiltration of inflammatory cells in animal models of colitis (21, 22, 50, 51). Additionally, the *N*-acylethanolamine PEA has also been shown to exert anti-inflammatory effects through activation of PPARα, including reduction of pro-inflammatory cytokine production (54). We therefore examined the mRNA expression of two key inflammatory markers, TNFα and IL-1β, in the intestine to explore a potential association with the increased AEA and PEA concentrations observed in the jejunum. Indeed, the reduction in mRNA expression of these pro-inflammatory cytokines by VA is consistent with previous observations in this rat model. VA treatment has been shown to normalize the production of IL-2 and TNFα in mesenteric gut-associated lymph nodes after mitogen stimulation in this rodent model of metabolic syndrome (4). Results from the present study provide further evidence for a potential anti-inflammatory effect of VA via activation of the ECS in the intestine. We wish to note that both CB and noncannabinoid receptor (e.g., PPAR) mechanisms may contribute to the anti-inflammatory effects of FAAH inhibition (52). Further, we have shown previously that VA feeding increases the expression of PPARα and PPARγ in jejunal mucosa (6). Therefore, increasing the availability of endogenous ligands to CB and PPAR receptors (e.g., AEA and PEA, respectively) may offer a mechanistic explanation for the anti-inflammatory effects of VA in this organ.

Results from this study also suggest a potential synergistic effect of VA and OEA on reducing the LPS-induced mRNA expression of TNFα in the Caco2 cell model (Fig. 8). The mechanisms for this interaction are not clear, but previous studies suggest that the anti-inflammatory effects of OEA are associated with reduced activation of the transcriptional cytokine activator, nuclear factor κB (NF-κB) (55, 56). Unlike industrially derived *trans* fatty acids, VA has been shown to protect against NF-κB activation (57) and inflammation, as measured by reduced T-helper cell cytokine production in a PPARγ-dependent manner (7). Therefore, it is plausible that OEA and VA may act synergistically to reduce the LPS-induced pro-inflammatory response via PPAR activation. Alternatively, VA and OEA may alter cell receptor function (e.g., toll-like receptor 4) and receptor-induced activation of NF-κB indirectly by altering membrane and lipid raft function, but this warrants further investigation.

In conclusion, we demonstrate that dietary supplementation with VA exerts a tissue-specific regulation of ECs that could be used as an attractive alternative approach to target the ECS during conditions of metabolic syndrome and intestinal inflammatory diseases. We have shown that VA effectively reduces liver and VAT 2-AG concentrations corresponding with its previously observed properties to beneficially modulate lipid storage compartments. We have also provided evidence that VA can act independently of CLA, which seems to be associated with its incorporation into tissue PLs. Additionally, the present findings delineate a unique opposing regulation of VA on AEA and its *N*-acylethanolamine analogs that cannot be explained by changes in their biosynthetic PL precursors. Rather, our results suggest an inhibitory effect of VA on the protein expression of FAAH in the intestine that may result in activation of protective pathways of the ECS in this organ. Collectively, findings from this study have provided a potential novel mechanism of action for the health benefits of VA and highlight the need for further investigation to explore the efficacy of VA on intestinal inflammatory diseases.

The authors thank Sharon Sokolik and Sandra Kelly for their excellent technical assistance associated with this project.

REFERENCES

1. US Food and Drug Administration. 2013. FDA takes step to further reduce *trans* fats in processed foods. Accessed February 7, 2016, at http://www.fda.gov/newsevents/newsroom/pressannouncements/ucm373939.htm.
2. Wang, Y., J. Lu, M. R. Ruth, S. D. Goruk, M. J. Reaney, D. R. Glimm, D. F. Vine, C. J. Field, and S. D. Proctor. 2008. Trans-11 vaccenic acid dietary supplementation induces hypolipidemic effects in JCR:LA-cp rats. *J. Nutr.* **138:** 2117–2122.
3. Wang, Y., M. M. Jacome-Sosa, M. R. Ruth, S. D. Goruk, M. J. Reaney, D. R. Glimm, D. C. Wright, D. F. Vine, C. J. Field, and S. D. Proctor. 2009. Trans-11 vaccenic acid reduces hepatic lipogenesis and chylomicron secretion in JCR:LA-cp rats. *J. Nutr.* **139:** 2049–2054.
4. Blewett, H. J., C. A. Gerdung, M. R. Ruth, S. D. Proctor, and C. J. Field. 2009. Vaccenic acid favourably alters immune function in obese JCR:LA-cp rats. *Br. J. Nutr.* **102:** 526–536.
5. Jacome-Sosa, M. M., F. Borthwick, R. Mangat, R. Uwiera, M. J. Reaney, J. Shen, A. D. Quiroga, R. L. Jacobs, R. Lehner, and S. D. Proctor. 2014. Diets enriched in trans-11 vaccenic acid alleviate ectopic lipid accumulation in a rat model of NAFLD and metabolic syndrome. *J. Nutr. Biochem.* **25:** 692–701.
6. Wang, Y., M. M. Jacome-Sosa, M. R. Ruth, J. Shen, M. J. Reaney, S. L. Scott, M. E. Dugan, H. D. Anderson, C. J. Field, S. D. Proctor, et al. 2012. The intestinal bioavailability of vaccenic acid and activation of peroxisome proliferator-activated receptor-α and -γ in a rodent model of dyslipidemia and the metabolic syndrome. *Mol. Nutr. Food Res.* **56:** 1234–1246.
7. Jaudszus, A., G. Jahreis, W. Schlörmann, J. Fischer, R. Kramer, C. Degen, C. Rohrer, A. Roth, H. Gabriel, D. Barz, et al. 2012. Vaccenic acid-mediated reduction in cytokine production is independent of c9,t11-CLA in human peripheral blood mononuclear cells. *Biochim. Biophys. Acta.* **1821:** 1316–1322.
8. Calder, P. C. 2006. n-3 Polyunsaturated fatty acids, inflammation, and inflammatory diseases. *Am. J. Clin. Nutr.* **83:** 1505S–1519S.
9. Banni, S., and V. Di Marzo. 2010. Effect of dietary fat on endocannabinoids and related mediators: consequences on energy homeostasis, inflammation and mood. *Mol. Nutr. Food Res.* **54:** 82–92.

10. Berger, A., G. Crozier, T. Bisogno, P. Cavaliere, S. Innis, and V. Di Marzo. 2001. Anandamide and diet: inclusion of dietary arachidonate and docosahexaenoate leads to increased brain levels of the corresponding N-acylethanolamines in piglets. *Proc. Natl. Acad. Sci. USA.* **98:** 6402–6406.
11. D'Asti, E., H. Long, J. Tremblay-Mercier, M. Grajzer, S. C. Cunnane, V. Di Marzo, and C. D. Walker. 2010. Maternal dietary fat determines metabolic profile and the magnitude of endocannabinoid inhibition of the stress response in neonatal rat offspring. *Endocrinology.* **151:** 1685–1694.
12. Watanabe, S., M. Doshi, and T. Hamazaki. 2003. n-3 Polyunsaturated fatty acid (PUFA) deficiency elevates and n-3 PUFA enrichment reduces brain 2-arachidonoylglycerol level in mice. *Prostaglandins Leukot. Essent. Fatty Acids.* **69:** 51–59.
13. Alvheim, A. R., M. K. Malde, D. Osei-Hyiaman, Y. H. Lin, R. J. Pawlosky, L. Madsen, K. Kristiansen, L. Frøyland, and J. R. Hibbeln. 2012. Dietary linoleic acid elevates endogenous 2-AG and anandamide and induces obesity. *Obesity (Silver Spring).* **20:** 1984–1994.
14. Engeli, S., J. Böhnke, M. Feldpausch, K. Gorzelniak, J. Janke, S. Bátkai, P. Pacher, J. Harvey-White, F. C. Luft, A. M. Sharma, et al. 2005. Activation of the peripheral endocannabinoid system in human obesity. *Diabetes.* **54:** 2838–2843.
15. Blüher, M., S. Engeli, N. Klöting, J. Berndt, M. Fasshauer, S. Bátkai, P. Pacher, M. R. Schön, J. Jordan, and M. Stumvoll. 2006. Dysregulation of the peripheral and adipose tissue endocannabinoid system in human abdominal obesity. *Diabetes.* **55:** 3053–3060.
16. Côté, M., I. Matias, I. Lemieux, S. Petrosino, N. Alméras, J. P. Després, and V. Di Marzo. 2007. Circulating endocannabinoid levels, abdominal adiposity and related cardiometabolic risk factors in obese men. *Int. J. Obes. (Lond).* **31:** 692–699.
17. Di Marzo, V., S. K. Goparaju, L. Wang, J. Liu, S. Bátkai, Z. Járai, F. Fezza, G. I. Miura, R. D. Palmiter, T. Sugiura, et al. 2001. Leptin-regulated endocannabinoids are involved in maintaining food intake. *Nature.* **410:** 822–825.
18. Osei-Hyiaman, D., M. DePetrillo, P. Pacher, J. Liu, S. Radaeva, S. Bátkai, J. Harvey-White, K. Mackie, L. Offertáler, L. Wang, et al. 2005. Endocannabinoid activation at hepatic CB1 receptors stimulates fatty acid synthesis and contributes to diet-induced obesity. *J. Clin. Invest.* **115:** 1298–1305.
19. Osei-Hyiaman, D., J. Liu, L. Zhou, G. Godlewski, J. Harvey-White, W. I. Jeong, S. Bátkai, G. Marsicano, B. Lutz, C. Buettner, et al. 2008. Hepatic CB1 receptor is required for development of diet-induced steatosis, dyslipidemia, and insulin and leptin resistance in mice. *J. Clin. Invest.* **118:** 3160–3169.
20. Cinar, R., G. Godlewski, J. Liu, J. Tam, T. Jourdan, B. Mukhopadhyay, J. Harvey-White, and G. Kunos. 2014. Hepatic CB1 receptors mediate diet-induced insulin resistance by increasing de novo synthesis of long chain ceramides. *Hepatology.* **59:** 143–153.
21. Massa, F., G. Marsicano, H. Hermann, A. Cannich, K. Monory, B. F. Cravatt, G. L. Ferri, A. Sibaev, M. Storr, and B. Lutz. 2004. The endogenous cannabinoid system protects against colonic inflammation. *J. Clin. Invest.* **113:** 1202–1209.
22. Singh, U. P., N. P. Singh, B. Singh, R. L. Price, M. Nagarkatti, and P. S. Nagarkatti. 2012. Cannabinoid receptor-2 (CB2) agonist ameliorates colitis in IL-10(-/-) mice by attenuating the activation of T cells and promoting their apoptosis. *Toxicol. Appl. Pharmacol.* **258:** 256–267.
23. Pintus, S., E. Murru, G. Carta, L. Cordeddu, B. Batetta, S. Accossu, D. Pistis, S. Uda, M. Elena Ghiani, M. Mele, et al. 2013. Sheep cheese naturally enriched in α-linolenic, conjugated linoleic and vaccenic acids improves the lipid profile and reduces anandamide in the plasma of hypercholesterolaemic subjects. *Br. J. Nutr.* **109:** 1453–1462.
24. Jacome-Sosa, M. M., J. Lu, Y. Wang, M. R. Ruth, D. C. Wright, M. J. Reaney, J. Shen, C. J. Field, D. F. Vine, and S. D. Proctor. 2010. Increased hypolipidemic benefits of cis-9, trans-11 conjugated linoleic acid in combination with trans-11 vaccenic acid in a rodent model of the metabolic syndrome, the JCR:LA-cp rat. *Nutr. Metab. (Lond).* **7:** 60.
25. Fu, J., S. Gaetani, F. Oveisi, J. Lo Verme, A. Serrano, F. Rodríguez De Fonseca, A. Rosengarth, H. Luecke, B. Di Giacomo, G. Tarzia, et al. 2003. Oleylethanolamide regulates feeding and body weight through activation of the nuclear receptor PPAR-alpha. *Nature.* **425:** 90–93.
26. Schwartz, G. J., J. Fu, G. Astarita, X. Li, S. Gaetani, P. Campolongo, V. Cuomo, and D. Piomelli. 2008. The lipid messenger OEA links dietary fat intake to satiety. *Cell Metab.* **8:** 281–288.
27. Lo Verme, J., J. Fu, G. Astarita, G. La Rana, R. Russo, A. Calignano, and D. Piomelli. 2005. The nuclear receptor peroxisome proliferator-activated receptor-alpha mediates the anti-inflammatory actions of palmitoylethanolamide. *Mol. Pharmacol.* **67:** 15–19.
28. Russell, J. C., and S. D. Proctor. 2006. Small animal models of cardiovascular disease: tools for the study of the roles of metabolic syndrome, dyslipidemia, and atherosclerosis. *Cardiovasc. Pathol.* **15:** 318–330.
29. Vine, D. F., R. Takechi, J. C. Russell, and S. D. Proctor. 2007. Impaired postprandial apolipoprotein-B48 metabolism in the obese, insulin-resistant JCR:LA-cp rat: increased atherogenicity for the metabolic syndrome. *Atherosclerosis.* **190:** 282–290.
30. Motard-Bélanger, A., A. Charest, G. Grenier, P. Paquin, Y. Chouinard, S. Lemieux, P. Couture, and B. Lamarche. 2008. Study of the effect of trans fatty acids from ruminants on blood lipids and other risk factors for cardiovascular disease. *Am. J. Clin. Nutr.* **87:** 593–599.
31. Swain, M. L., and B. A. Brice. 1949. Formation of traces of conjugated tetraenoic and trienoic constitutents in autoxidized linolenic and linoleic acids and vegetable oils during alkali-isomerization. *J. Am. Oil Chem. Soc.* **26:** 272–277.
32. Cruz-Hernandez, C., J. K. G. Kramer, J. J. Kennelly, D. R. Glimm, B. M. Sorensen, E. K. Okine, L. A. Goonewardene, and R. J. Weselake. 2007. Evaluating the conjugated linoleic acid and trans 18:1 isomers in milk fat of dairy cows fed increasing amounts of sunflower oil and a constant level of fish oil. *J. Dairy Sci.* **90:** 3786–3801.
33. Folch, J., M. Lees, and G. H. Sloane Stanley. 1957. A simple method for the isolation and purification of total lipids from animal tissues. *J. Biol. Chem.* **226:** 497–509.
34. Lehner, R., and D. E. Vance. 1999. Cloning and expression of a cDNA encoding a hepatic microsomal lipase that mobilizes stored triacylglycerol. *Biochem. J.* **343:** 1–10.
35. Zoerner, A. A., F. M. Gutzki, S. Batkai, M. May, C. Rakers, S. Engeli, J. Jordan, and D. Tsikas. 2011. Quantification of endocannabinoids in biological systems by chromatography and mass spectrometry: a comprehensive review from an analytical and biological perspective. *Biochim. Biophys. Acta.* **1811:** 706–723.
36. Lu, J., F. Borthwick, Z. Hassanali, Y. Wang, R. Mangat, M. Ruth, D. Shi, A. Jaeschke, J. C. Russell, C. J. Field, et al. 2011. Chronic dietary n-3 PUFA intervention improves dyslipidaemia and subsequent cardiovascular complications in the JCR:LA-*cp* rat model of the metabolic syndrome. *Br. J. Nutr.* **105:** 1572–1582.
37. Fu, J., G. Astarita, S. Gaetani, J. Kim, B. F. Cravatt, K. Mackie, and D. Piomelli. 2007. Food intake regulates oleoylethanolamide formation and degradation in the proximal small intestine. *J. Biol. Chem.* **282:** 1518–1528.
38. Mohankumar, S. K., D. Hanke, L. Siemens, A. Cattini, J. Enns, J. Shen, M. Reaney, P. Zahradka, and C. G. Taylor. 2013. Dietary supplementation of trans-11-vaccenic acid reduces adipocyte size but neither aggravates nor attenuates obesity-mediated metabolic abnormalities in fa/fa Zucker rats. *Br. J. Nutr.* **109:** 1628–1636.
39. Tyburczy, C., C. Major, A. L. Lock, F. Destaillats, P. Lawrence, J. T. Brenna, A. M. Salter, and D. E. Bauman. 2009. Individual trans octadecenoic acids and partially hydrogenated vegetable oil differentially affect hepatic lipid and lipoprotein metabolism in golden Syrian hamsters. *J. Nutr.* **139:** 257–263.
40. Guagnini, F., M. Valenti, S. Mukenge, I. Matias, A. Bianchetti, S. Di Palo, G. Ferla, V. Di Marzo, and T. Croci. 2006. Neural contractions in colonic strips from patients with diverticular disease: role of endocannabinoids and substance P. *Gut.* **55:** 946–953.
41. D'Argenio, G., S. Petrosino, C. Gianfrani, M. Valenti, G. Scaglione, I. Grandone, S. Nigam, I. Sorrentini, G. Mazzarella, and V. Di Marzo. 2007. Overactivity of the intestinal endocannabinoid system in celiac disease and in methotrexate-treated rats. *J. Mol. Med. (Berl).* **85:** 523–530.
42. Ligresti, A., T. Bisogno, I. Matias, L. De Petrocellis, M. G. Cascio, V. Cosenza, G. D'argenio, G. Scaglione, M. Bifulco, I. Sorrentini, et al. 2003. Possible endocannabinoid control of colorectal cancer growth. *Gastroenterology.* **125:** 677–687.
43. Christensen, R., P. K. Kristensen, E. M. Bartels, H. Bliddal, and A. Astrup. 2007. Efficacy and safety of the weight-loss drug rimonabant: a meta-analysis of randomised trials. *Lancet.* **370:** 1706–1713.
44. Batetta, B., M. Griinari, G. Carta, E. Murru, A. Ligresti, L. Cordeddu, E. Giordano, F. Sanna, T. Bisogno, S. Uda, et al. 2009. Endocannabinoids may mediate the ability of (n-3) fatty acids to reduce ectopic fat and inflammatory mediators in obese Zucker rats. *J. Nutr.* **139:** 1495–1501.

45. Pagano, C., C. Pilon, A. Calcagno, R. Urbanet, M. Rossato, G. Milan, K. Bianchi, R. Rizzuto, P. Bernante, G. Federspil, et al. 2007. The endogenous cannabinoid system stimulates glucose uptake in human fat cells via phosphatidylinositol 3-kinase and calcium-dependent mechanisms. *J. Clin. Endocrinol. Metab.* **92:** 4810–4819.
46. Verhoeckx, K. C., T. Voortman, M. G. Balvers, H. F. Hendriks, H. M. Wortelboer, and R. F. Witkamp. 2011. Presence, formation and putative biological activities of N-acyl serotonins, a novel class of fatty-acid derived mediators, in the intestinal tract. *Biochim. Biophys. Acta.* **1811:** 578–586.
47. Waleh, N. S., B. F. Cravatt, A. Apte-Deshpande, A. Terao, and T. S. Kilduff. 2002. Transcriptional regulation of the mouse fatty acid amide hydrolase gene. *Gene.* **291:** 203–210.
48. Maccarrone, M., M. Di Rienzo, A. Finazzi-Agrò, and A. Rossi. 2003. Leptin activates the anandamide hydrolase promoter in human T lymphocytes through STAT3. *J. Biol. Chem.* **278:** 13318–13324.
49. Dainese, E., G. De Fabritiis, A. Sabatucci, S. Oddi, C. B. Angelucci, C. Di Pancrazio, T. Giorgino, N. Stanley, M. Del Carlo, B. F. Cravatt, et al. 2014. Membrane lipids are key modulators of the endocannabinoid-hydrolase FAAH. *Biochem. J.* **457:** 463–472.
50. Storr, M. A., C. M. Keenan, D. Emmerdinger, H. Zhang, B. Yüce, A. Sibaev, F. Massa, N. E. Buckley, B. Lutz, B. Göke, et al. 2008. Targeting endocannabinoid degradation protects against experimental colitis in mice: involvement of CB1 and CB2 receptors. *J. Mol. Med. (Berl).* **86:** 925–936.
51. Storr, M. A., C. M. Keenan, H. Zhang, K. D. Patel, A. Makriyannis, and K. A. Sharkey. 2009. Activation of the cannabinoid 2 receptor (CB2) protects against experimental colitis. *Inflamm. Bowel Dis.* **15:** 1678–1685.
52. Schlosburg, J. E., S. G. Kinsey, and A. H. Lichtman. 2009. Targeting fatty acid amide hydrolase (FAAH) to treat pain and inflammation. *AAPS J.* **11:** 39–44.
53. Starowicz, K. M., L. Cristino, I. Matias, R. Capasso, A. Racioppi, A. A. Izzo, and V. Di Marzo. 2008. Endocannabinoid dysregulation in the pancreas and adipose tissue of mice fed with a high-fat diet. *Obesity (Silver Spring).* **16:** 553–565.
54. Di Paola, R., D. Impellizzeri, A. Torre, E. Mazzon, A. Cappellani, C. Faggio, E. Esposito, F. Trischitta, and S. Cuzzocrea. 2012. Effects of palmitoylethanolamide on intestinal injury and inflammation caused by ischemia-reperfusion in mice. *J. Leukoc. Biol.* **91:** 911–920.
55. Sayd, A., M. Antón, F. Alén, J. R. Caso, J. Pavón, J. C. Leza, F. Rodríguez de Fonseca, B. García-Bueno, and L. Orio. 2014. Systemic administration of oleoylethanolamide protects from neuroinflammation and anhedonia induced by LPS in rats. *Int. J. Neuropsychopharmacol.* **18:** pyu111.
56. Sun, Y., S. P. Alexander, M. J. Garle, C. L. Gibson, K. Hewitt, S. P. Murphy, D. A. Kendall, and A. J. Bennett. 2007. Cannabinoid activation of PPAR alpha; a novel neuroprotective mechanism. *Br. J. Pharmacol.* **152:** 734–743.
57. Iwata, N. G., M. Pham, N. O. Rizzo, A. M. Cheng, E. Maloney, and F. Kim. 2011. Trans fatty acids induce vascular inflammation and reduce vascular nitric oxide production in endothelial cells. *PLoS One.* **6:** e29600.

Supplemental Table 1 Fat composition of designed control and experimental diets

Fat ingredient	Control diet	VA diet	CLA diet	VA+CLA diet
	g/kg of diet			
Butter	48.75	57.3	59.6	102.50
Sunflower oil	14.25	21.6	22.5	0
Safflower oil	0	0	0	22.13
Flaxseed	3.75	3.9	3.9	3.9
Fully hydrogenated canola oil	6.75	6.6	6.75	0
Olive oil	52.5	28.5	25.5	0
Lard	24	19.4	13.5	0
Vaccenic acid	0	12.66	0	13.82
Conjugated linoleic acid	0	0	18.2	8.25

Values are expressed as g per kg of diet. Adapted from reference 5.